NASA/TM–1999–209336

Aeroacoustic Data for a High Reynolds Number Axisymmetric Subsonic Jet

Michael K. Ponton
Langley Research Center, Hampton, Virginia

Lawrence S. Ukeiley
Langley Research Center, Hampton, Virginia

Sang W. Lee
The George Washington University Joint Institute for Advancement of Flight Sciences
Langley Research Center, Hampton, Virginia

May 1999

The NASA STI Program Office ... in Profile

Since its founding, NASA has been dedicated to the advancement of aeronautics and space science. The NASA Scientific and Technical Information (STI) Program Office plays a key part in helping NASA maintain this important role.

The NASA STI Program Office is operated by Langley Research Center, the lead center for NASA's scientific and technical information. The NASA STI Program Office provides access to the NASA STI Database, the largest collection of aeronautical and space science STI in the world. The Program Office is also NASA's institutional mechanism for disseminating the results of its research and development activities. These results are published by NASA in the NASA STI Report Series, which includes the following report types:

- TECHNICAL PUBLICATION. Reports of completed research or a major significant phase of research that present the results of NASA programs and include extensive data or theoretical analysis. Includes compilations of significant scientific and technical data and information deemed to be of continuing reference value. NASA counterpart and peer-reviewed formal professional papers, but having less stringent limitations on manuscript length and extent of graphic presentations.

- TECHNICAL MEMORANDUM. Scientific and technical findings that are preliminary or of specialized interest, e.g., quick release reports, working papers, and bibliographies that contain minimal annotation. Does not contain extensive analysis.

- CONTRACTOR REPORT. Scientific and technical findings by NASA-sponsored contractors and grantees.

- CONFERENCE PUBLICATION. Collected papers from scientific and technical conferences, symposia, seminars, or other meetings sponsored or co-sponsored by NASA.

- SPECIAL PUBLICATION. Scientific, technical, or historical information from NASA programs, projects, and missions, often concerned with subjects having substantial public interest.

- TECHNICAL TRANSLATION. English-language translations of foreign scientific and technical material pertinent to NASA's mission.

Specialized services that complement the STI Program Office's diverse offerings include creating custom thesauri, building customized databases, organizing and publishing research results... even providing videos.

For more information about the NASA STI Program Office, see the following:

- Access the NASA STI Program Home Page at ***http://www.sti.nasa.gov***

- E-mail your question via the Internet to help@sti.nasa.gov

- Fax your question to the NASA STI Help Desk at (301) 621–0134

- Phone the NASA STI Help Desk at (301) 621–0390

- Write to:
  NASA STI Help Desk
  NASA Center for AeroSpace Information
  7121 Standard Drive
  Hanover, MD 21076–1320

NASA/TM–1999–209336

Aeroacoustic Data for a High Reynolds Number Axisymmetric Subsonic Jet

Michael K. Ponton
Langley Research Center, Hampton, Virginia

Lawrence S. Ukeiley
Langley Research Center, Hampton, Virginia

Sang W. Lee
The George Washington University Joint Institute for Advancement of Flight Sciences
Langley Research Center, Hampton, Virginia

National Aeronautics and
Space Administration

Langley Research Center
Hampton, Virginia 23681–2199

May 1999

Acknowledgment

Lawrence Ukeiley would like to acknowledge National Research Council where he has a NASA LaRC Research Associateship.

Available from:

NASA Center for AeroSpace Information (CASI)
7121 Standard Drive
Hanover, MD 21076–1320
(301) 621–0390

National Technical Information Service (NTIS)
5285 Port Royal Road
Springfield, VA 22161–2171
(703) 605–6000

Summary

The near field fluctuating pressure and aerodynamic mean flow characteristics of a cold subsonic jet issuing from a contoured convergent nozzle are presented. The data are presented for nozzle exit Mach numbers of 0.30, 0.60, and 0.85 at a constant jet stagnation temperature of 104°F. The fluctuating pressure measurements were acquired via linear and semi-circular microphone arrays and the presented results include plots of narrowband spectra, contour maps, streamwise/azimuthal spatial correlations for zero time delay, and cross-spectra of the azimuthal correlations. A pitot probe was used to characterize the mean flow velocity by assuming the subsonic flow to be pressure-balanced with the ambient field into which it exhausts. Presented are mean flow profiles and the momentum thickness of the free shear layer as a function of streamwise position.

Introduction

The noise due to the engine exhausts of current subsonic commercial transports continues to be a major environmental concern to airport communities. This noise is created by the turbulent mixing of the exhausted jet plume with the ambient thus creating pressure fluctuations in the hydrodynamic near field and acoustic far field regions of the jet flow. Wlezien et al. (1998) state that this acoustic emission has limited aircraft operation to designated hours in many airports and that local noise standards for acceptable acoustic levels (more restrictive than current FAA guidelines) may be imposed upon entering aircraft. They assert that noise abatement may be facilitated by the incorporation of control methods designed to alter the turbulent noise sources residing in the free shear layer of the jet plume.

Seiner (1998) proposes that control schemes may be based upon a low-dimensional model of the turbulent flow field. He posits that these dynamical models can be generated by applying the Proper Orthogonal Decomposition (POD) (Holmes, Lumley & Berkooz, 1996) technique to the correlations of turbulent two-point statistics. Seiner (1998) asserts that upon completion of such a model, Lighthill's (1952) acoustic analogy approach to understanding aerodynamically generated sound may be used to determine which low order turbulent spatial structures are responsible for noise generation thus providing the base state for the design of control methodologies. Ukeiley, Seiner, and Ponton (1999) provide insight into the spatial structure of the turbulent velocity properties of a subsonic jet by application of the POD. However, further work is necessary to establish the relationship between these turbulent velocity structures and the turbulent pressure structures responsible for far field noise generation.

Michalke and Fuchs (1975) provide insight into the azimuthal structure of the turbulent pressure and velocity fields in a subsonic jet (Mach 0.2) shear layer while Arndt, Long, and Glauser (1997) use the POD technique to define the structure of the near field pressure fluctuations surrounding a Mach 0.07 jet. The purpose of this paper is to continue characterizing the near fluctuating pressure field thus enabling additional insights into the nature of acoustic noise sources at higher subsonic Mach numbers. To facilitate meaningful comparisons with research data acquired in other facilities, the aerodynamic characteristics of the plume's flow field are also presented.

Symbols

D	nozzle exit diameter, 2 in.
f_c	center frequency of the emitted broadband jet noise
Ma_e	local jet Mach number at the nozzle exit based upon the nozzle pressure ratio
OASPL	Overall SPL in dB re 20×10^{-6} N/m^2
p_a	test cell ambient pressure
p_t	local jet total pressure from the pitot probe
r	radial coordinate perpendicular to x; referenced from the jet centerline
SPL	Sound Pressure Level in dB re 20×10^{-6} N/m^2
x	axial coordinate parallel to the jet centerline; referenced from the nozzle exit plane
U	local jet velocity
U_e	nozzle exit velocity
Θ	compressible momentum thickness

Experimental Details

The experiments were conducted in the Small Anechoic Jet Facility (SAJF) located at the NASA Langley Research Center. Model hardware and instrumentation are available within the SAJF for research directed at measuring the fluid dynamic and acoustic characteristics associated with internal and external air flows. The interior walls of the SAJF are anechoically treated with acoustic wedges that absorb in excess of 99% of the incident sound for frequencies above 100 Hz. The internal dimensions of the SAJF (within the wedge tips) are 10.5 ft by 10 ft by 12 ft along the x-direction. Research models are connected to an air delivery system capable of supplying 2.5 lbm/s of continuous dry air. A 275 kW resistance heater is used to create a constant *cold* stagnation temperature of 104°F thereby establishing an operating temperature independent of variations in supply temperatures. An electronically controlled valve maintains the nozzle pressure ratio to within 0.5% of the desired set point and pressure transducers used by the flow control system receive frequent in-situ calibration.

The subsonic nozzle consists of a contoured transition section connecting a 6 inch settling chamber to a 2 inch inside diameter convergent nozzle. Metallic honeycomb is installed in the settling chamber to diminish large scale propagating disturbances. The nozzle is designed for parallel exit flow. A 2 ft diameter circular duct treated with fine mesh screen is positioned concentric to the nozzle assembly thus facilitating co-flow aspiration.

The linear and semi-circular arrays (Figure 1) incorporated seven 1/4 inch phase-matched microphone systems. The separation distance between each microphone on the linear array was 1 D (i.e., 2 inches) and the array was positioned parallel to the jet centerline. On the semi-circular array, a constant azimuthal separation of 30° was used with each sensor positioned at r/D = 2. The plane of this array was perpendicular to the jet centerline. For data acquisition, both arrays were traversed in

the x-direction while only the linear array was traversed in the r-direction. Data were acquired using the semi-circular array at x/D = 0, 1, 2, 3, 4, 5, 6, 7 and 8. For the linear array, data were acquired at r/D = 3, 4, 6, 8, 10, 12, 14, 16 and 18 and the array was traversed axially whereby the upstream microphone varied in position from x/D = 0, 4, 7 to 13. For the linear array data, each microphone signal was digitized at 50 kHz and bandpass filtered between 160 Hz and 20 kHz. For the semi-circular array data, the signals were digitized at 30 kHz and bandpass filtered between 160 Hz and 12.5 kHz. For all microphone data, 128 independent blocks of 1024 usable data points were recorded.

Aerodynamic Results

Presented in figures 2 and 3 are the radial distributions for the axial mean velocity profiles and the computed compressible momentum thickness, respectively. The data were reduced using pitot probe measurements of total pressure by assuming a statically pressure balanced jet. Additionally, the stagnation temperature was assumed to be a constant 104°F for all calculations even at large radial positions. Because the ambient temperature within the SAJF elevated quickly when the experiment was conducted, the difference between the test cell ambient and the jet stagnation temperatures introduce negligible errors in velocity and momentum thickness computations. Isentropic ideal gas flow is assumed and the ratio of specific heats at constant pressure to constant volume was taken to be 1.40. The local speed of sound was calculated using the local jet static temperature as determined from the stagnation temperature and the Mach number based upon the local pressure ratio, p_t/p_a. For momentum thickness calculations, the local static density was determined via isentropic equations relating total to static density.

Acoustic Results

Presented in figures 5 through 63 are the narrowband spectra for the data acquired using the linear microphone array. To facilitate comparisons, the amplitude range plotted is constant. Because the spectral processes of primary interest are dominant at low frequencies, a logarithmic frequency scale is employed. A reduced data set is presented for $\mathrm{Ma}_e = 0.3$ due to the presence of strong reflections from the near field array supports that convolute the amplitude distribution at large radial distances. Table 1 contains a description of the data presented within these figures. Each spectrum was computed using 128 averages of Fast Fourier Transformed (FFT) spectral images. Each FFT image was computed from 1024 temporal data points.

Figures 64 and 65 contain the near field pressure contour maps of OASPL as well as SPL in select frequency bands, f_c, for $\mathrm{Ma}_e = 0.6$ and 0.85. The data were reduced by digitally filtering the FFT generated spectra in select 488.3 Hz bands. The lowest f_c value plotted corresponds to the approximate peak frequency of the emitted jet noise as indicated from the microphone data acquired at x/D = 19 and r/D = 8. This position was used to determine the peak frequency because the end of the potential core is located at approximately x/D = 5 and jet noise is primarily emitted from this location at a polar angle of about 30° with respect to the jet centerline. The additional f_c values plotted correspond to

Fig	Ma_e	r/D	x/D	Fig	Ma_e	r/D	x/D
4	0.30	3	0-5	34	0.60	18	0-5
5	0.30	3	8-11	35	0.60	18	8-11
6	0.30	4	0-5	36	0.60	18	12-17
7	0.30	4	8-11	37	0.85	3	0-5
8	0.30	6	0-5	38	0.85	3	8-11
9	0.30	6	8-11	39	0.85	3	12-17
10	0.60	3	0-5	40	0.85	4	0-5
11	0.60	3	8-11	41	0.85	4	8-11
12	0.60	3	12-17	42	0.85	4	12-17
13	0.60	4	0-5	43	0.85	6	0-5
14	0.60	4	8-11	44	0.85	6	8-11
15	0.60	4	12-17	45	0.85	6	12-17
16	0.60	6	0-5	46	0.85	8	0-5
17	0.60	6	8-11	47	0.85	8	8-11
18	0.60	6	12-17	48	0.85	8	12-17
19	0.60	8	0-5	49	0.85	10	0-5
20	0.60	8	8-11	50	0.85	10	8-11
21	0.60	8	12-17	51	0.85	10	12-17
22	0.60	10	0-5	52	0.85	12	0-5
23	0.60	10	8-11	53	0.85	12	8-11
24	0.60	10	12-17	54	0.85	12	12-17
25	0.60	12	0-5	55	0.85	14	0-5
26	0.60	12	8-11	56	0.85	14	8-11
27	0.60	12	12-17	57	0.85	14	12-17
28	0.60	14	0-5	58	0.85	16	0-5
29	0.60	14	8-11	59	0.85	16	8-11
30	0.60	14	12-17	60	0.85	16	12-17
31	0.60	16	0-5	61	0.85	18	0-5
32	0.60	16	8-11	62	0.85	18	8-11
33	0.60	16	12-17	63	0.85	18	12-17

Table 1: List of Figures for Narrowband Autospectra

the second, fourth, and sixth harmonics of the peak jet noise frequency.

Presented in figures 66 through 74 are the cross-correlation coefficients of the linear array data for zero time delay; thus, these plots indicate the level of axial spatial correlation. Each microphone on the array was processed as the reference microphone and correlated with the remaining six microphone signals. The legend beside each plot indicates the symbols used to designate the reference microphone. Table 2 contains a description of the data presented within these figures.

Figures 75 and 76 present the cross-correlation coefficients of the semi-circular array data for $Ma_e = 0.6$ and 0.85, respectively, where the microphone positioned at 0° was processed as the reference microphone. Also included are the correlations for data digitally filtered about the

Fig	Ma_e	r/D	x/D	Fig	Ma_e	r/D	x/D
66	0.30	3-4	0-13	71	0.85	3-16	0-6
67	0.60	3-16	0-6	72	0.85	3-16	4-10
68	0.60	3-16	4-10	73	0.85	3-16	7-13
69	0.60	3-16	7-13	74	0.85	3-16	13-19
70	0.60	3-16	13-19				

Table 2: List of Figures for Zero Time Lag Pressure Correlations

peak jet noise frequency. These data indicate the level of azimuthal spatial correlation. For the digitally unfiltered data, figures 77 through 79 contain the cross-spectra of the azimuthal cross-correlations for $Ma_e = 0.3$, 0.6, and 0.85. These figures provide insight into the spatial structure of the azimuthal pressure field at r/D=2. The cross-correlation levels are consistent with the limited measurements presented by Pao and Maestrello (1976).

Concluding Remarks

Near field pressure and mean flow data, acquired at the NASA Langley Research Center, are presented for a contoured convergent nozzle. Velocity profiles and momentum thickness distributions are given as well as spectra, contour maps, cross-correlations, and cross-spectra of the fluctuating pressure field. The data are presented for nozzle exit Mach numbers of 0.30, 0.60, and 0.85 at a constant jet stagnation temperature of 104°F. These measurements should prove useful in furthering the understanding of the spatial characteristics of the hydrodynamic pressure field and the structure of noise generating mechanisms. Such an understanding will ultimately lead to the development of control methodologies that minimize acoustic emissions thereby reducing the environmental impact caused by subsonic commercial transports.

References

[1] Arndt, R. E. A., Long, D. F., & Glauser, M. N. (1997). "The Proper Orthogonal Decomposition of Pressure Fluctuations Surrounding a Turbulent Jet." *Journal of Fluid Mechanics* **340**, 1-33.

[2] Holmes, P., Lumley, J. L., & Berkooz, G. (1996). "Turbulence, Coherent Structures, Synamical Systems and Symmetry." Cambridge, Great Britain: Cambridge University Press.

[3] Lighthill, M. J. (1952). "On Sound Generated Aerodynamically." *Proceedings of the Royal Society* **211**(1106), 564-587.

[4] Michalke, A., & Fuchs, H. V. (1975). "On Turbulence and Noise of an Axisymmetric Shear Flow." *Journal of Fluid Mechanics* **70**, 179-205.

[5] Pao, S.P. and Maestrello, L. (1976). "Evidence of the Beam Pattern Concept of Subsonic Jet Noise Emission." NASA TN D-8104.

[6] Seiner, J. M. (1998). A New National Approach to Jet Noise Reduction." *Theoretical and Computational Fluid Dynamics* **10**, 373-383.

[7] Ukeiley, L. S., Seiner, J. M., & Ponton, M. K. (1999, July). "Azimuthal Structure of an Axisymmetric Jet Mixing Layer." Paper presented at the 3rd ASME/JSME Joint Fluids Engineering Conference, San Francisco, CA.

[8] Wlezien, R. W., Horner, G. C., McGowan, A. R., Padula, S. L., Scott, M. A., Silcox, R. J., & Simpson, J. O. (1998, April). "The Aircraft Morphing Program." AIAA Paper 98-1927 presented at the 39th Structures, Structural Dynamics, and Materials Conference and Exhibit, Long Beach, CA.

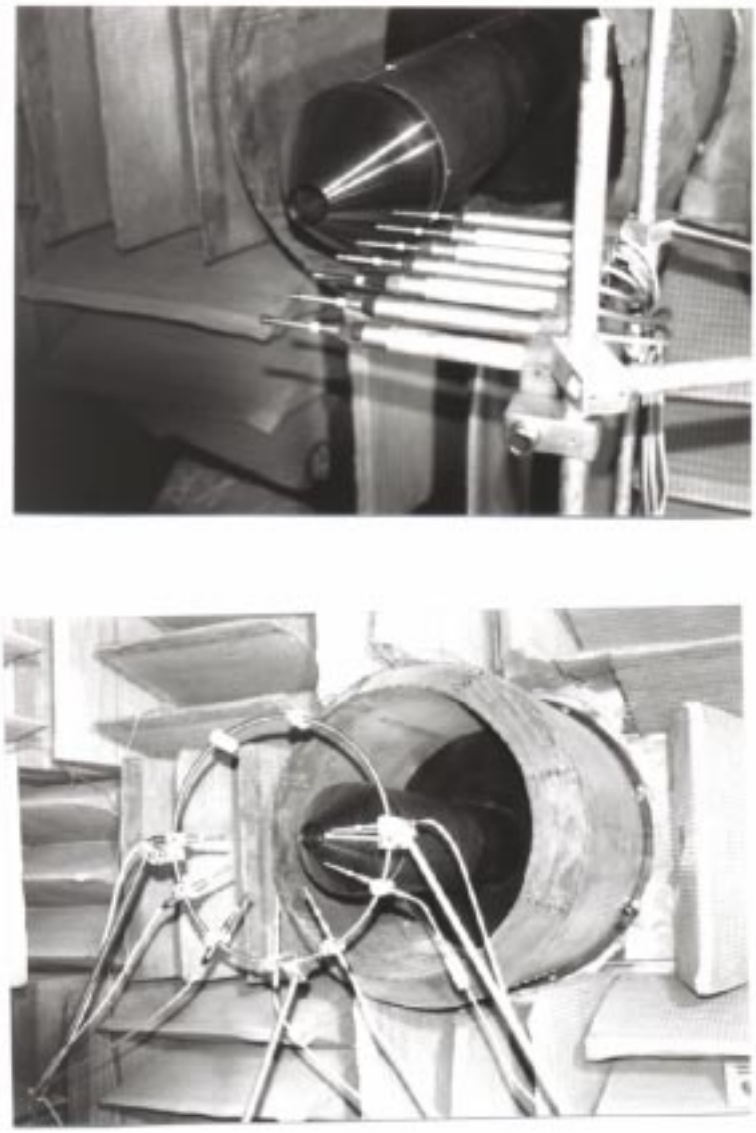

Figure 1: Near Field Microphone Arrays

Ma_e=0.30

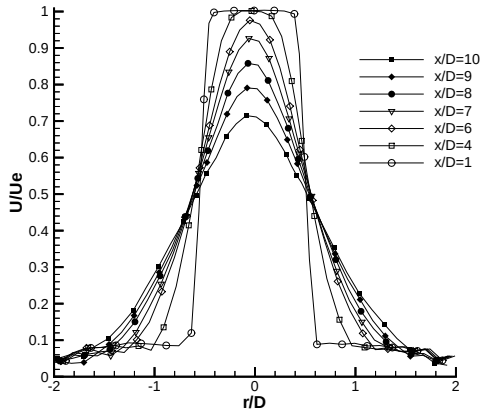

Ma_e=0.60

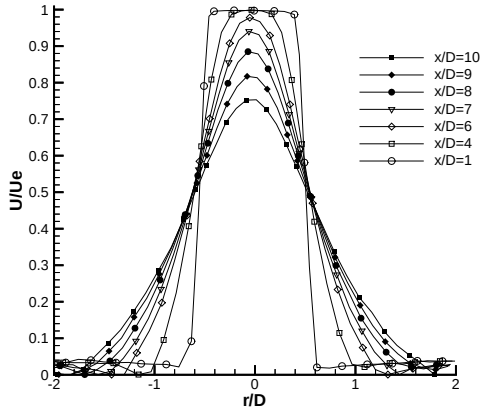

Ma_e=0.85

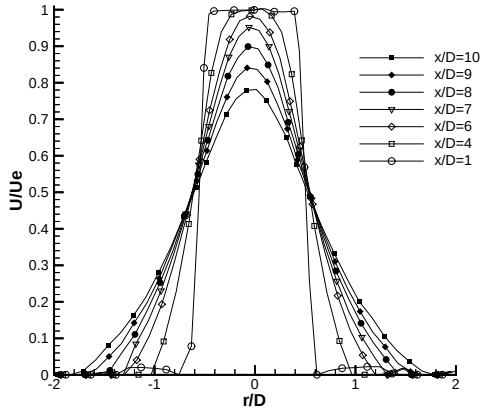

Figure 2: Mean Streamwise Velocity Profiles

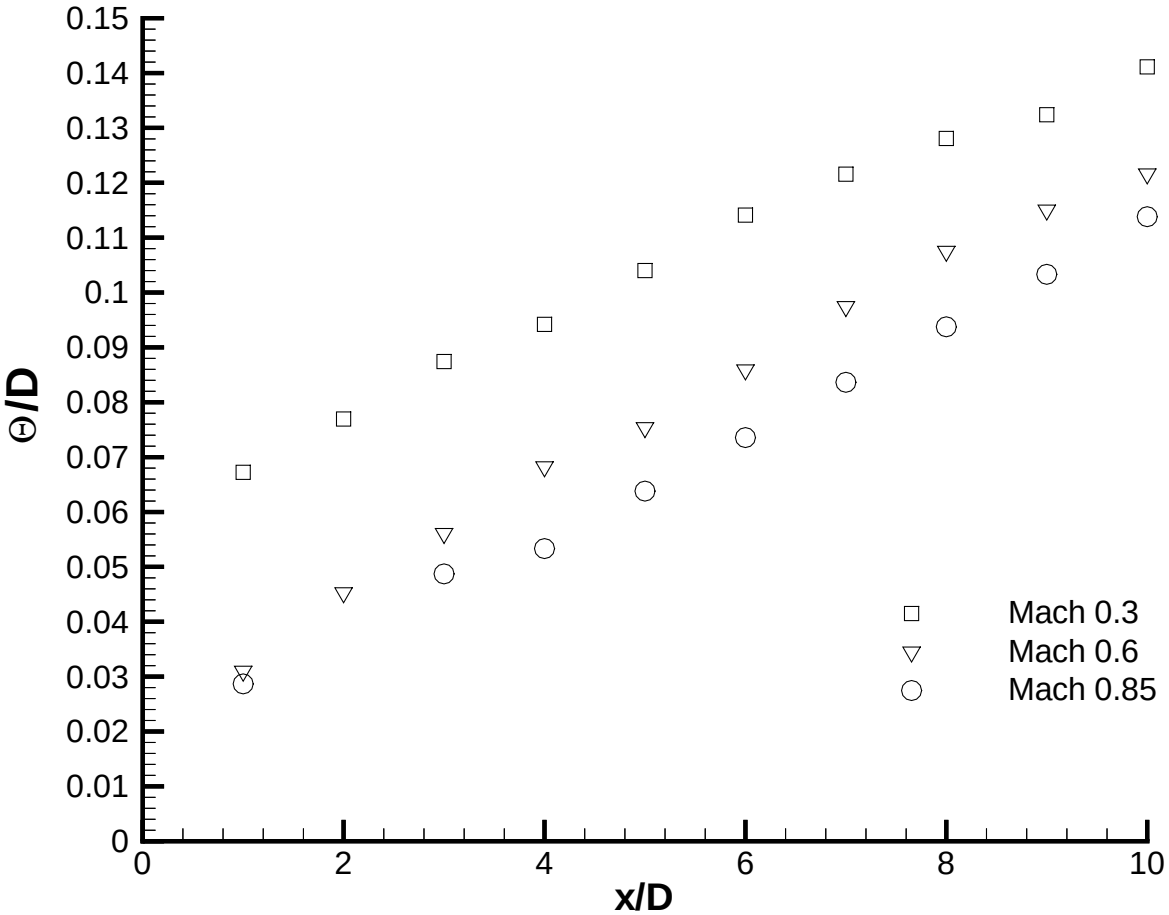

Figure 3: Momentum Thickness

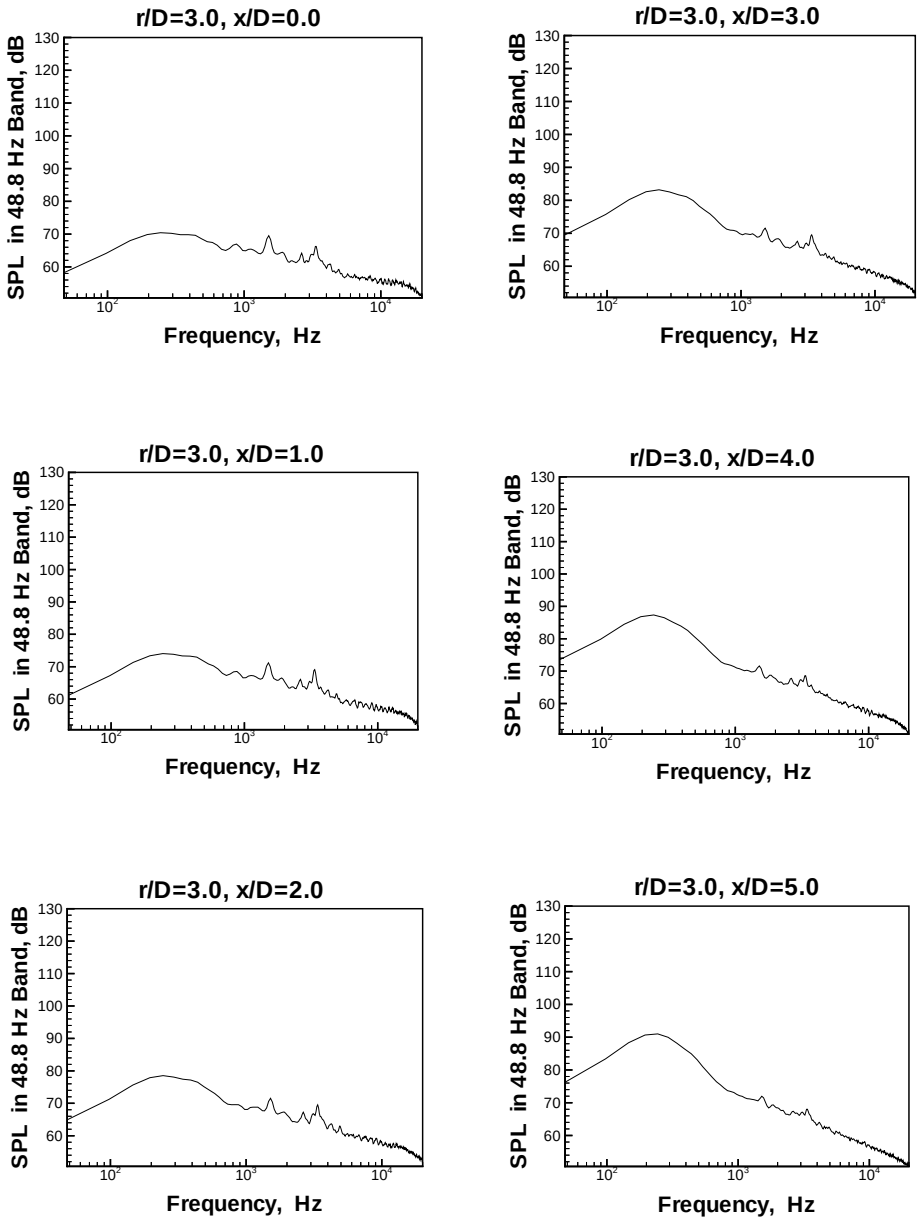

Figure 4: Near Field Pressure Spectra, Ma_e=0.30, r/D=3.0

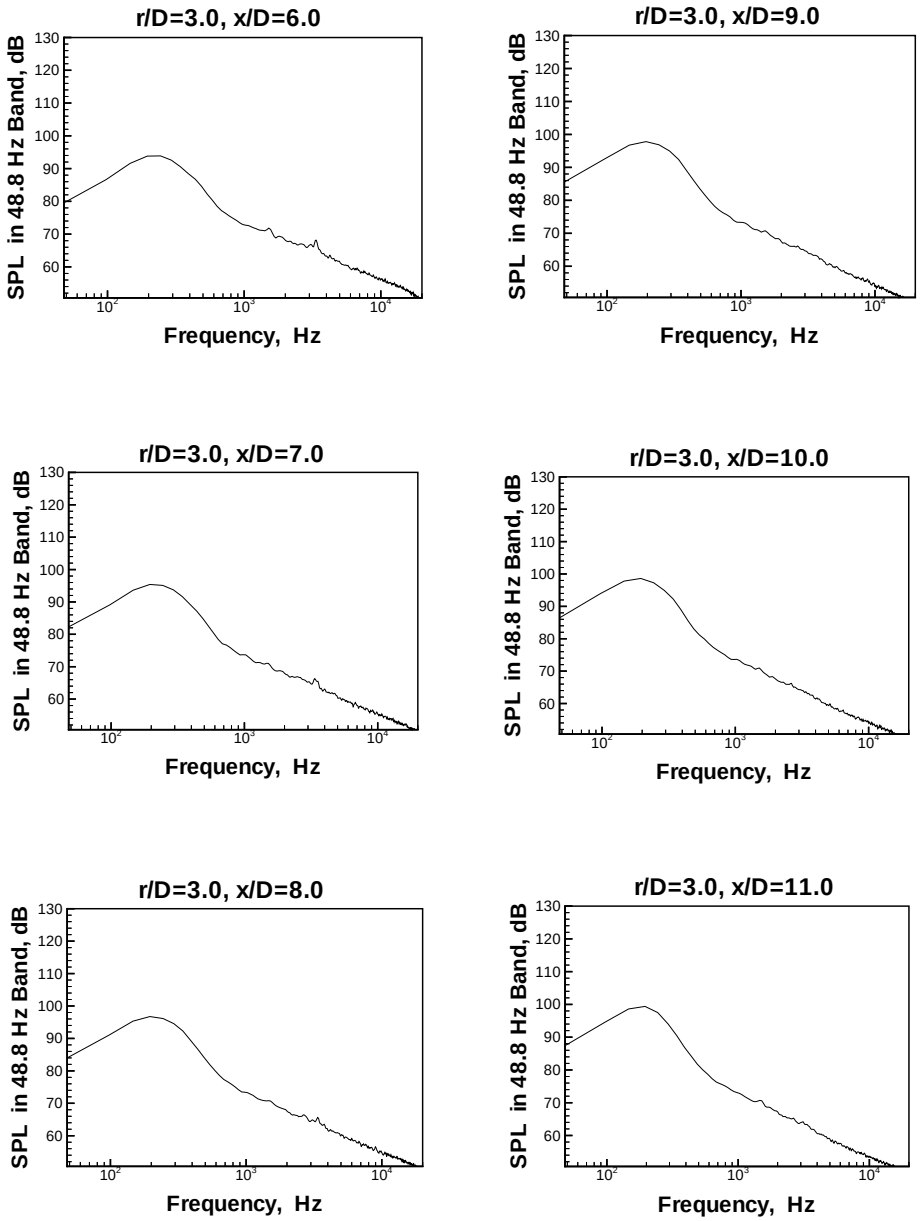

Figure 5: Near Field Pressure Spectra, Ma_e=0.30, r/D=3.0

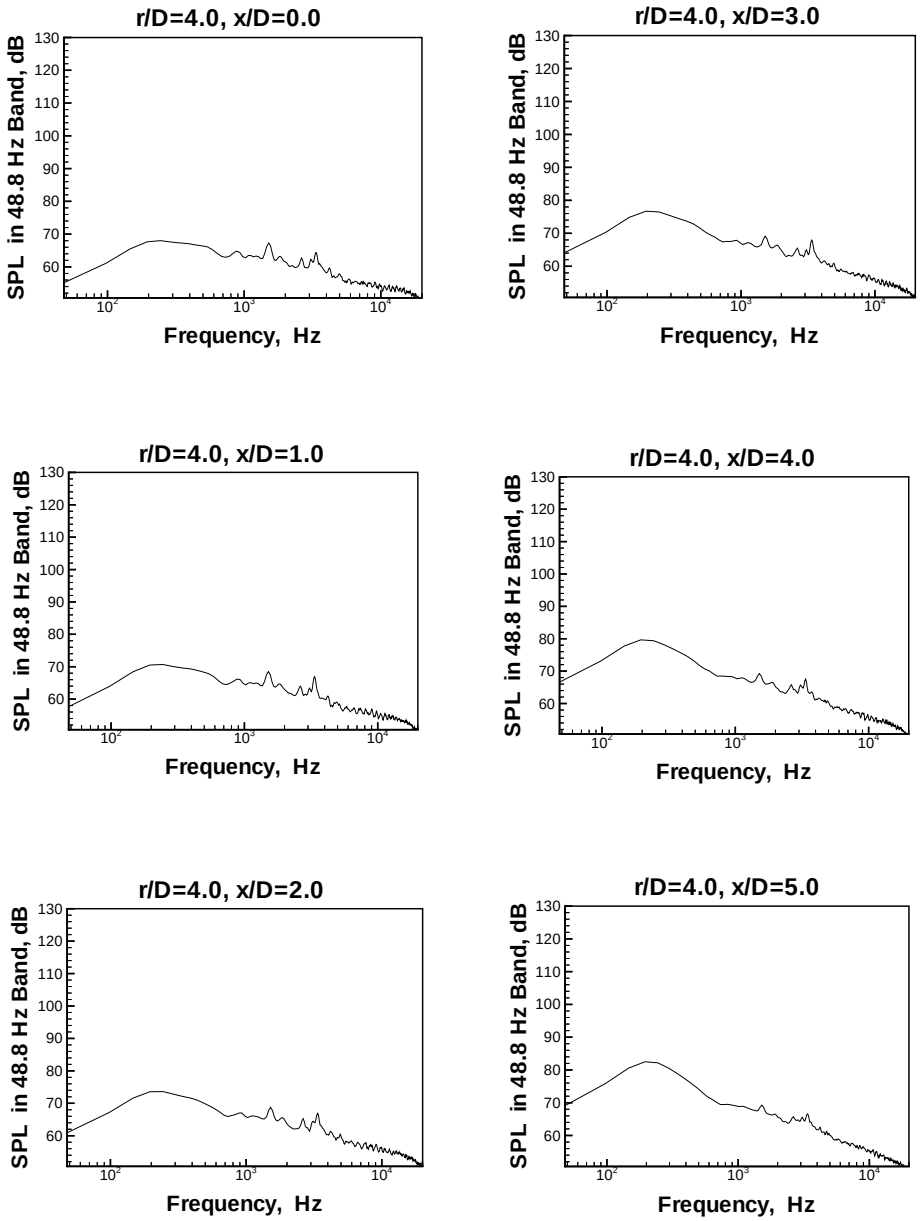

Figure 6: Near Field Pressure Spectra, Ma_e=0.30, r/D=4.0

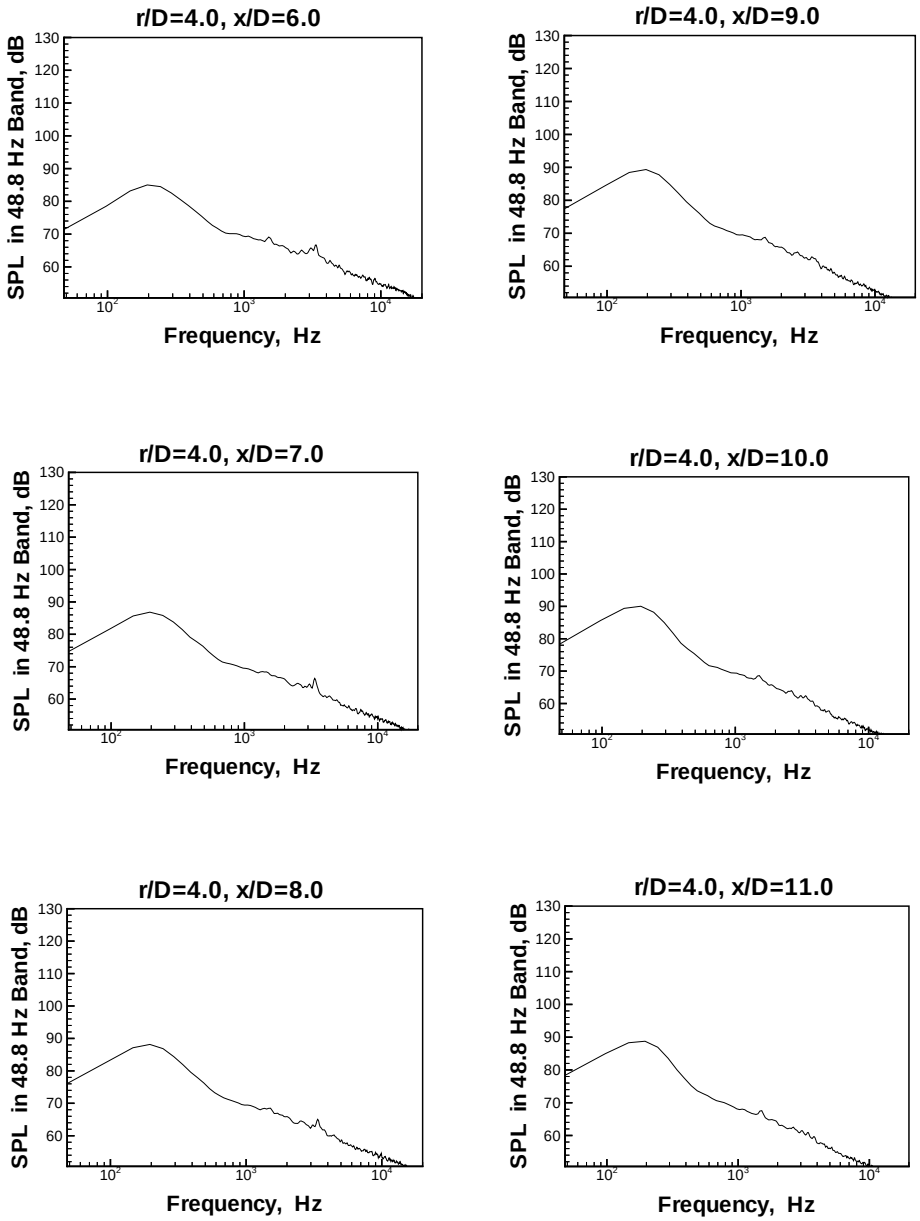

Figure 7: Near Field Pressure Spectra, Ma_e=0.30, r/D=4.0

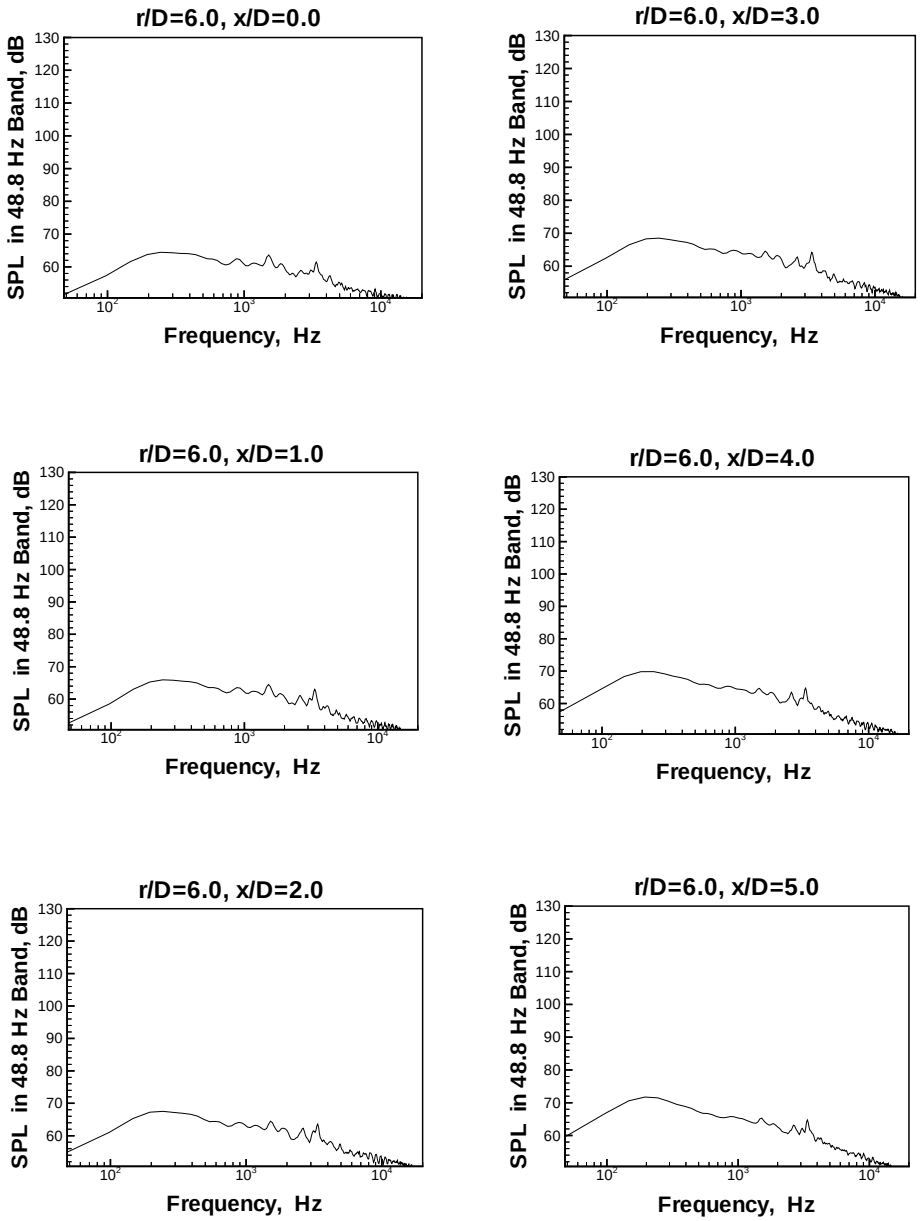

Figure 8: Near Field Pressure Spectra, Ma_e=0.30, r/D=6.0

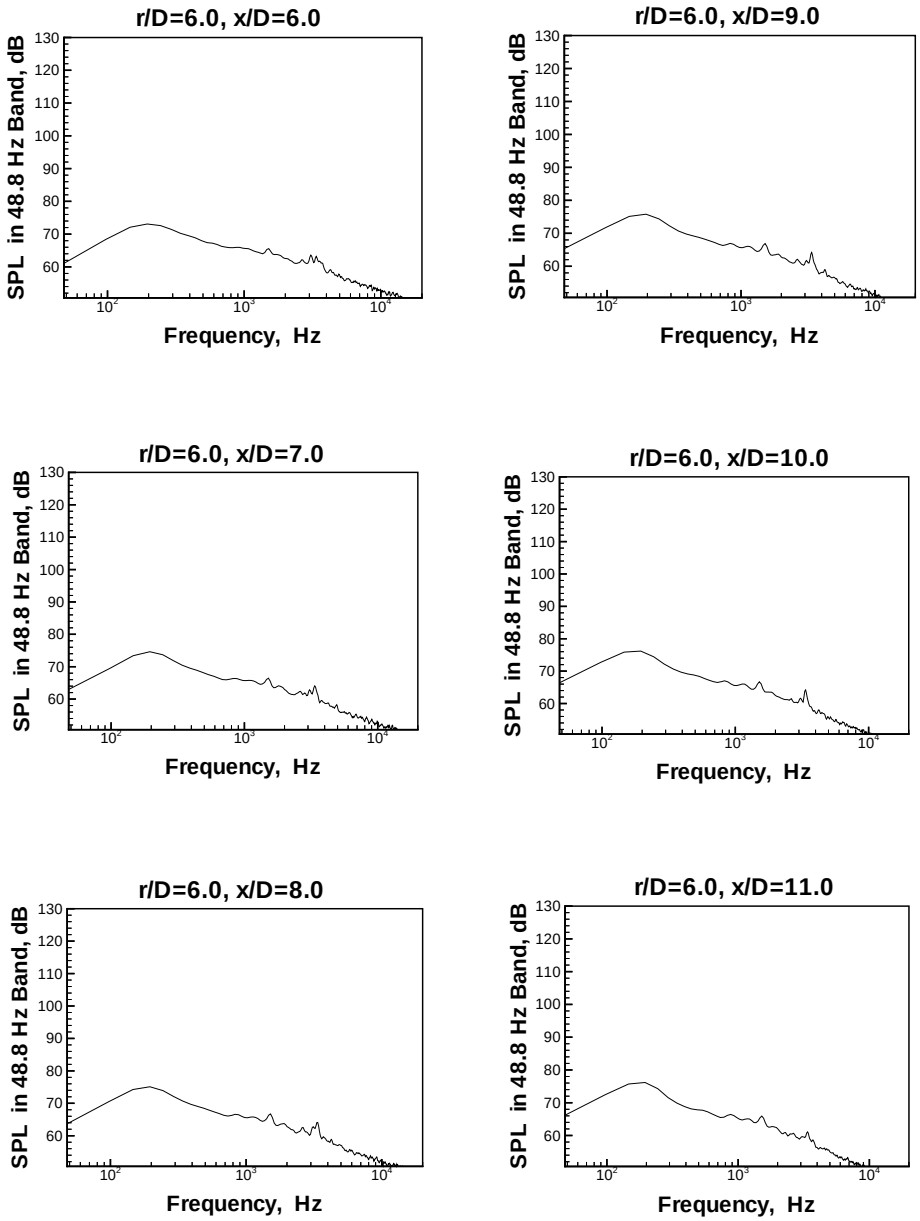

Figure 9: Near Field Pressure Spectra, Ma_e=0.30, r/D=6.0

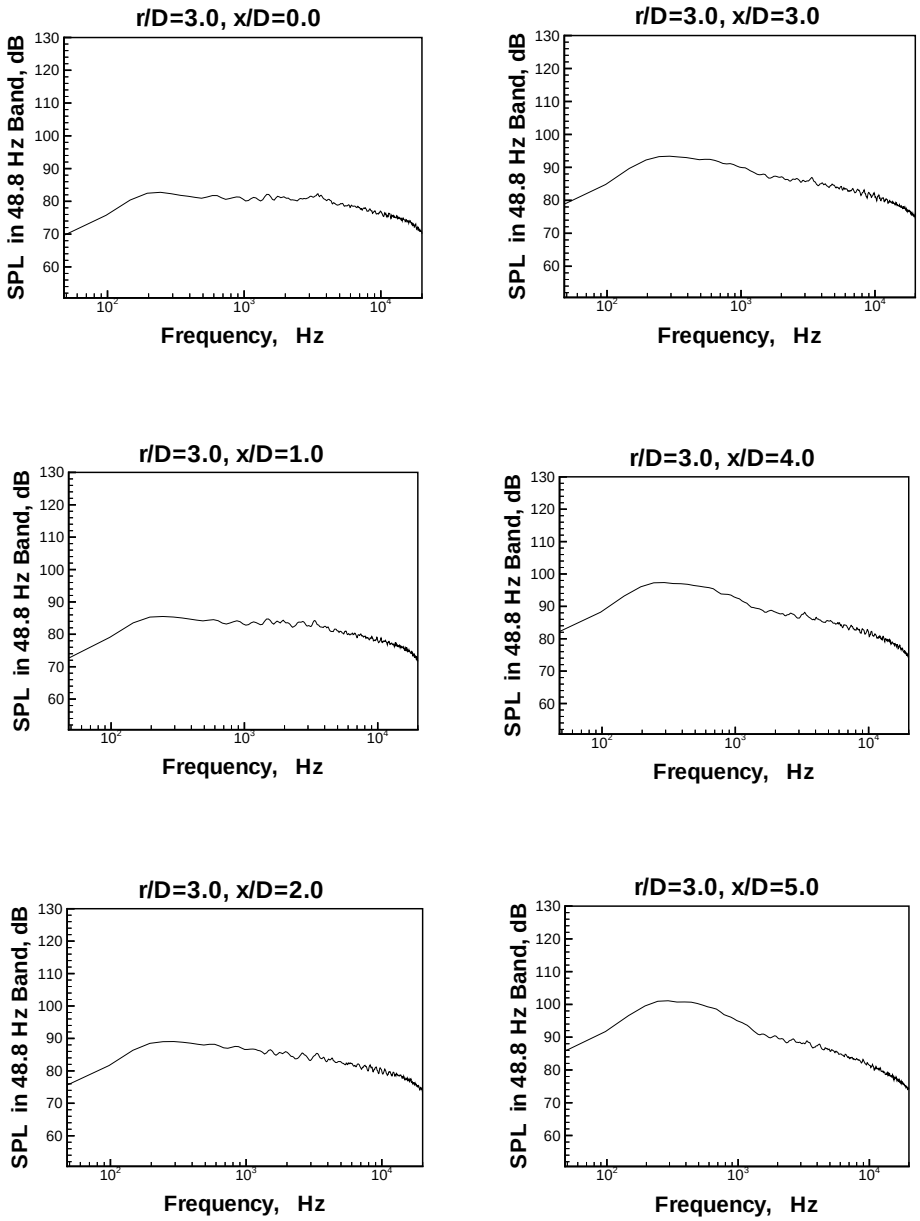

Figure 10: Near Field Pressure Spectra, Ma_e=0.60, r/D=3.0

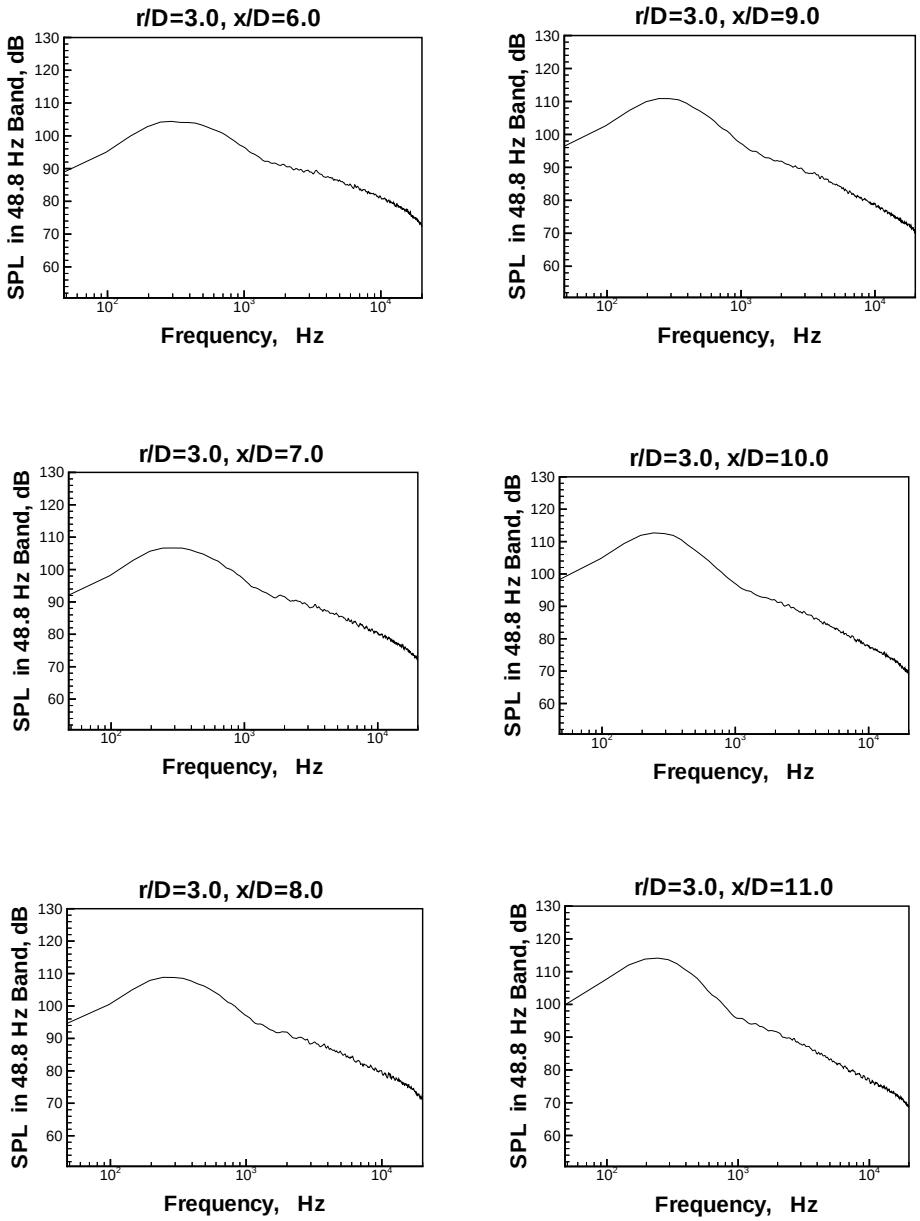

Figure 11: Near Field Pressure Spectra, Ma_e=0.60, r/D=3.0

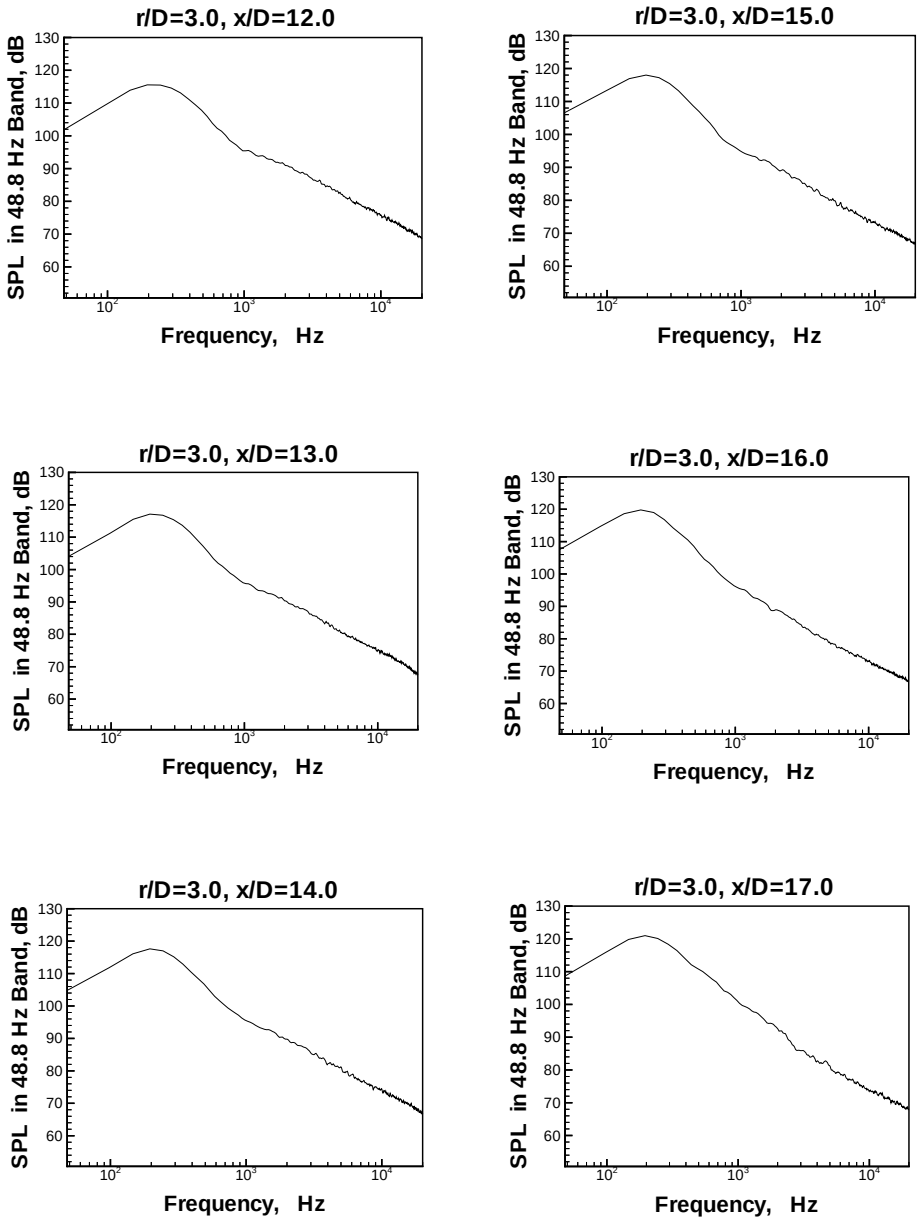

Figure 12: Near Field Pressure Spectra, Ma_e=0.60, r/D=3.0

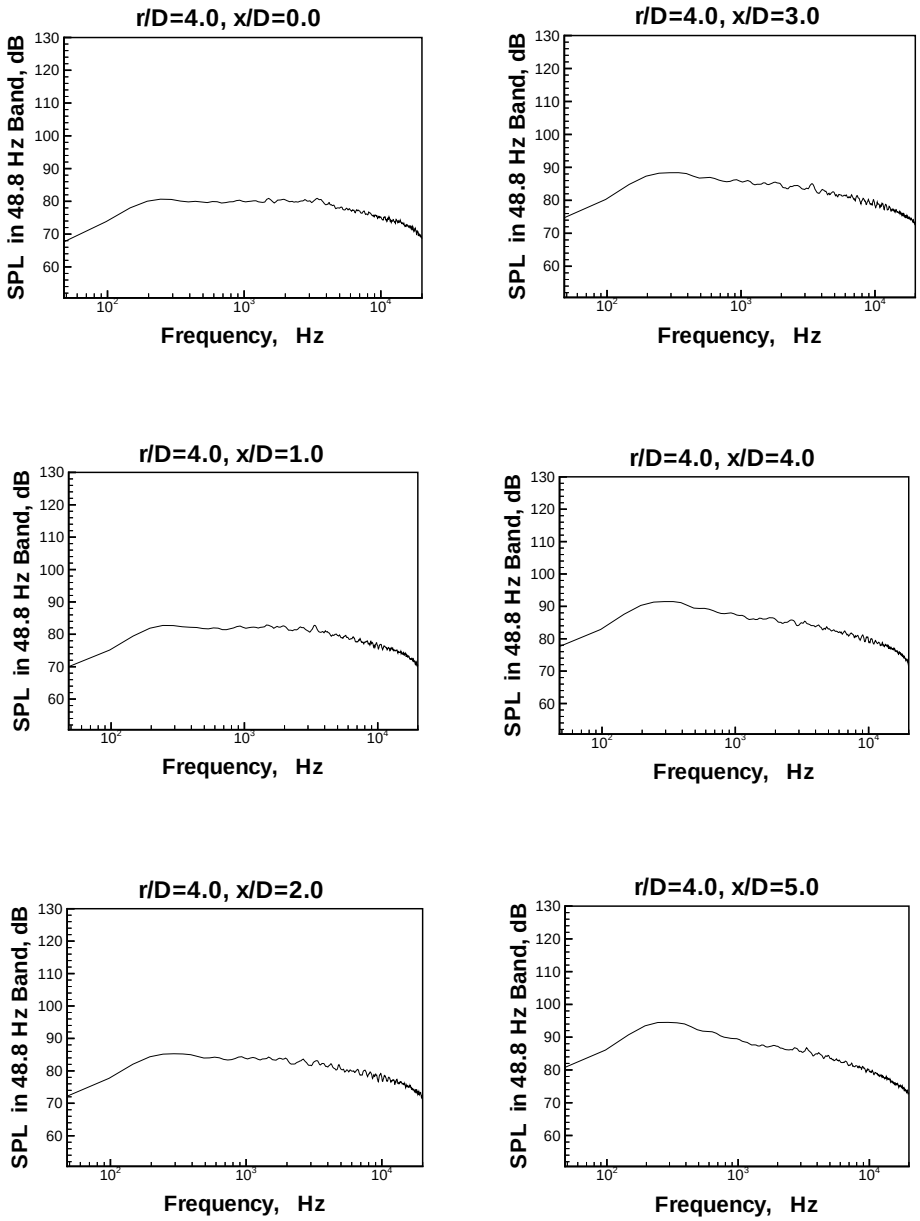

Figure 13: Near Field Pressure Spectra, Ma_e=0.60, r/D=4.0

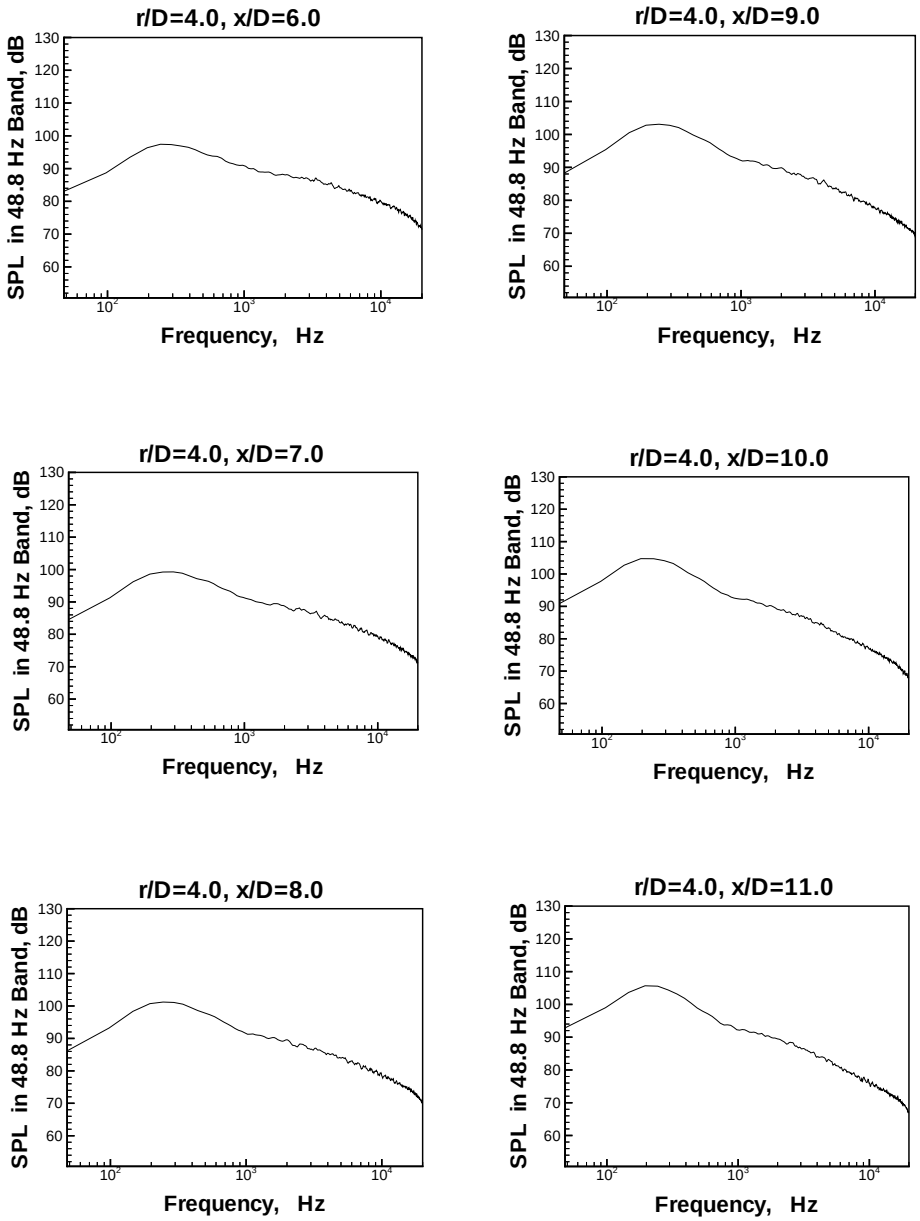

Figure 14: Near Field Pressure Spectra, Ma_e=0.60, r/D=4.0

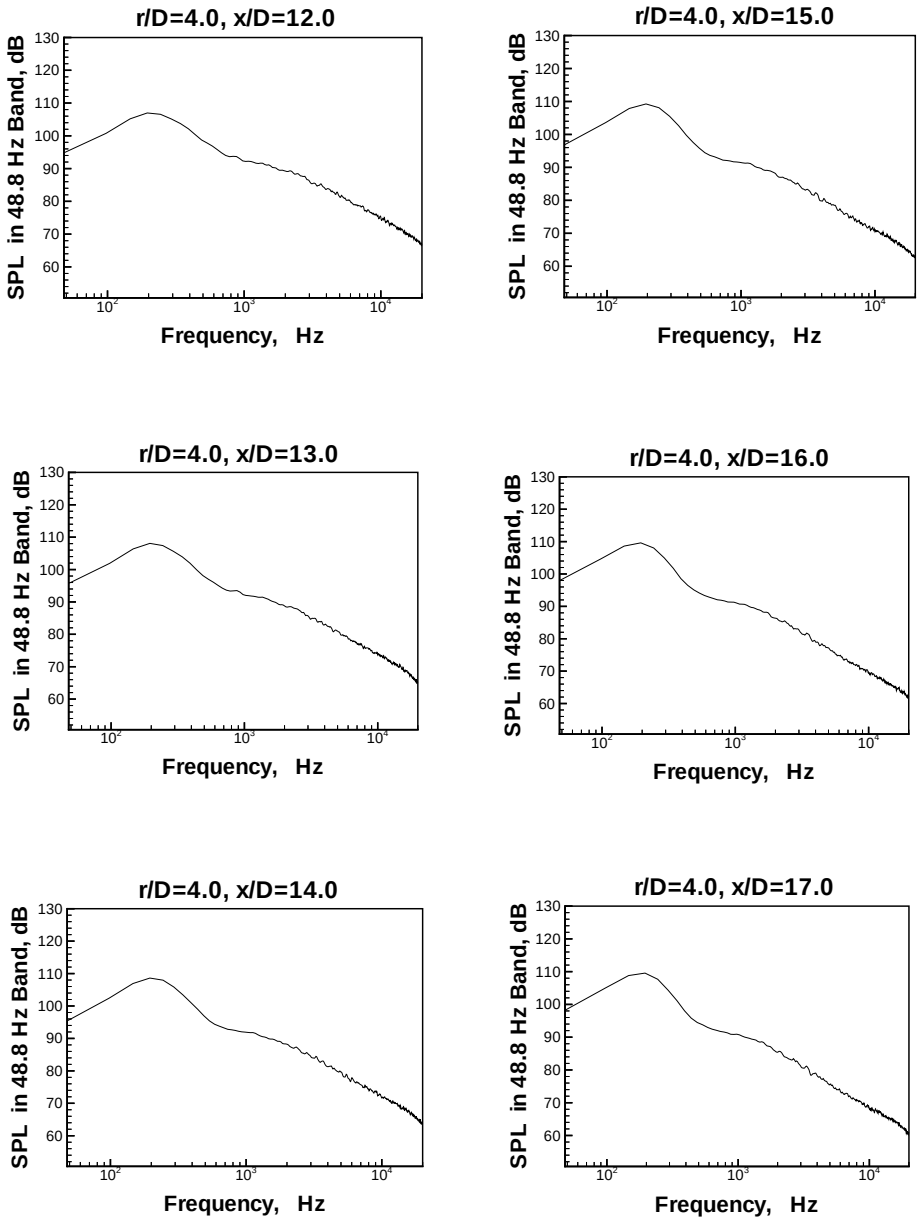

Figure 15: Near Field Pressure Spectra, Ma_e=0.60, r/D=4.0

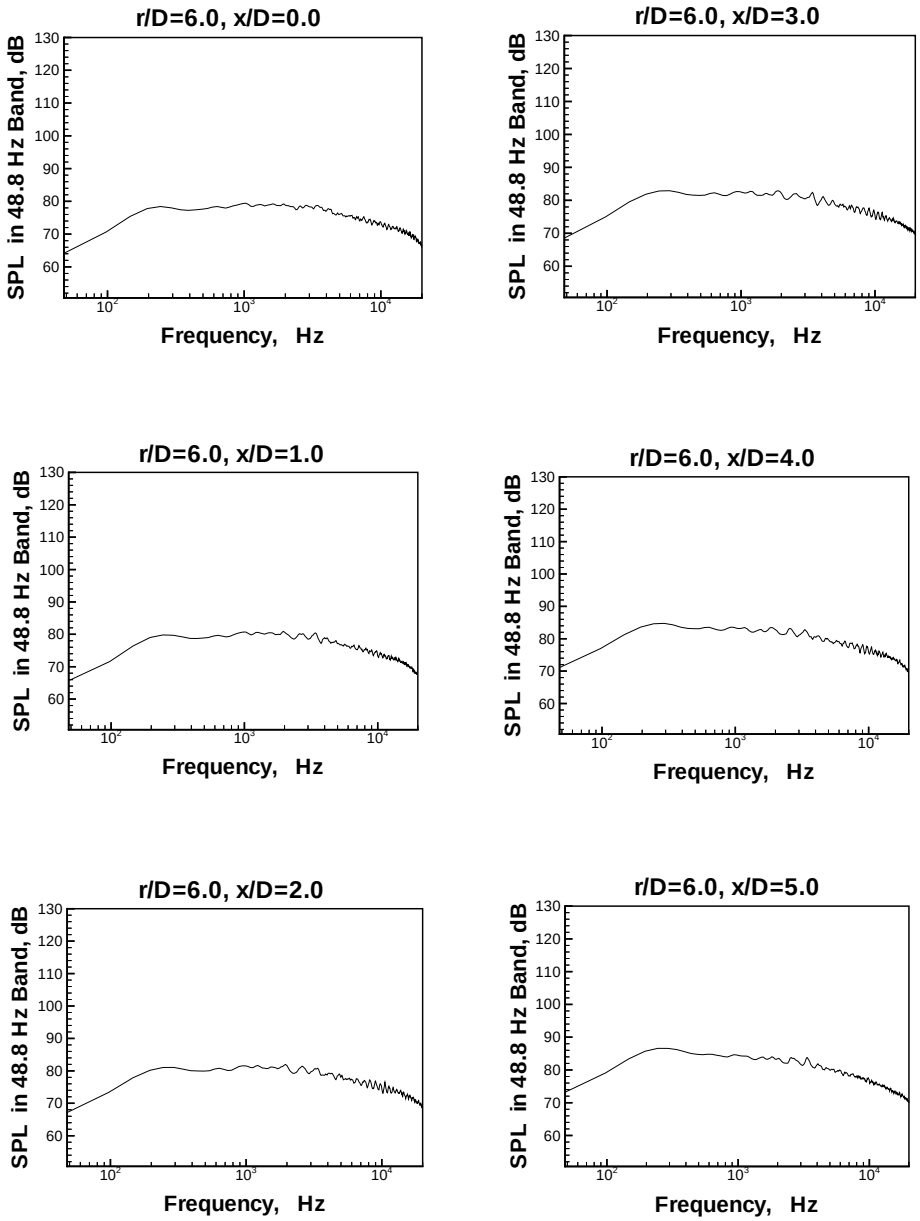

Figure 16: Near Field Pressure Spectra, Ma_e=0.60, r/D=6.0

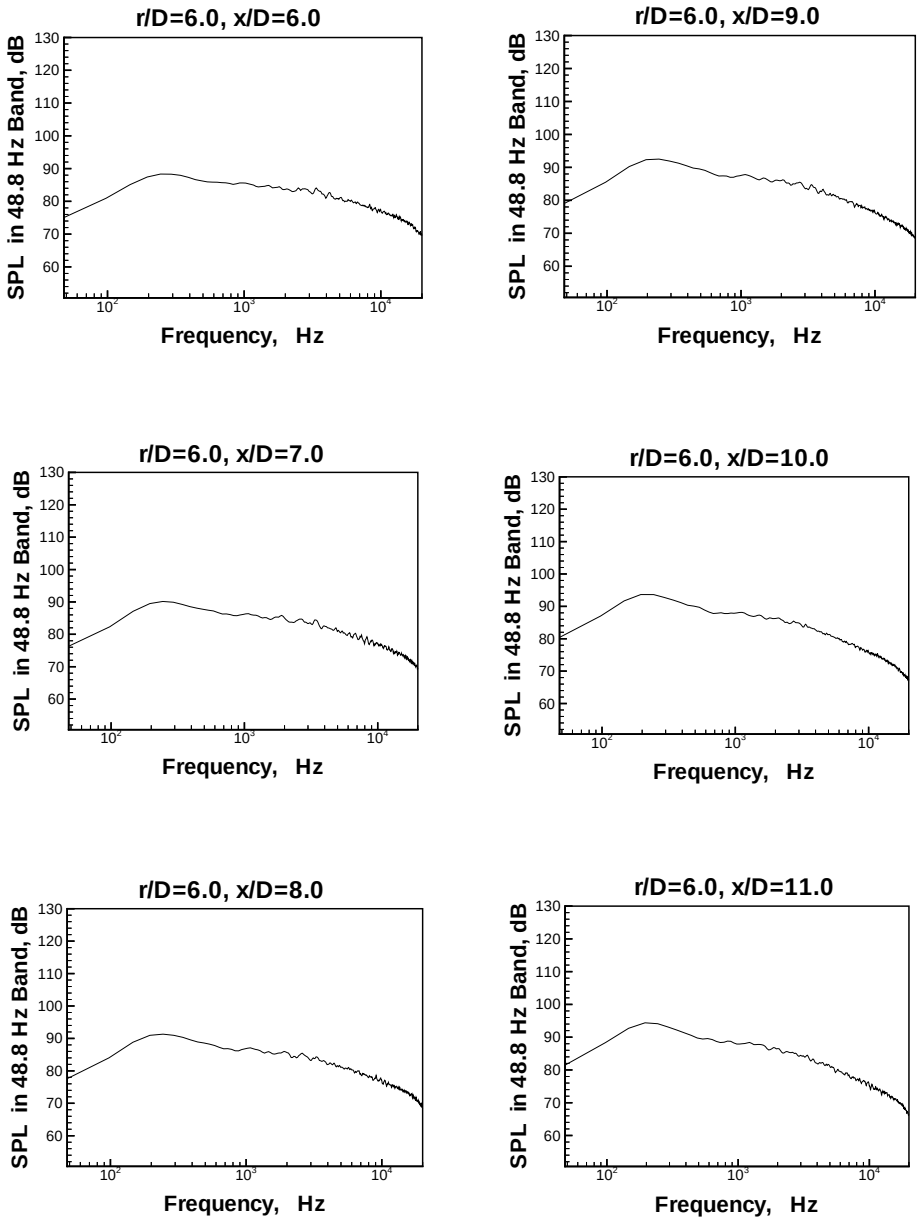

Figure 17: Near Field Pressure Spectra, Ma_e=0.60, r/D=6.0

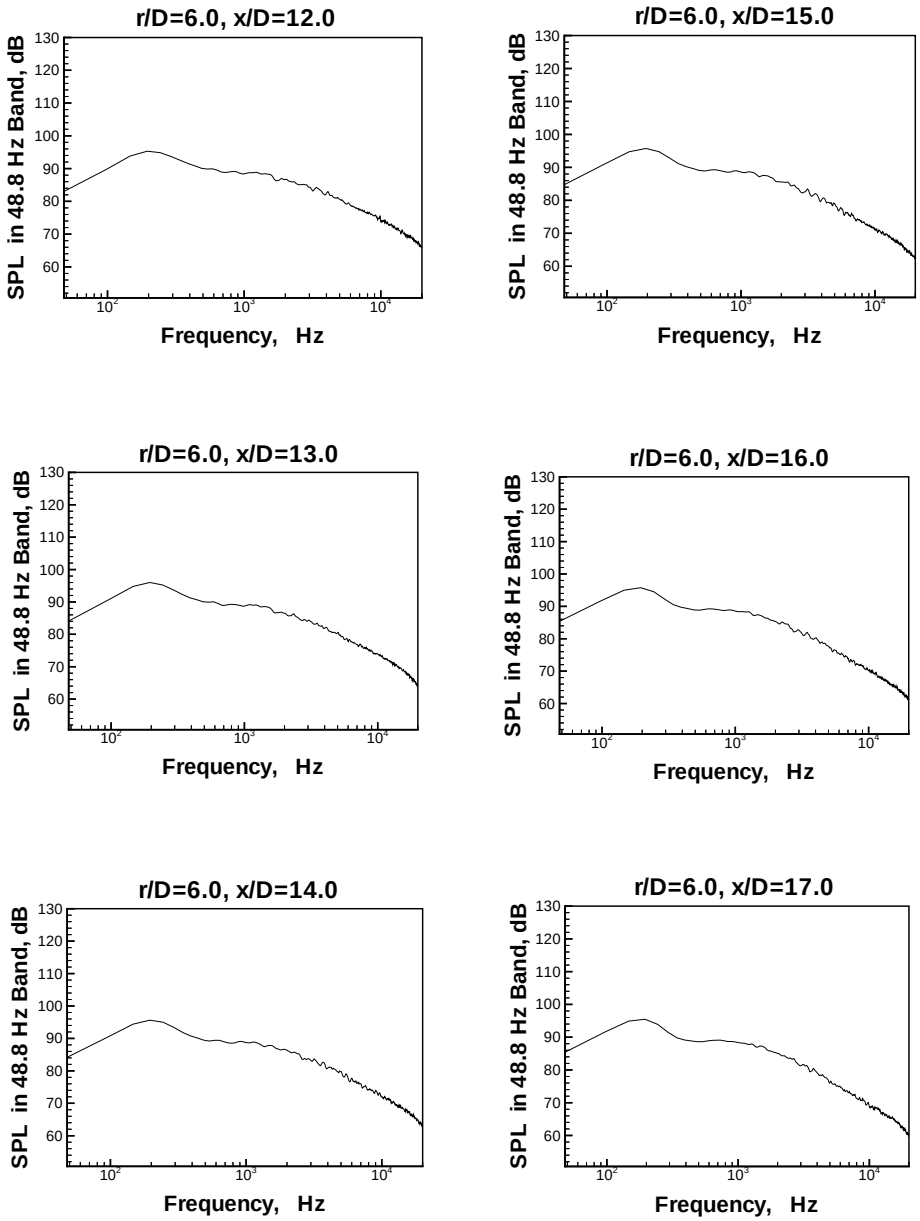

Figure 18: Near Field Pressure Spectra, Ma_e=0.60, r/D=6.0

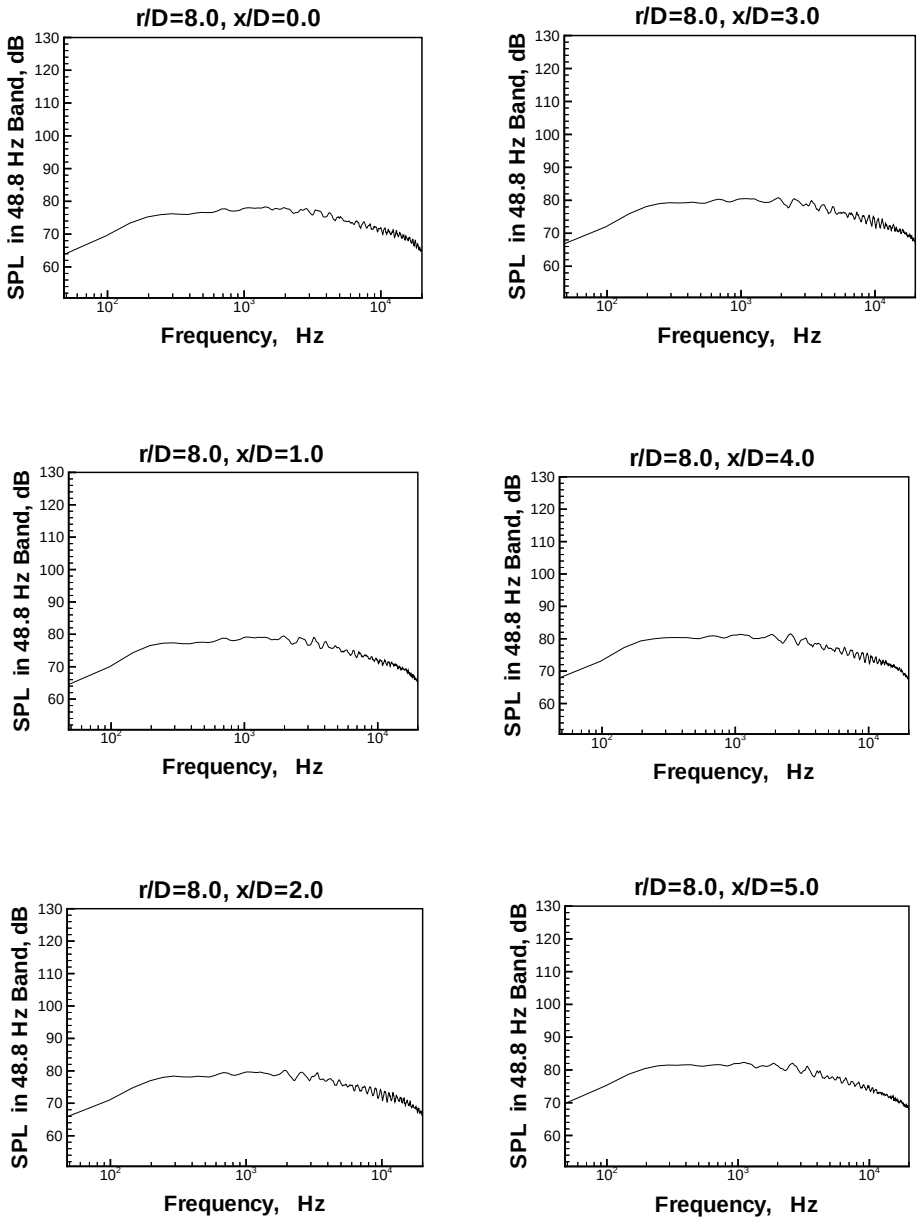

Figure 19: Near Field Pressure Spectra, Ma_e=0.60, r/D=8.0

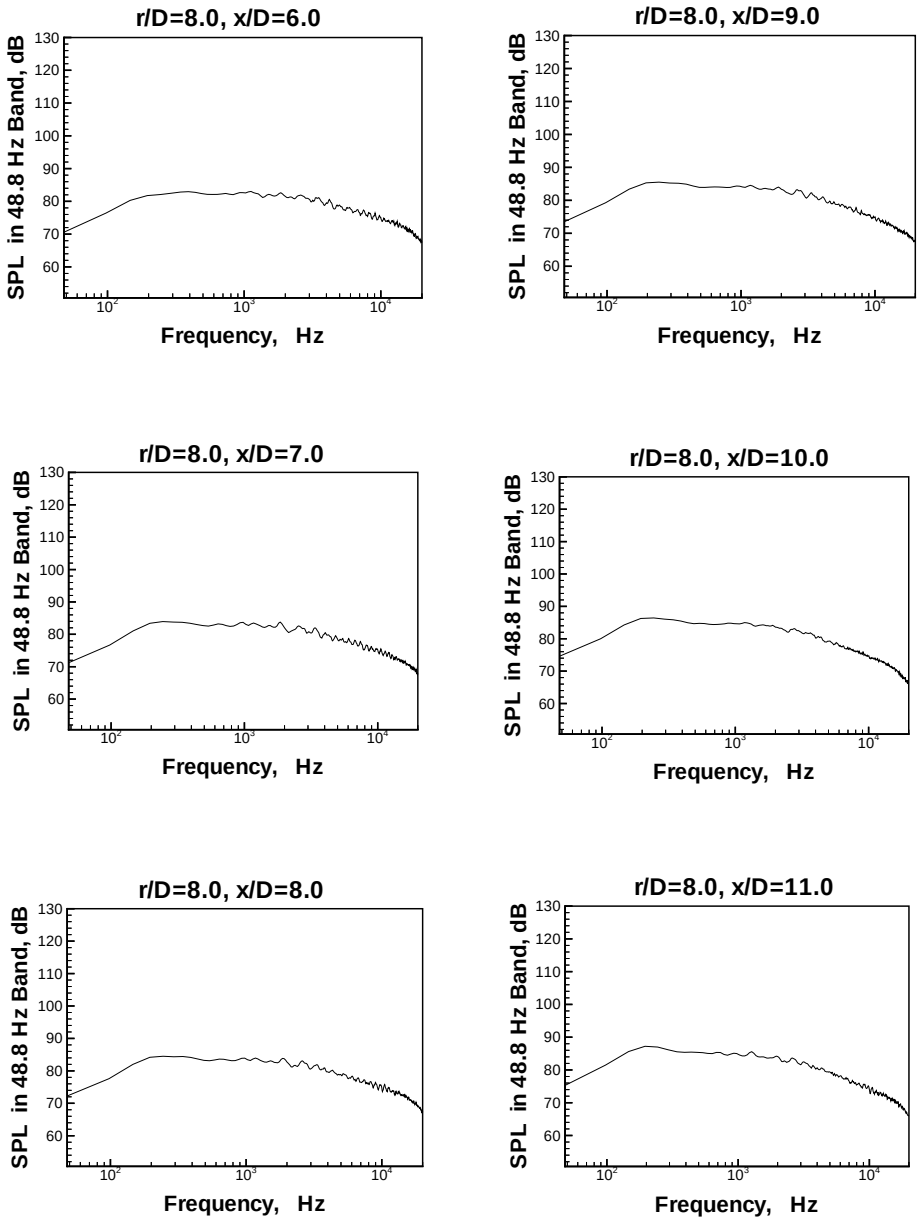

Figure 20: Near Field Pressure Spectra, Ma_e=0.60, r/D=8.0

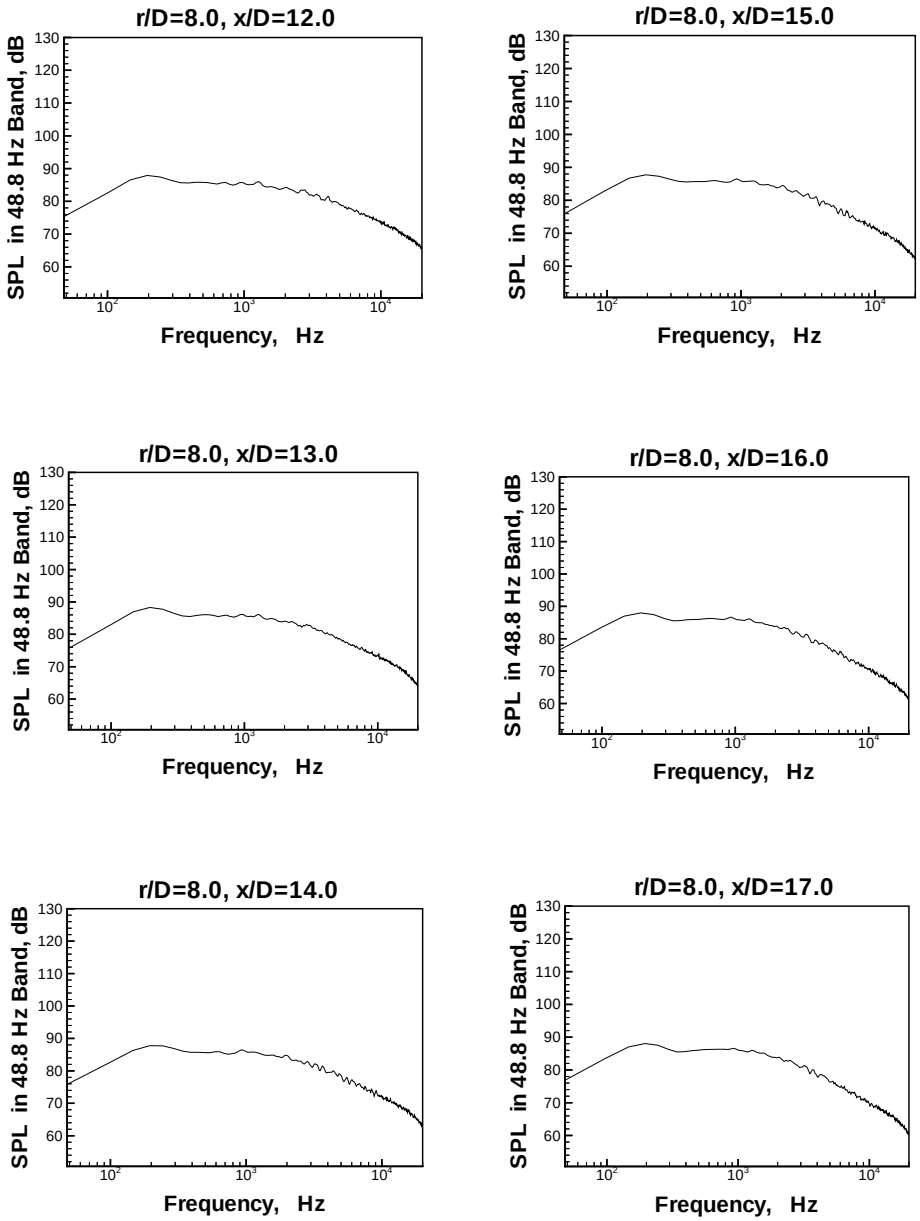

Figure 21: Near Field Pressure Spectra, Ma_e=0.60, r/D=8.0

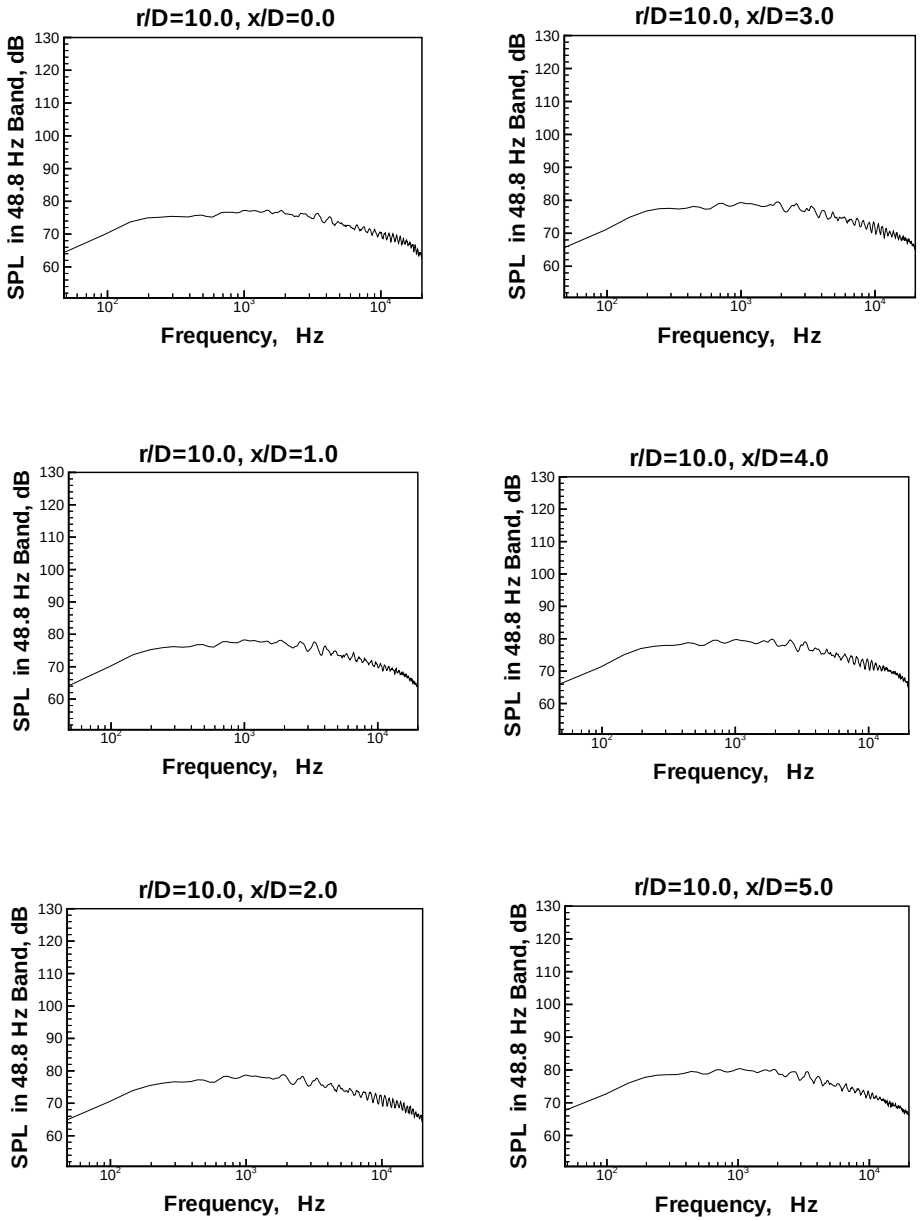

Figure 22: Near Field Pressure Spectra, Ma_e=0.60, r/D=10.0

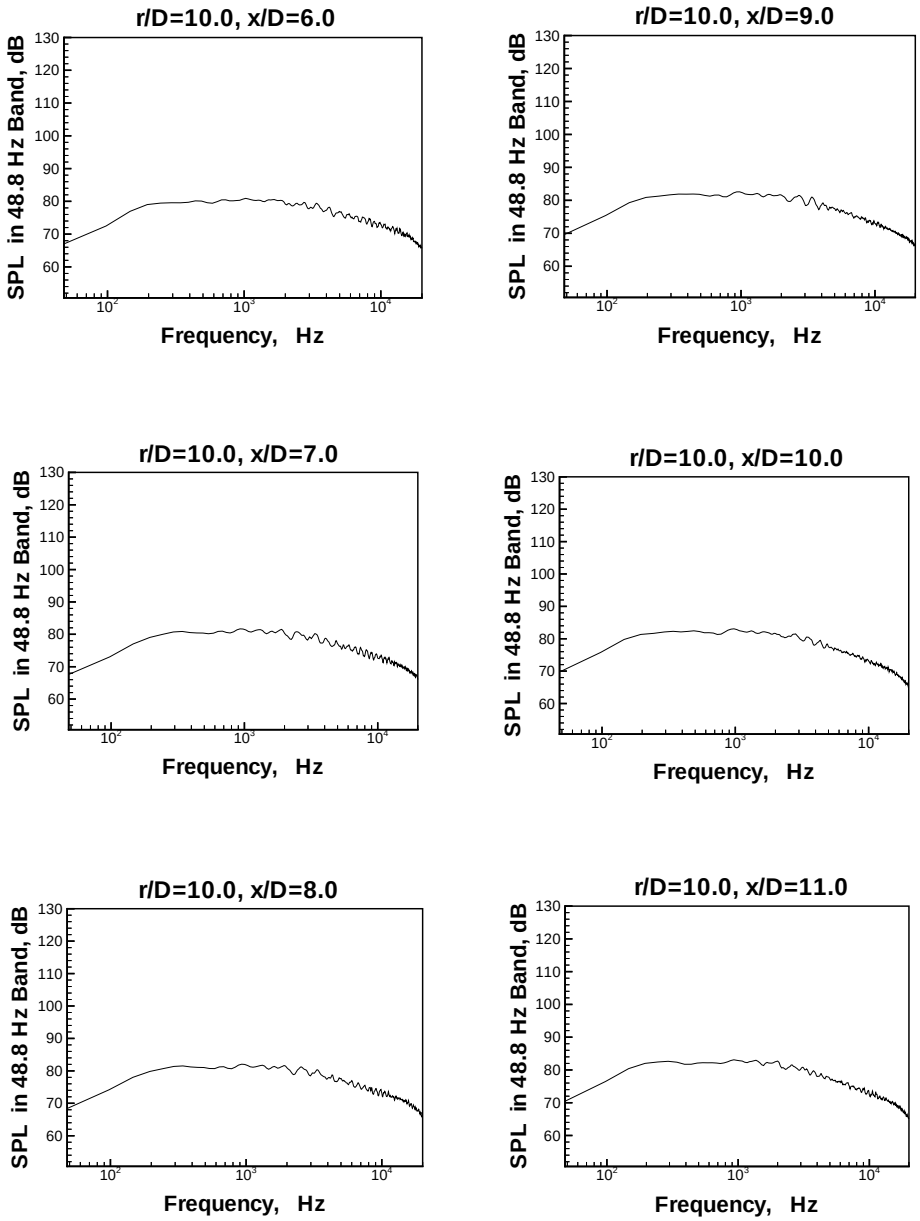

Figure 23: Near Field Pressure Spectra, Ma_e=0.60, r/D=10.0

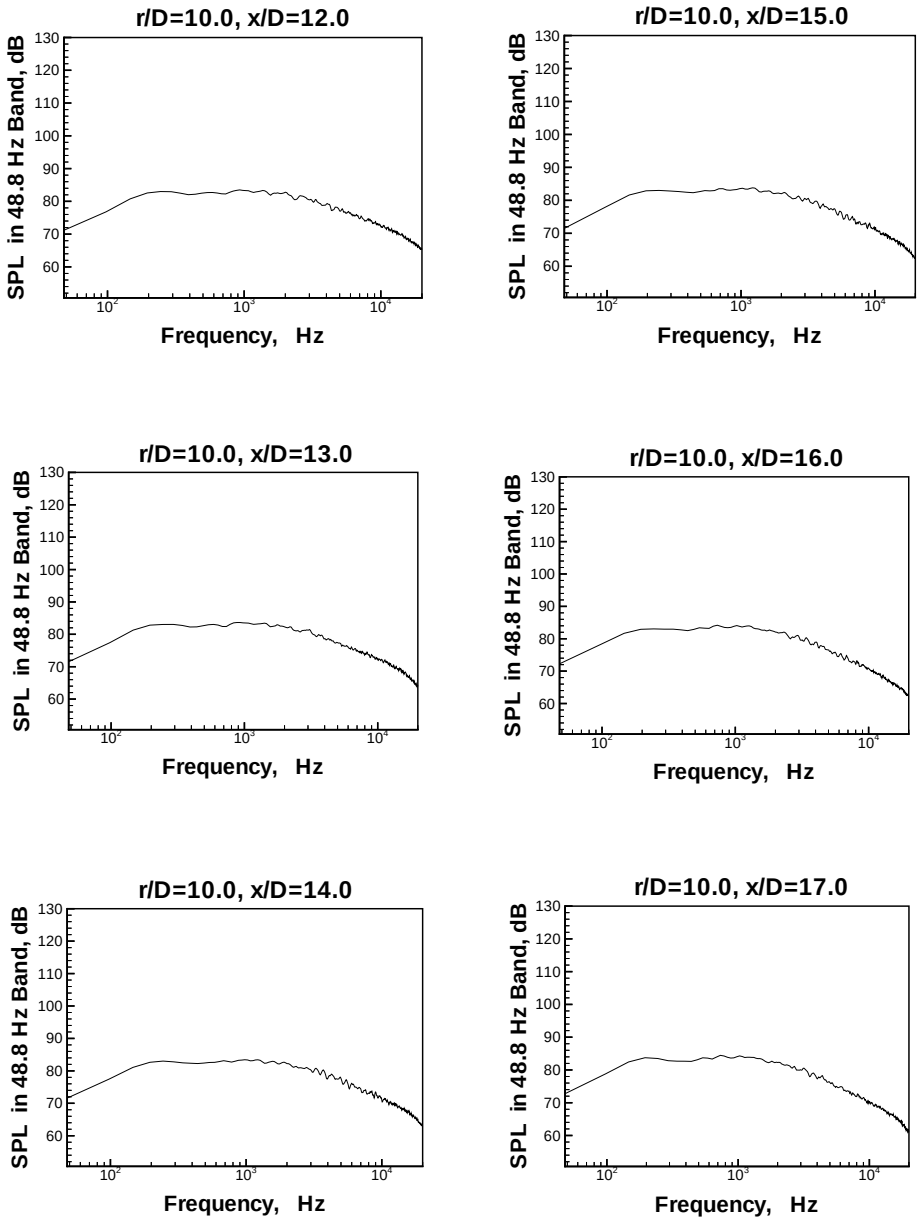

Figure 24: Near Field Pressure Spectra, Ma_e=0.60, r/D=10.0

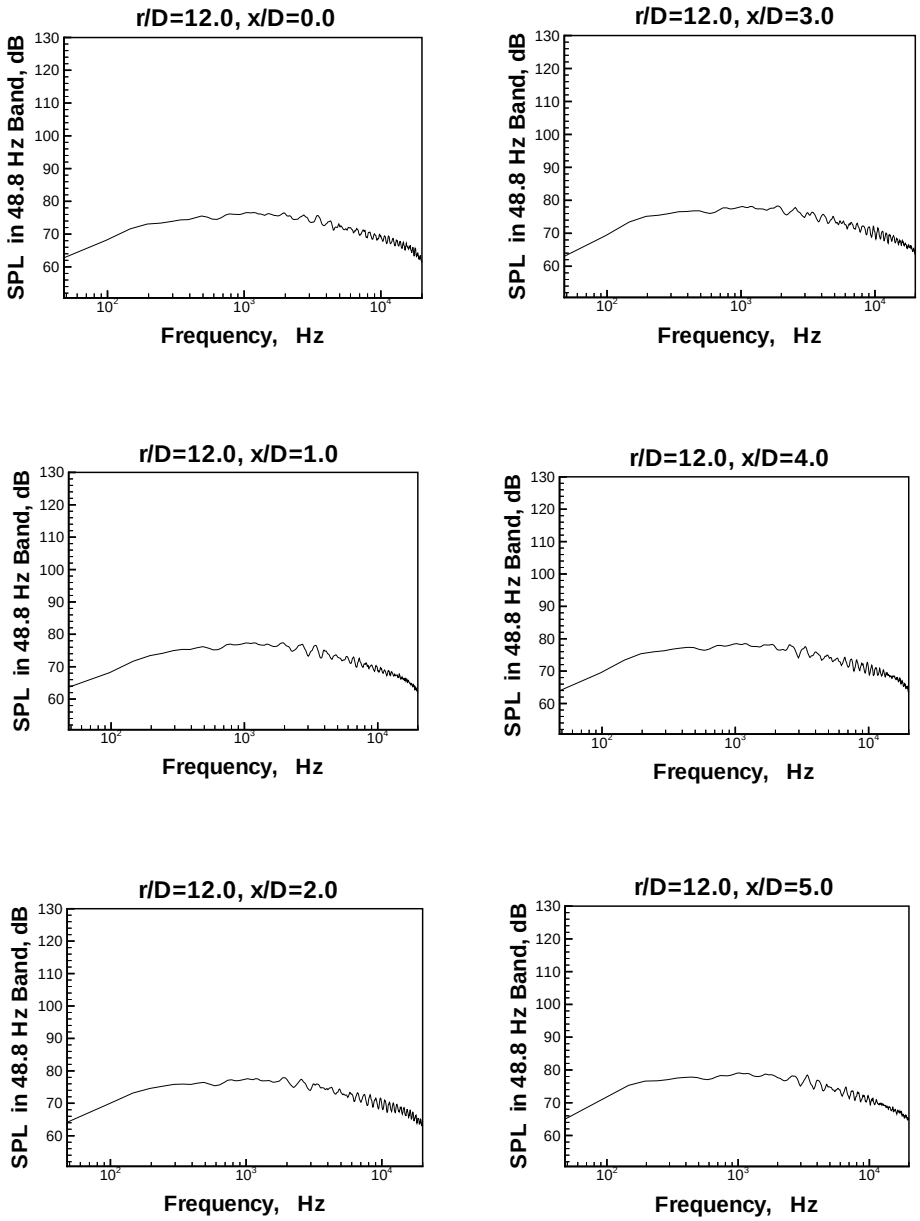

Figure 25: Near Field Pressure Spectra, Ma_e=0.60, r/D=12.0

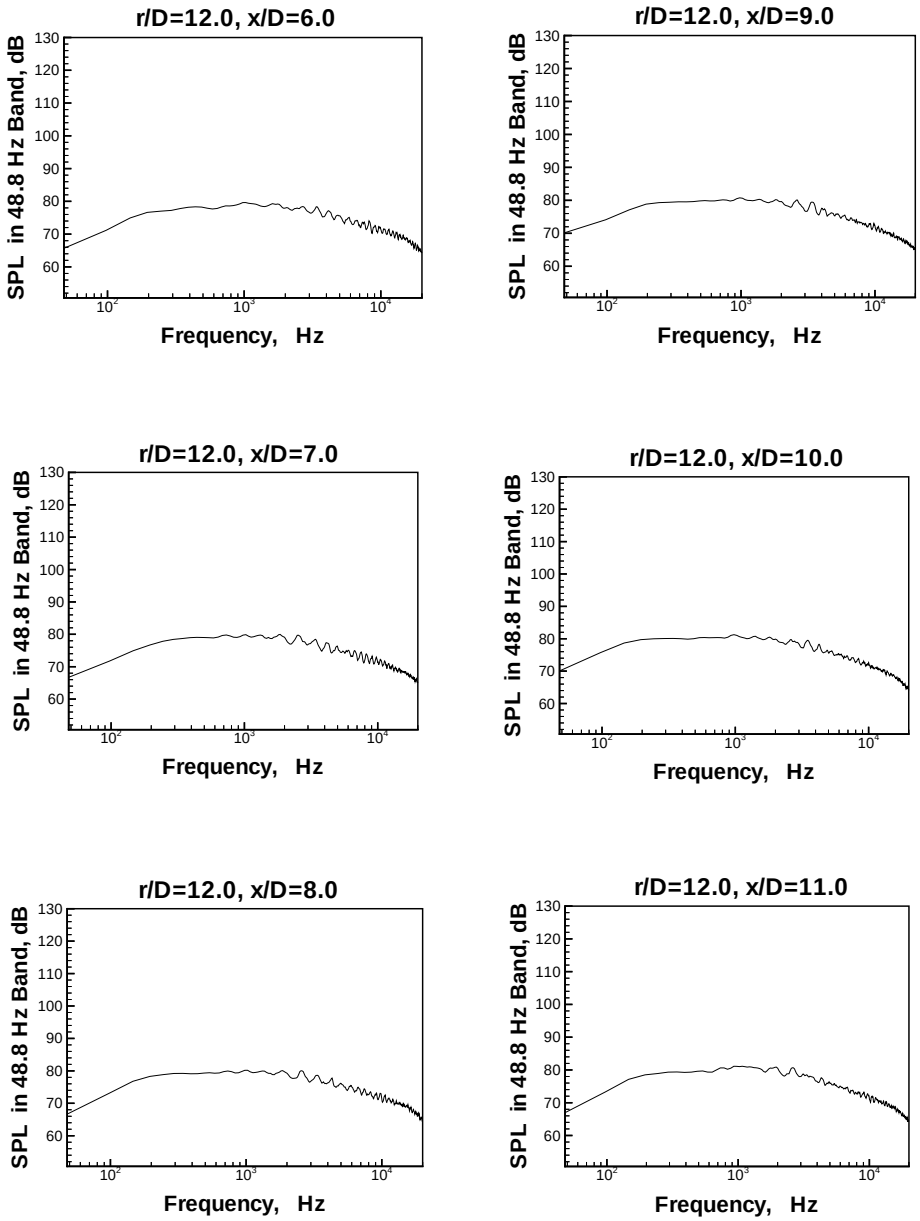

Figure 26: Near Field Pressure Spectra, Ma_e=0.60, r/D=12.0

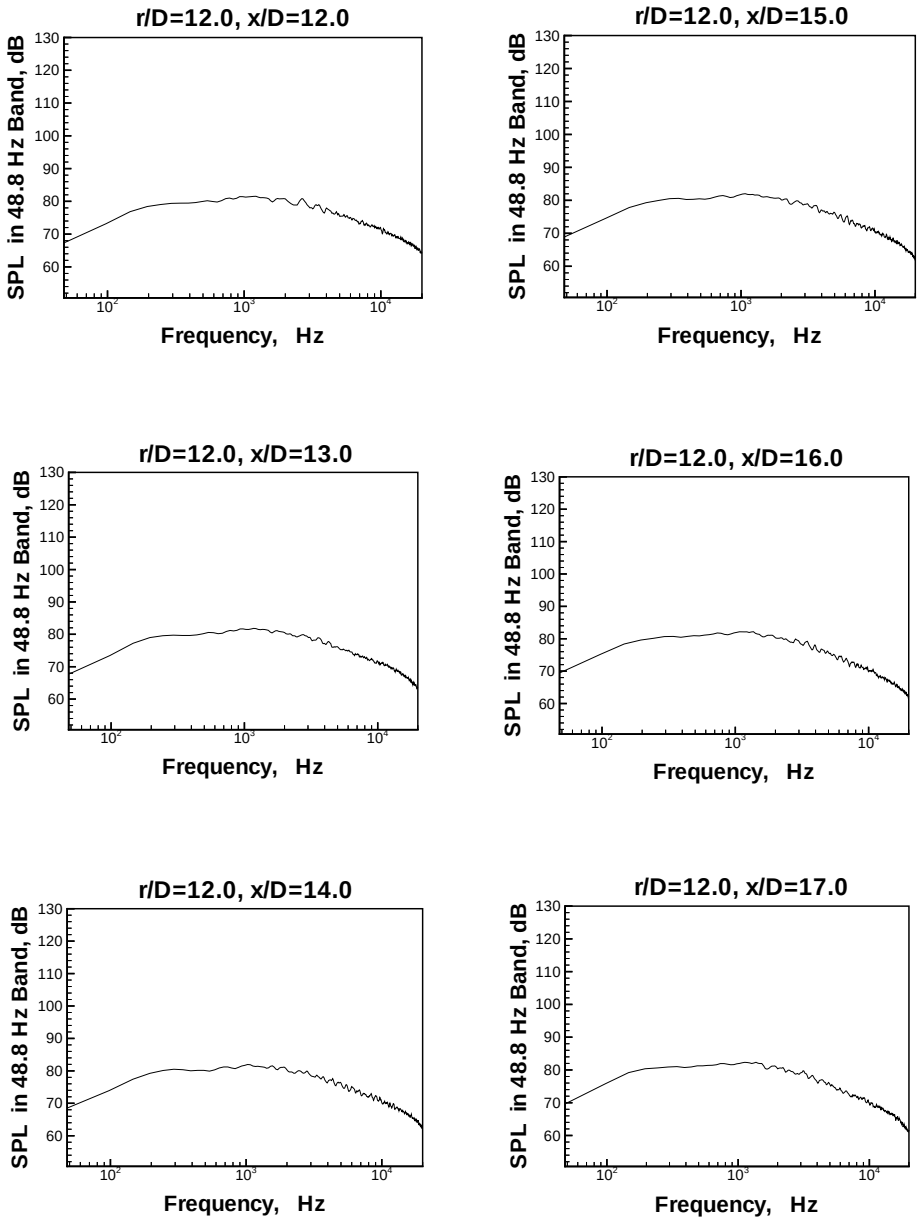

Figure 27: Near Field Pressure Spectra, Ma_e=0.60, r/D=12.0

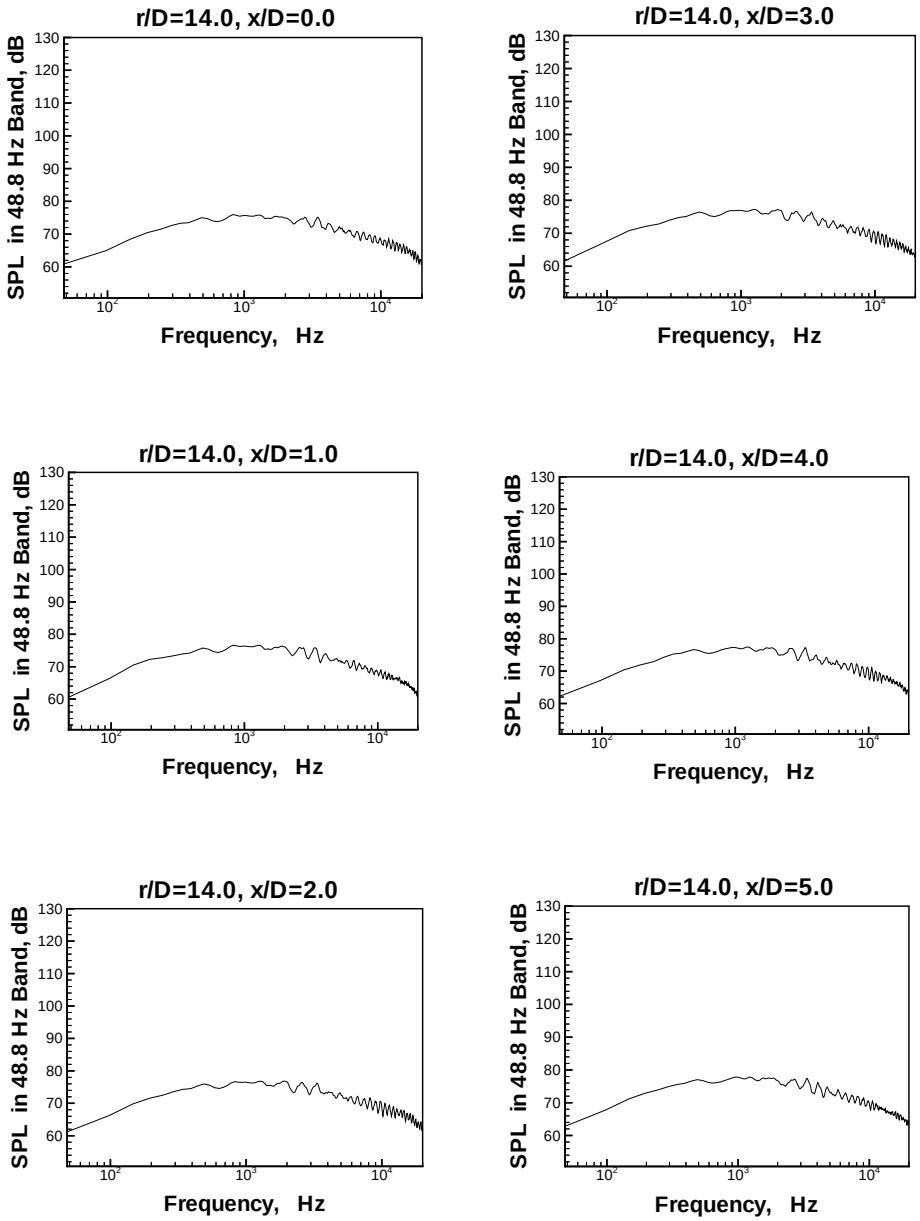

Figure 28: Near Field Pressure Spectra, Ma_e=0.60, r/D=14.0

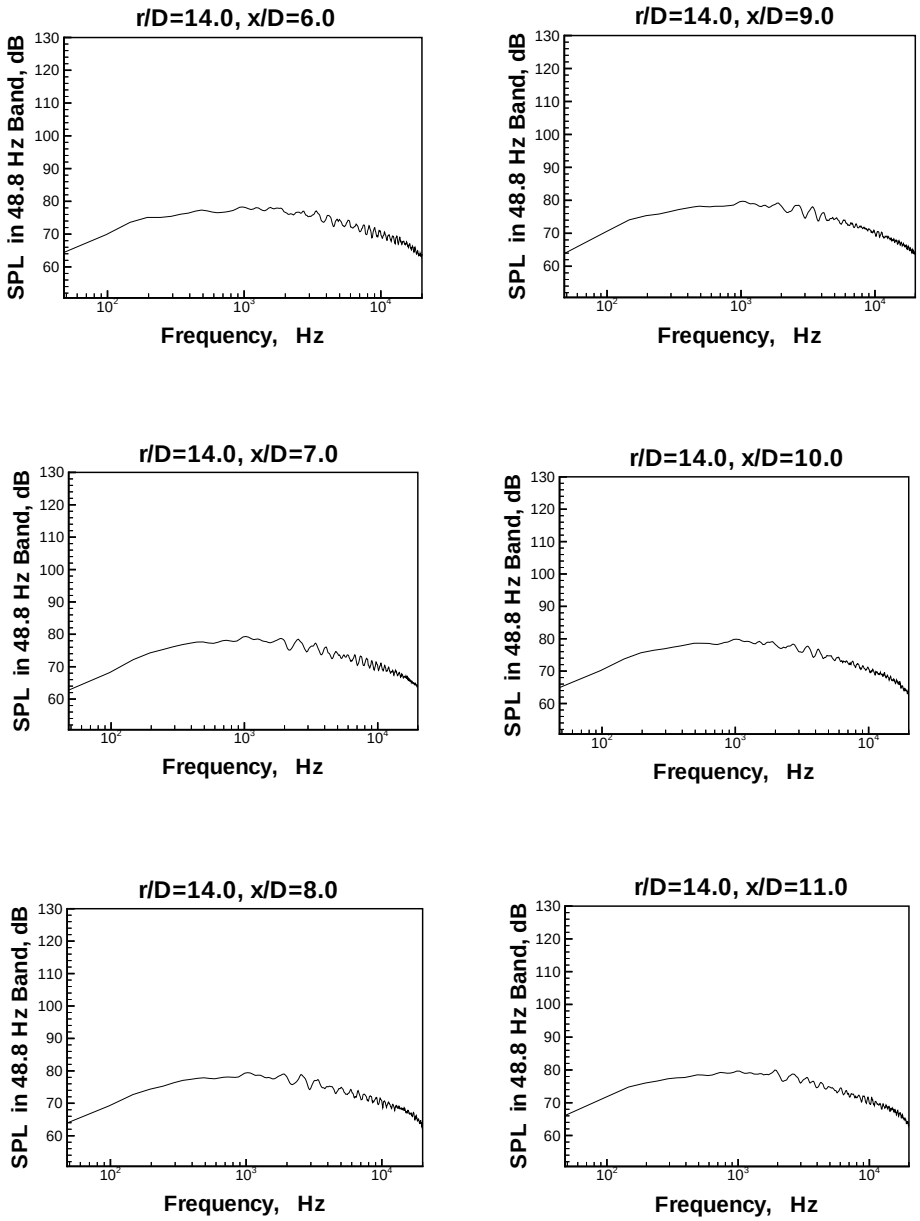

Figure 29: Near Field Pressure Spectra, Ma_e=0.60, r/D=14.0

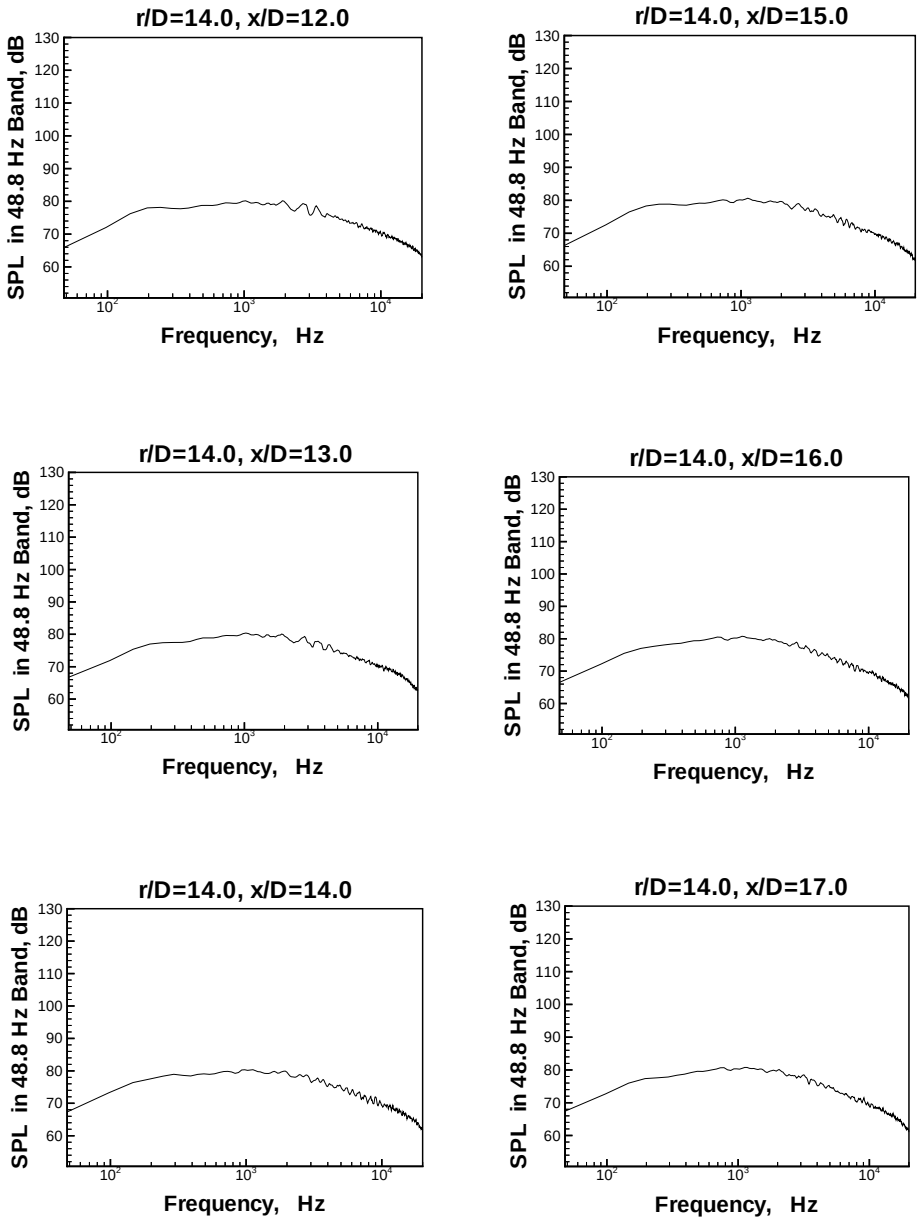

Figure 30: Near Field Pressure Spectra, Ma_e=0.60, r/D=14.0

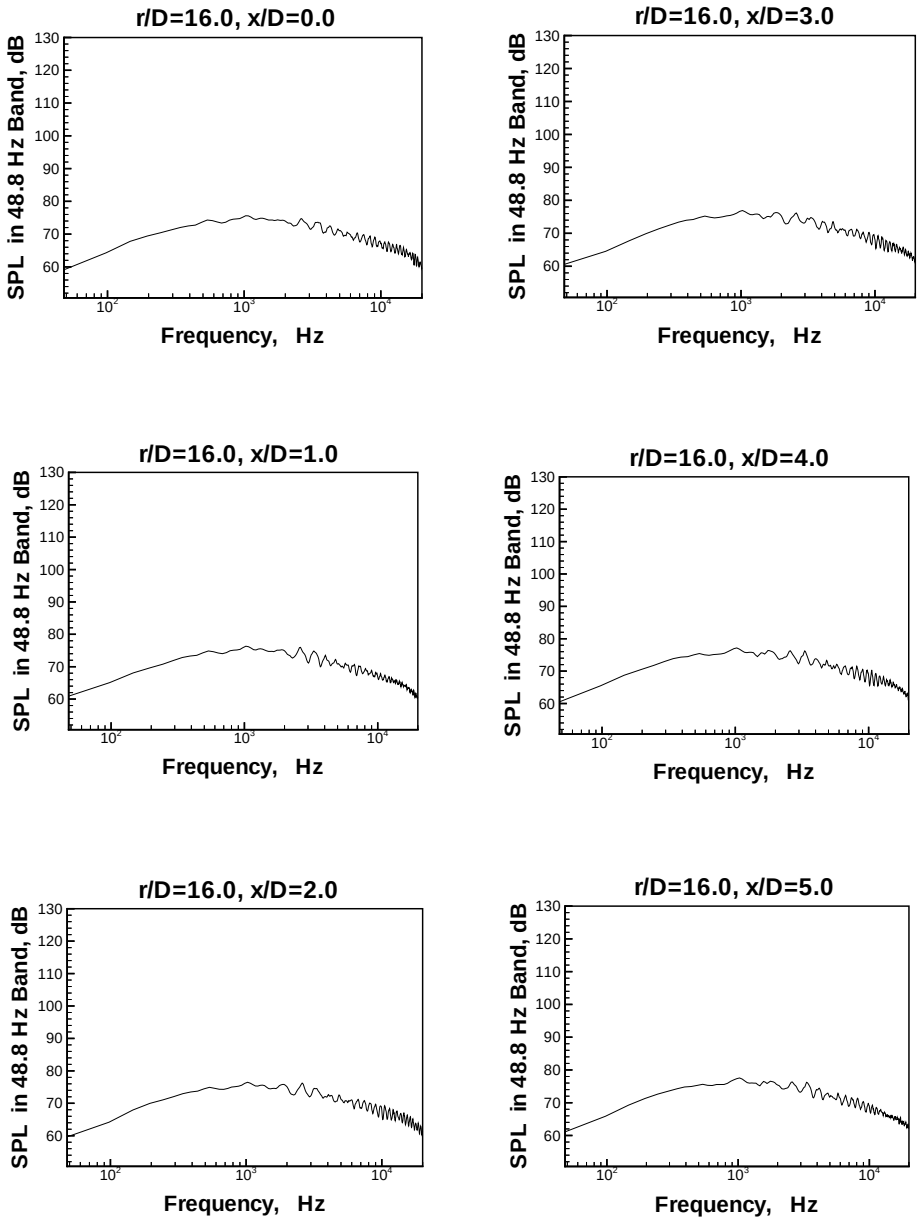

Figure 31: Near Field Pressure Spectra, Ma_e=0.60, r/D=16.0

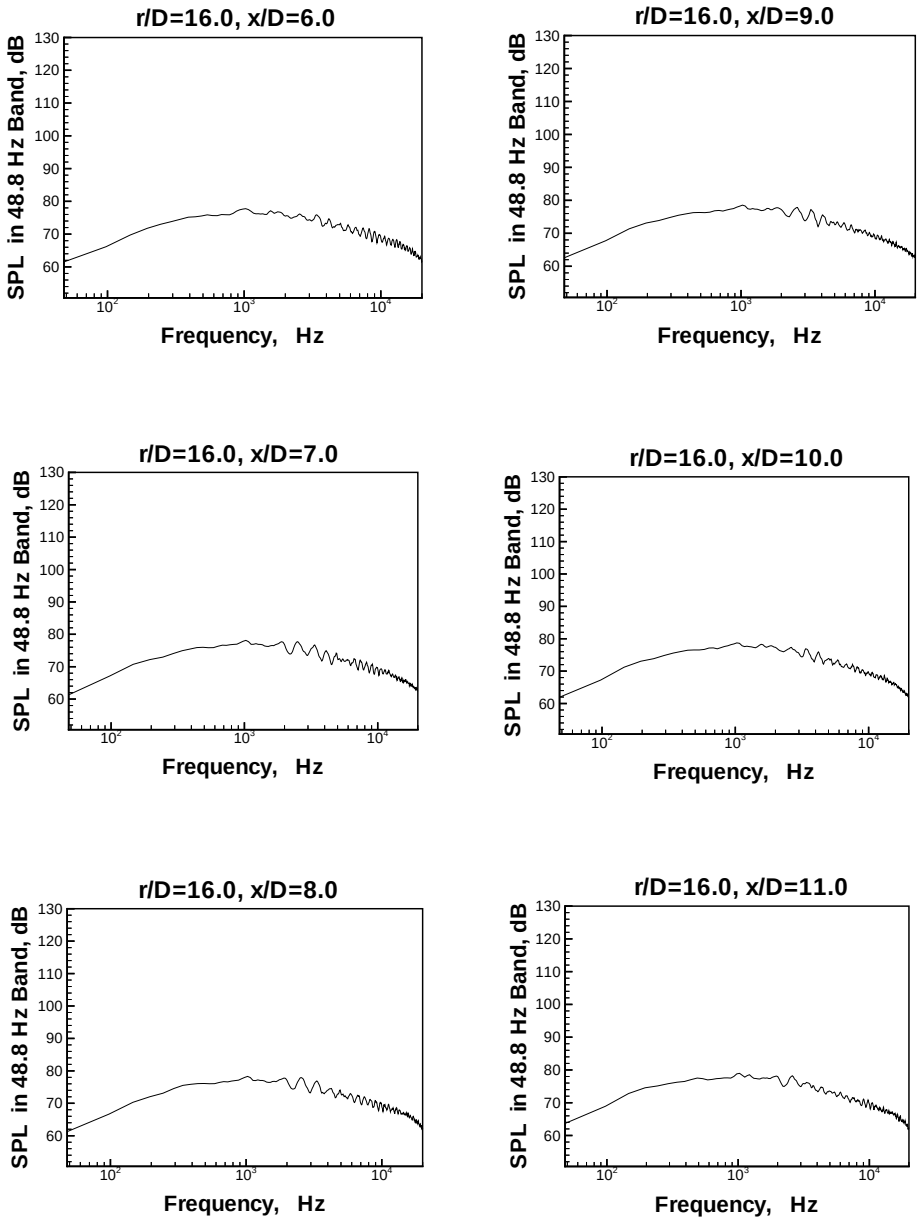

Figure 32: Near Field Pressure Spectra, Ma_e=0.60, r/D=16.0

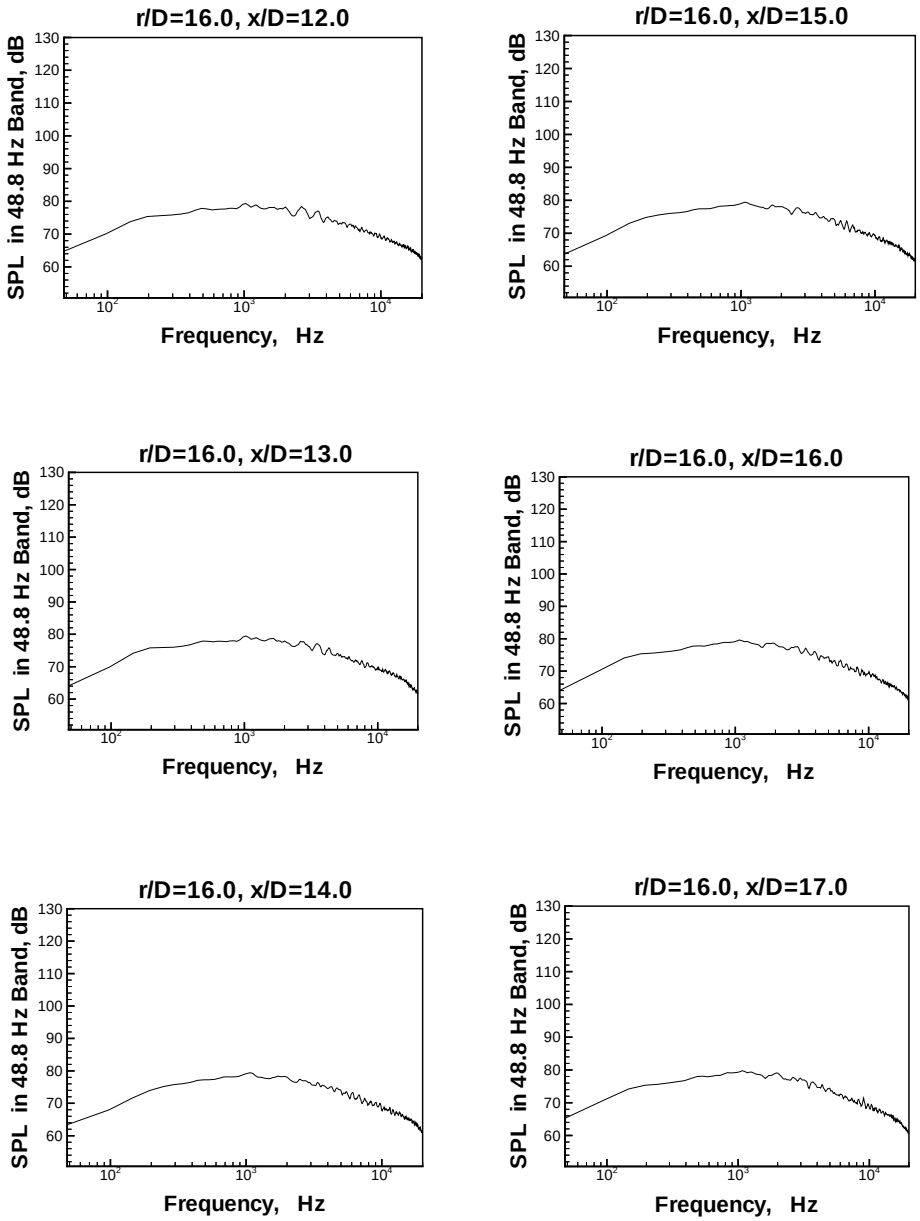

Figure 33: Near Field Pressure Spectra, Ma_e=0.60, r/D=16.0

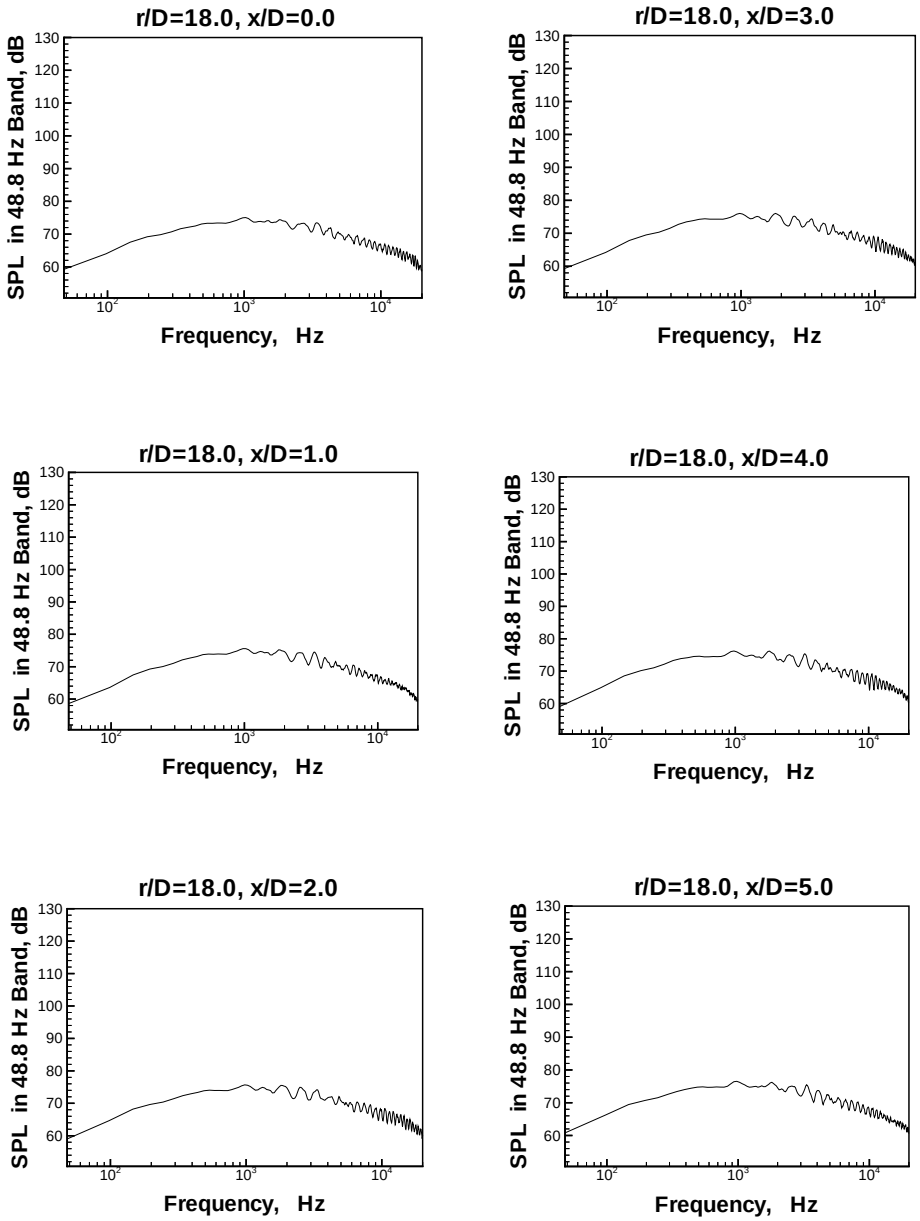

Figure 34: Near Field Pressure Spectra, Ma_e=0.60, r/D=18.0

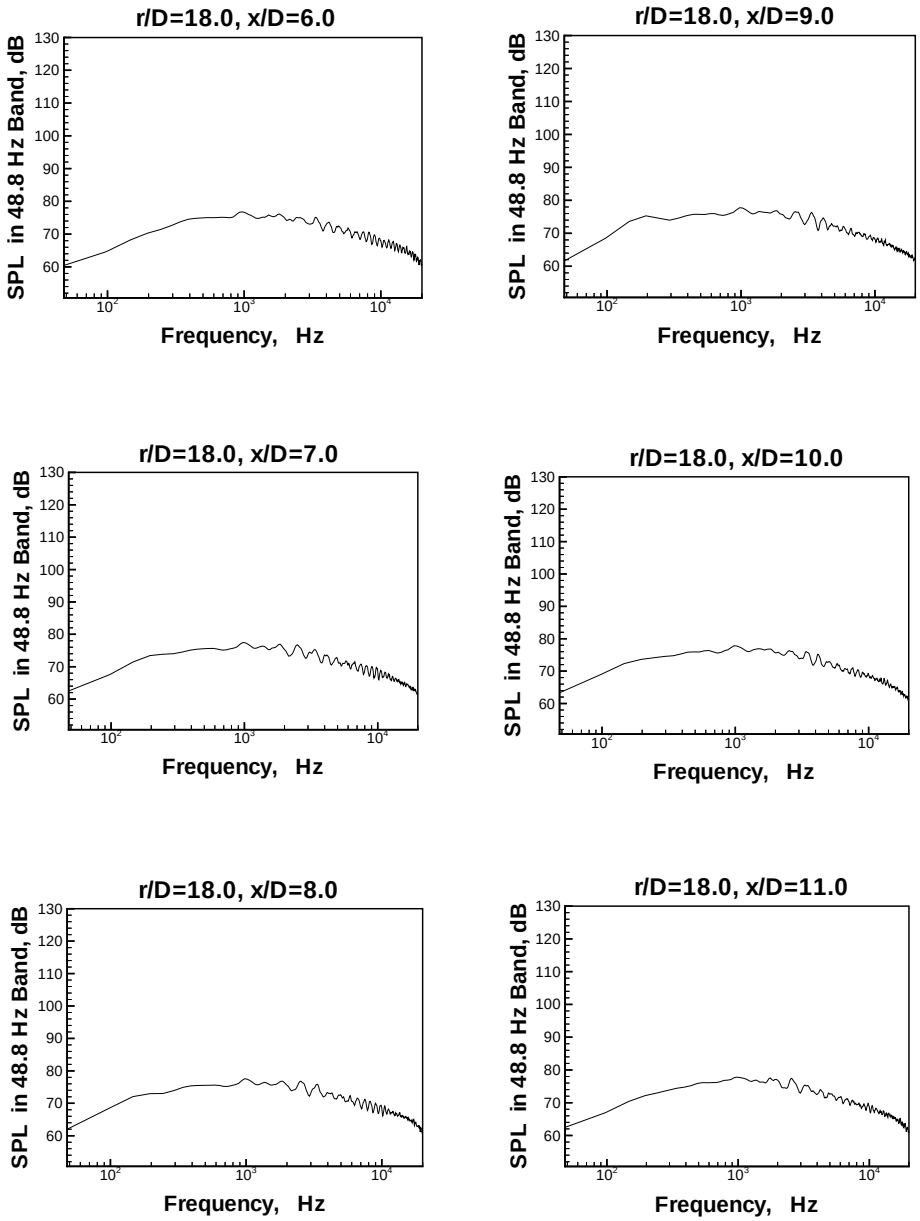

Figure 35: Near Field Pressure Spectra, Ma_e=0.60, r/D=18.0

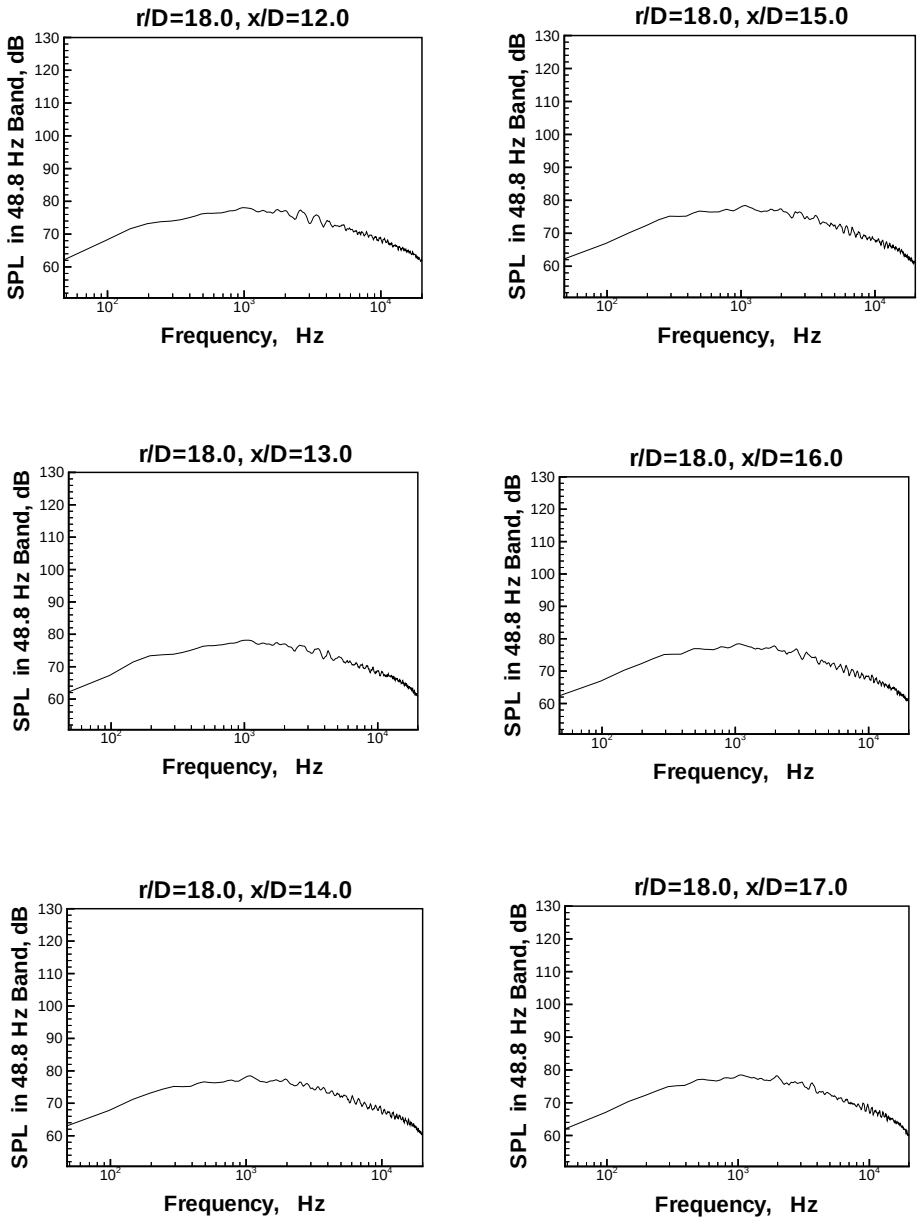

Figure 36: Near Field Pressure Spectra, Ma_e=0.60, r/D=18.0

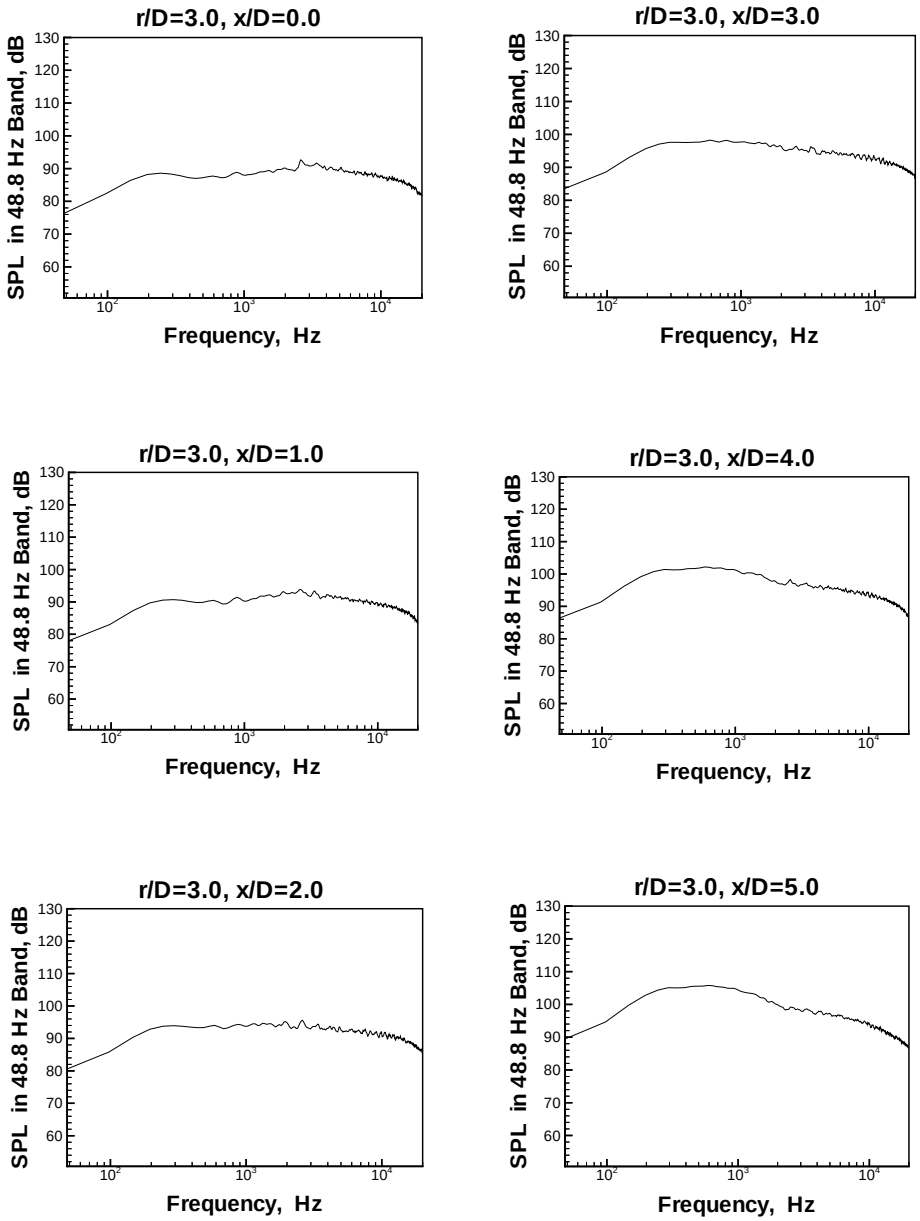

Figure 37: Near Field Pressure Spectra, Ma_e=0.85, r/D=3.0

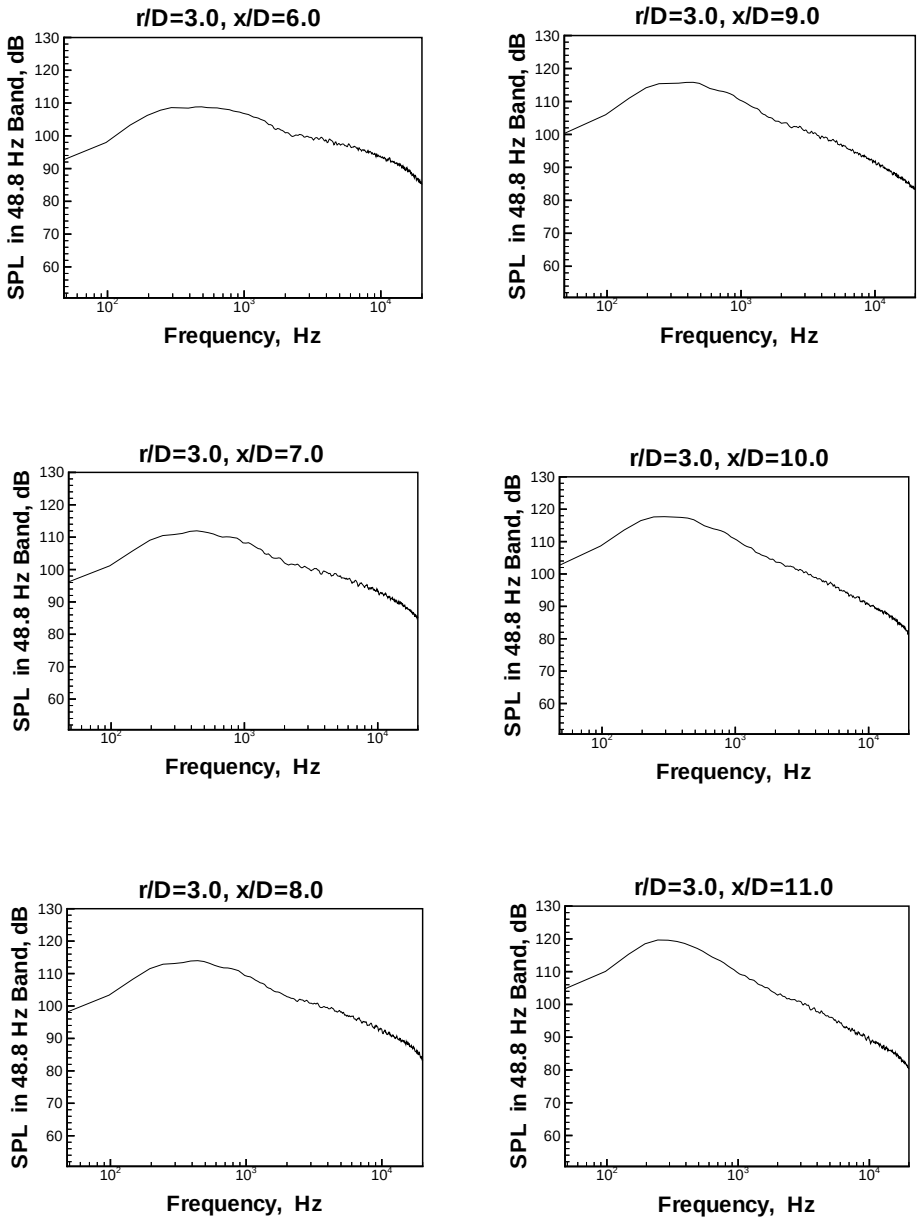

Figure 38: Near Field Pressure Spectra, Ma_e=0.85, r/D=3.0

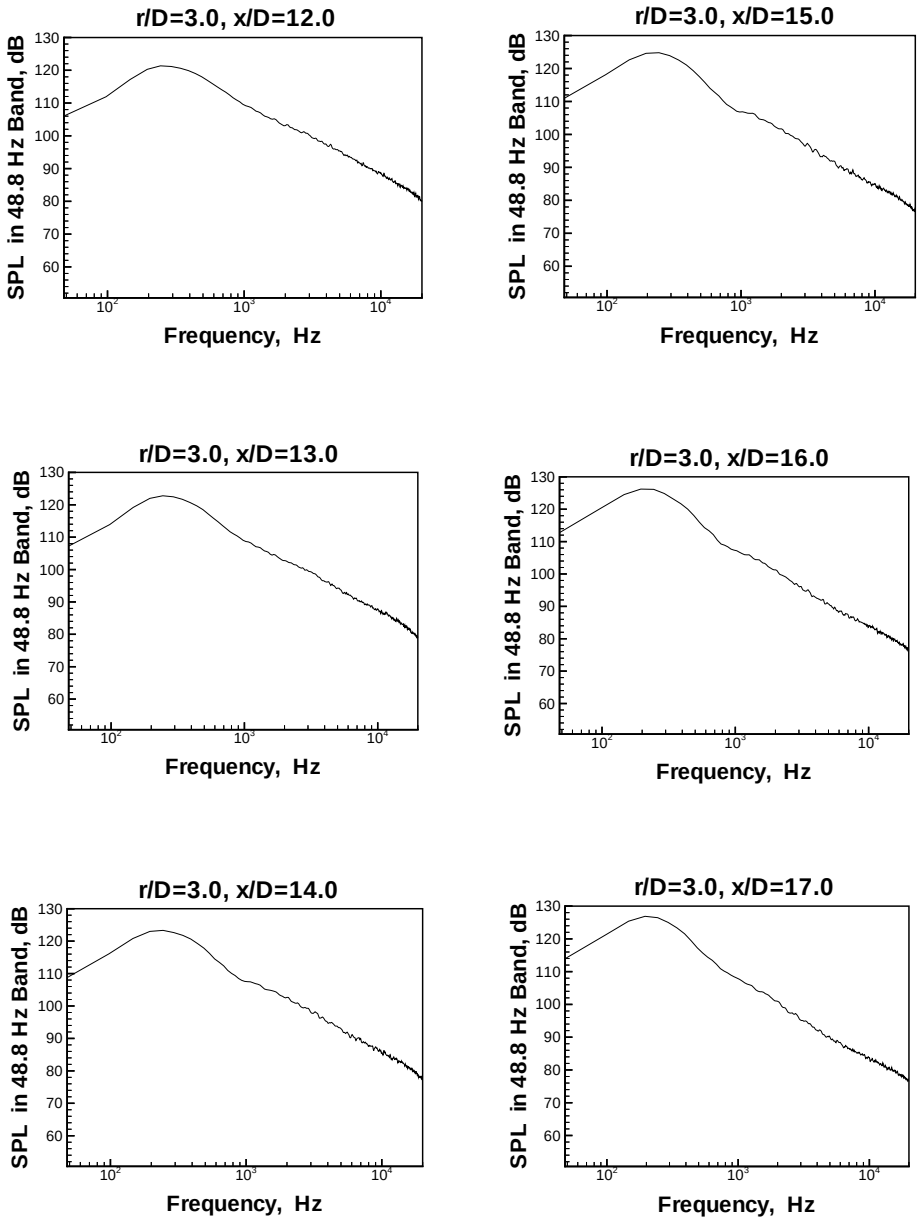

Figure 39: Near Field Pressure Spectra, Ma_e=0.85, r/D=3.0

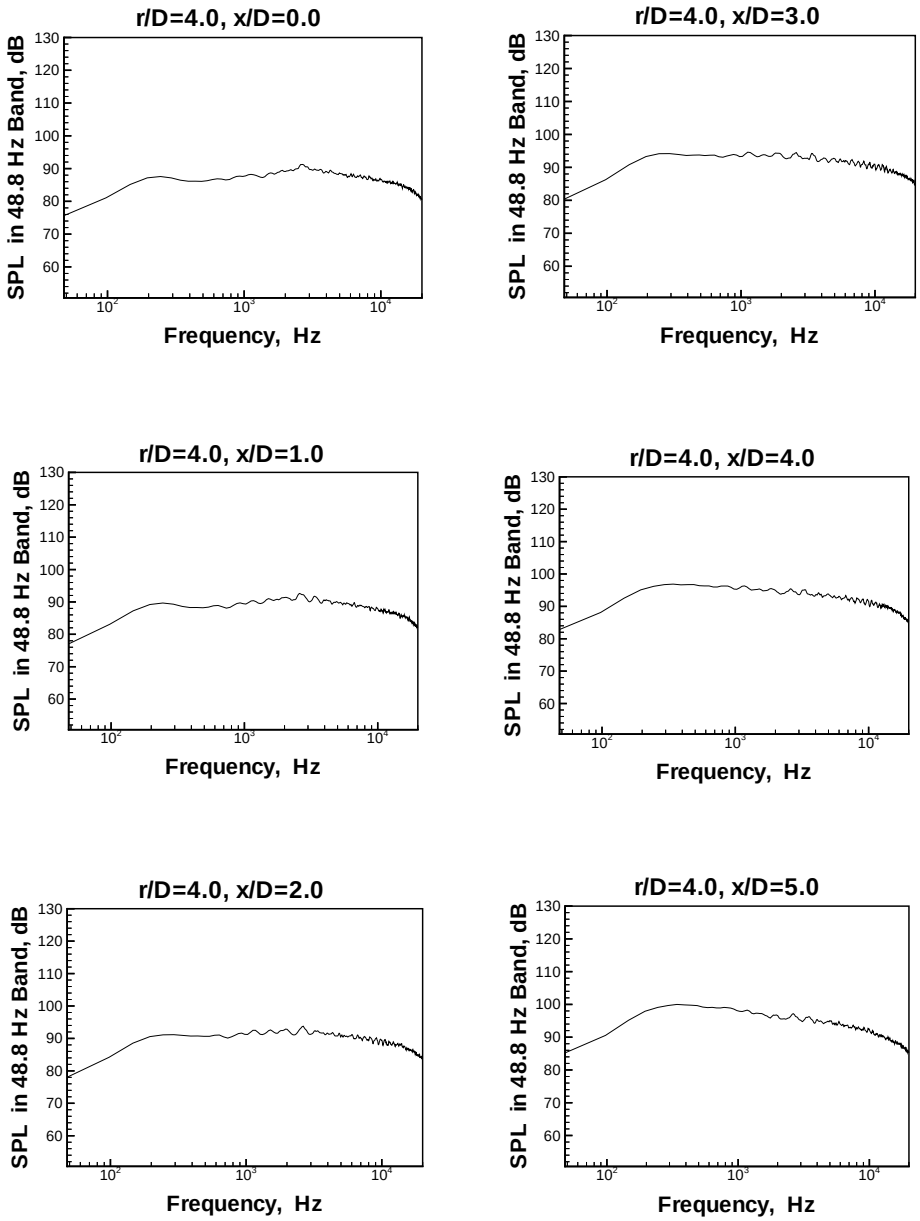

Figure 40: Near Field Pressure Spectra, Ma_e=0.85, r/D=4.0

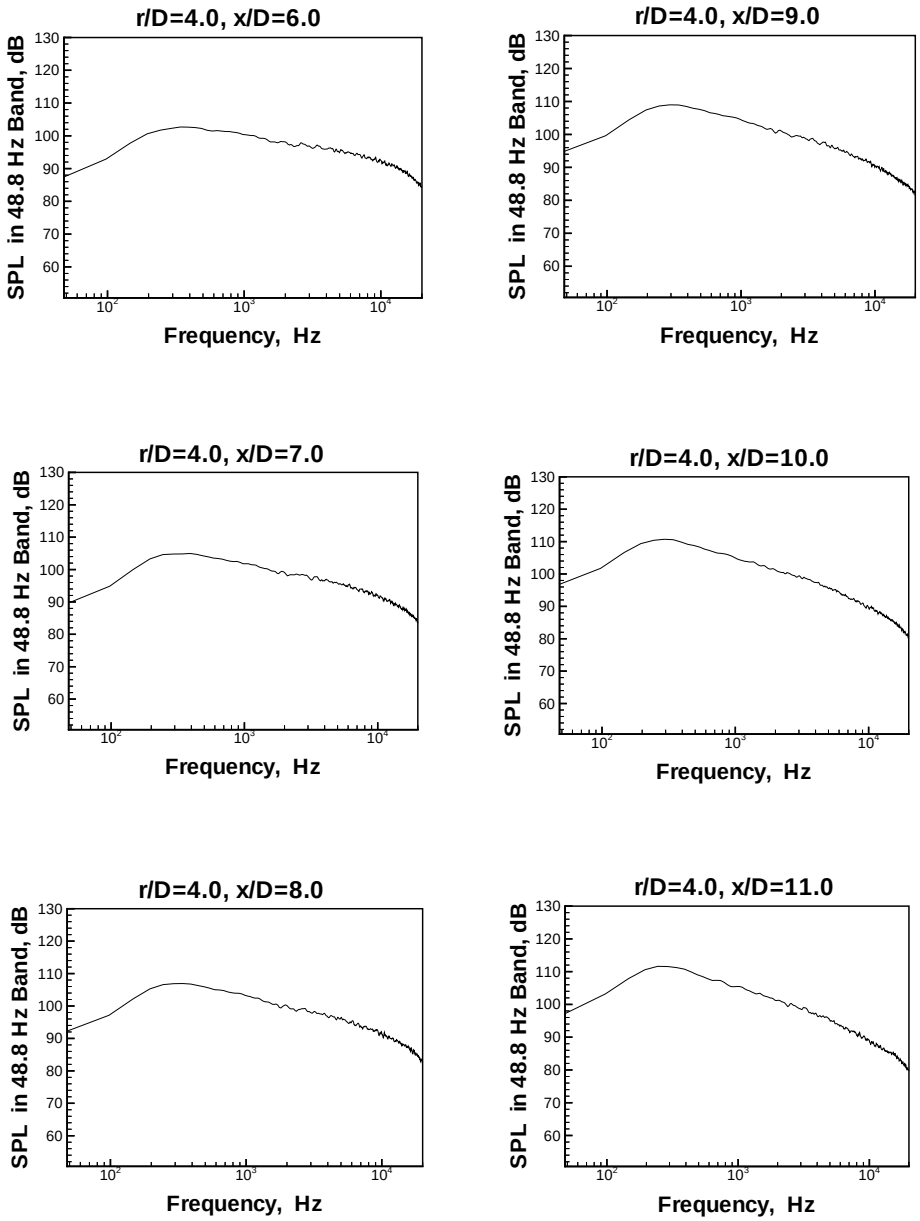

Figure 41: Near Field Pressure Spectra, Ma_e=0.85, r/D=4.0

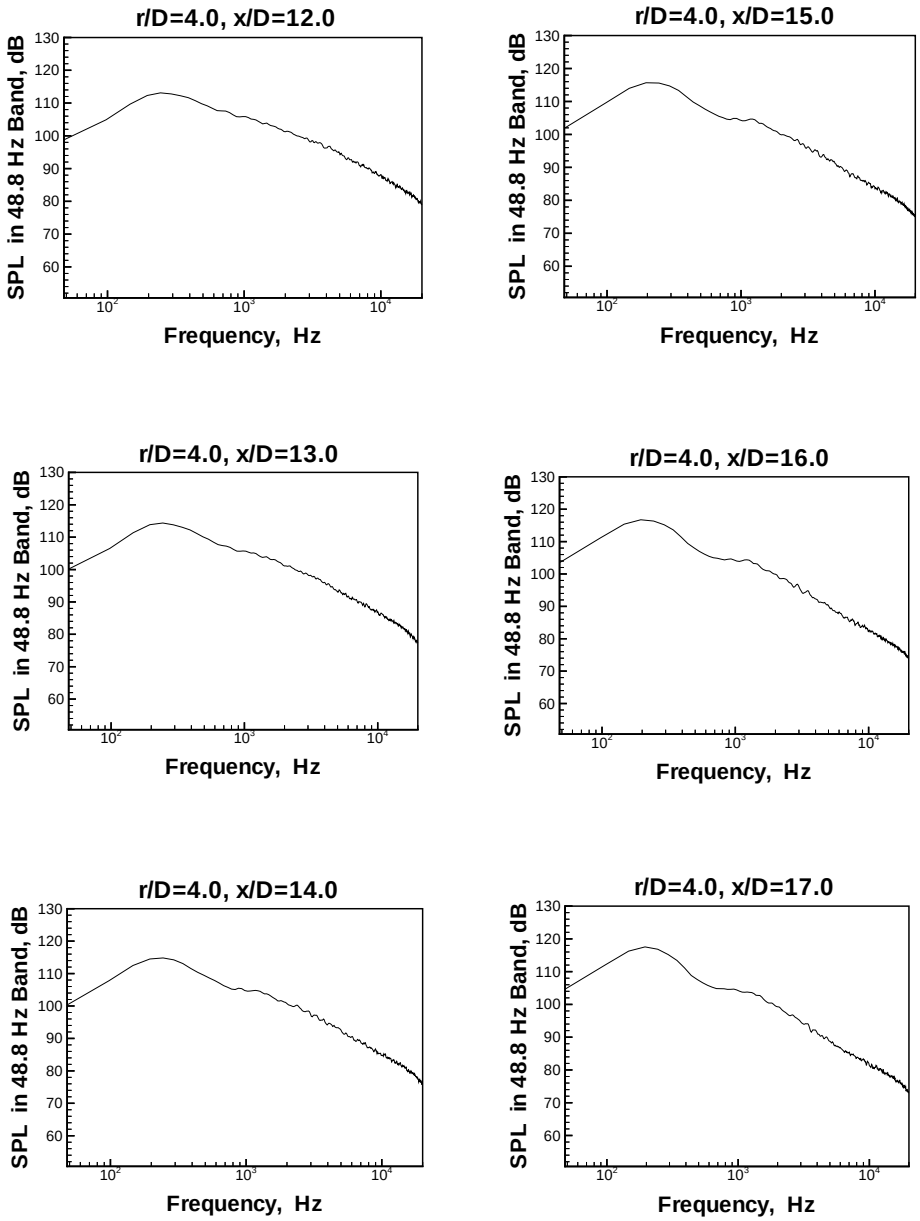

Figure 42: Near Field Pressure Spectra, Ma_e=0.85, r/D=4.0

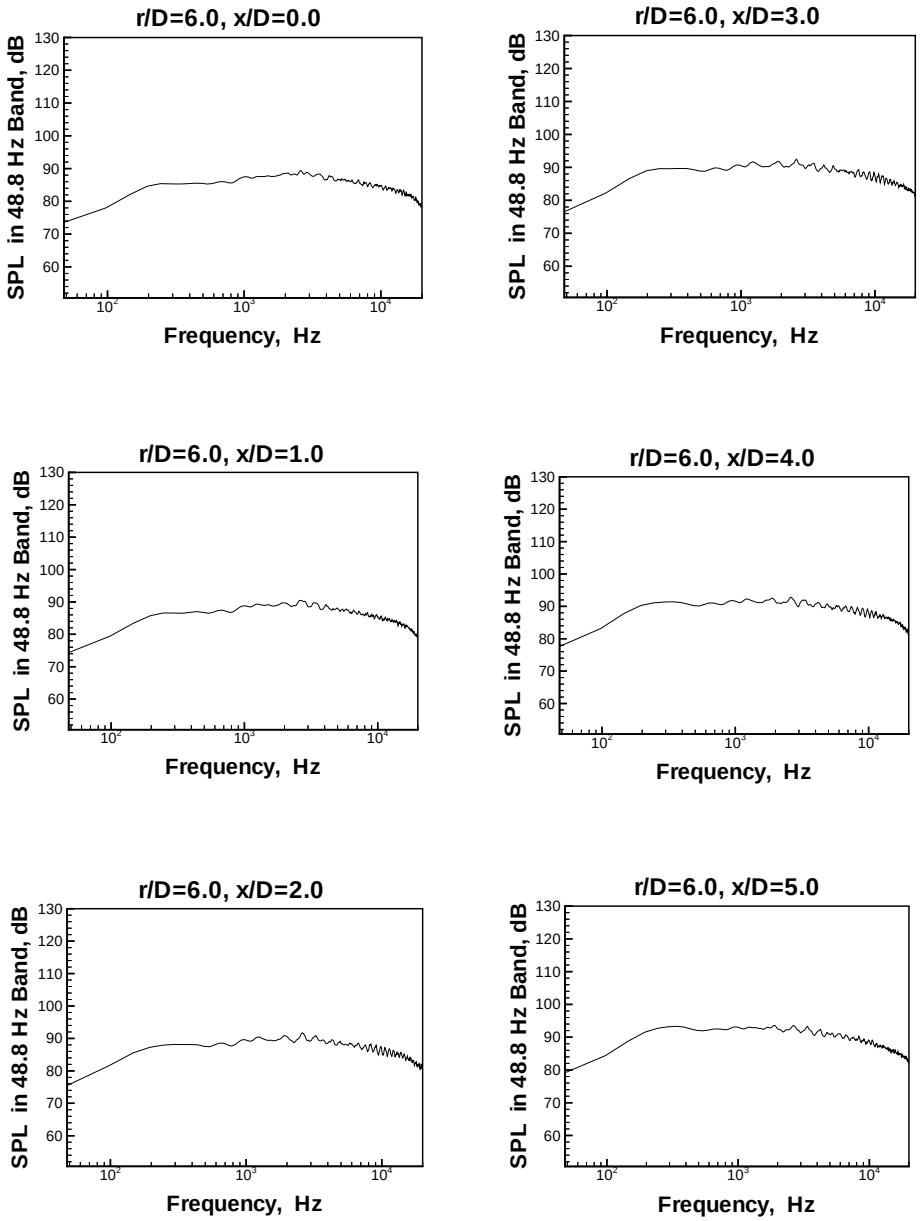

Figure 43: Near Field Pressure Spectra, Ma_e=0.85, r/D=6.0

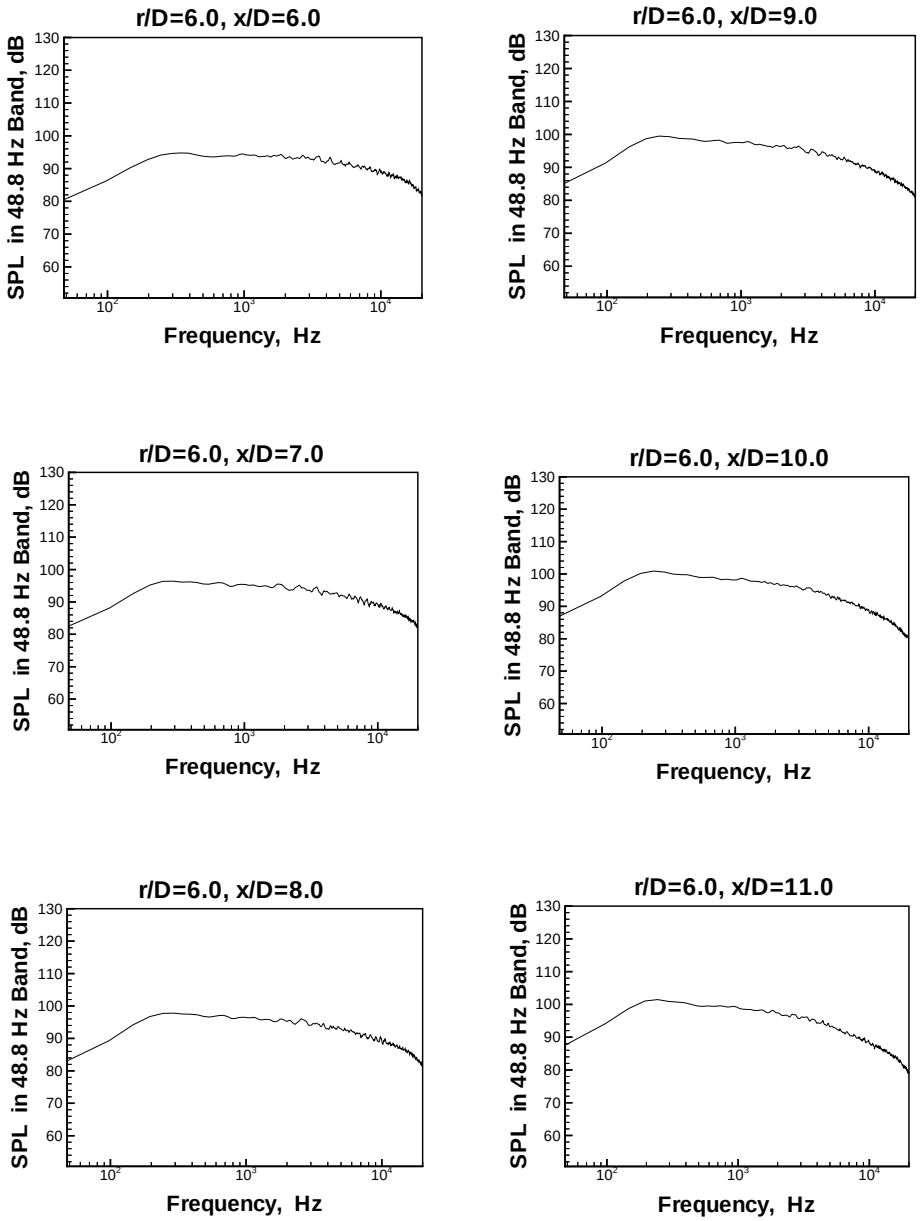

Figure 44: Near Field Pressure Spectra, Ma_e=0.85, r/D=6.0

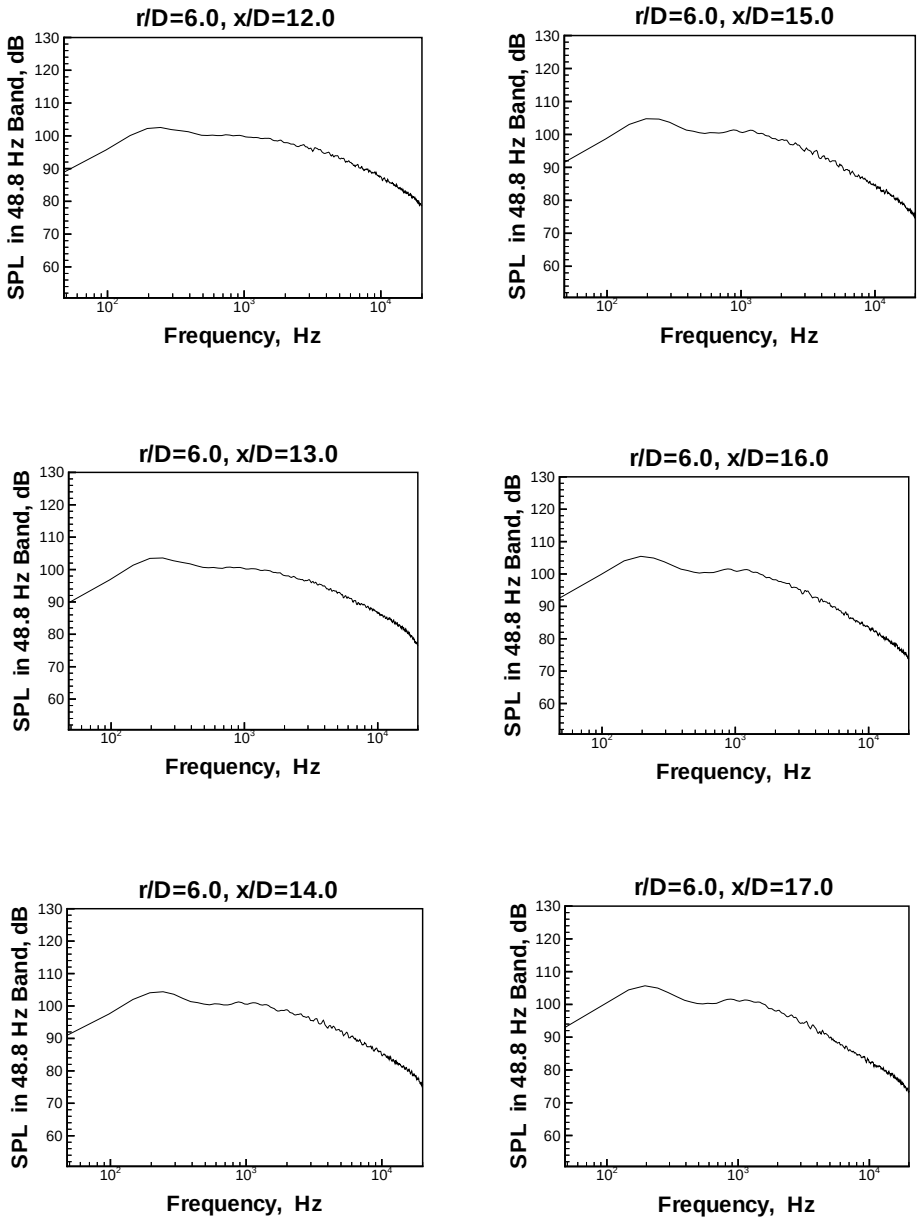

Figure 45: Near Field Pressure Spectra, Ma_e=0.85, r/D=6.0

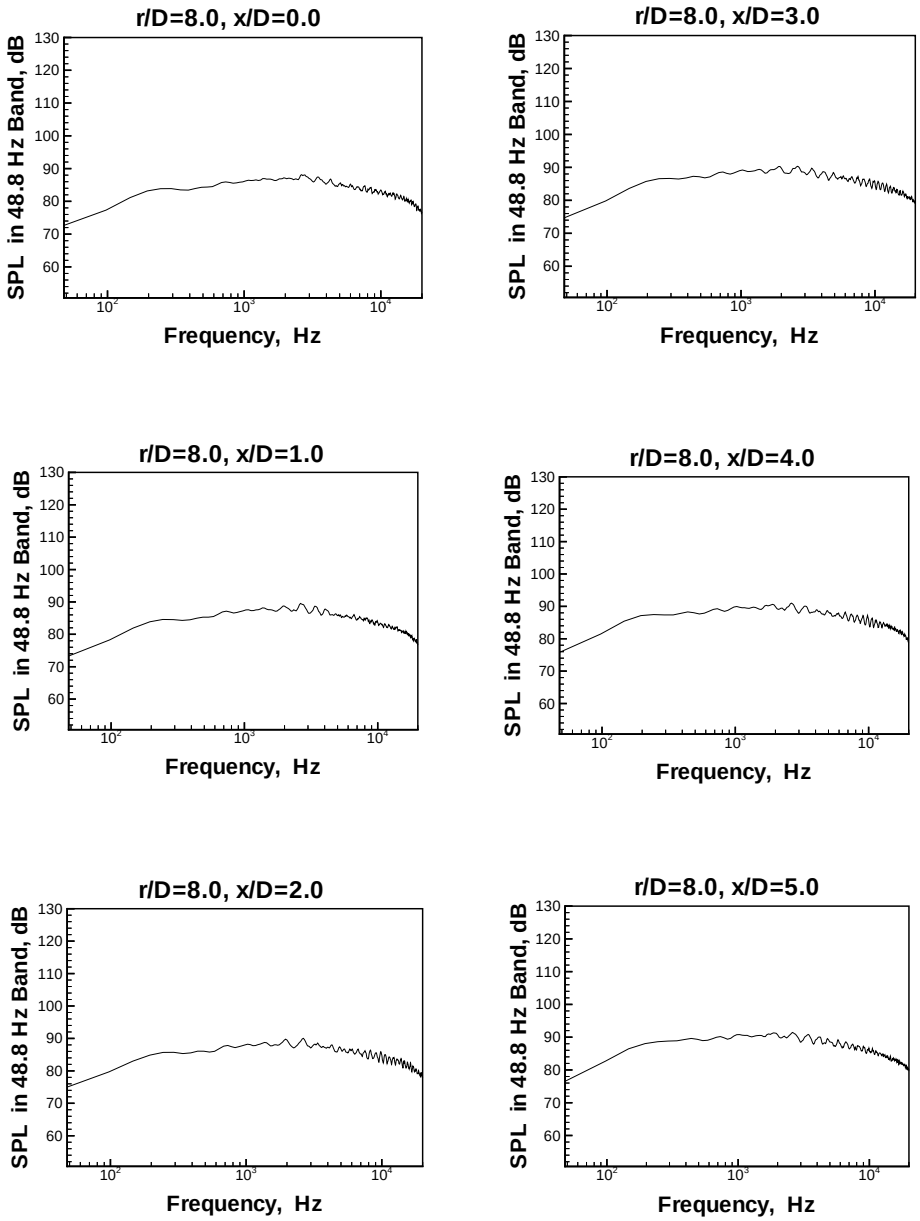

Figure 46: Near Field Pressure Spectra, Ma_e=0.85, r/D=8.0

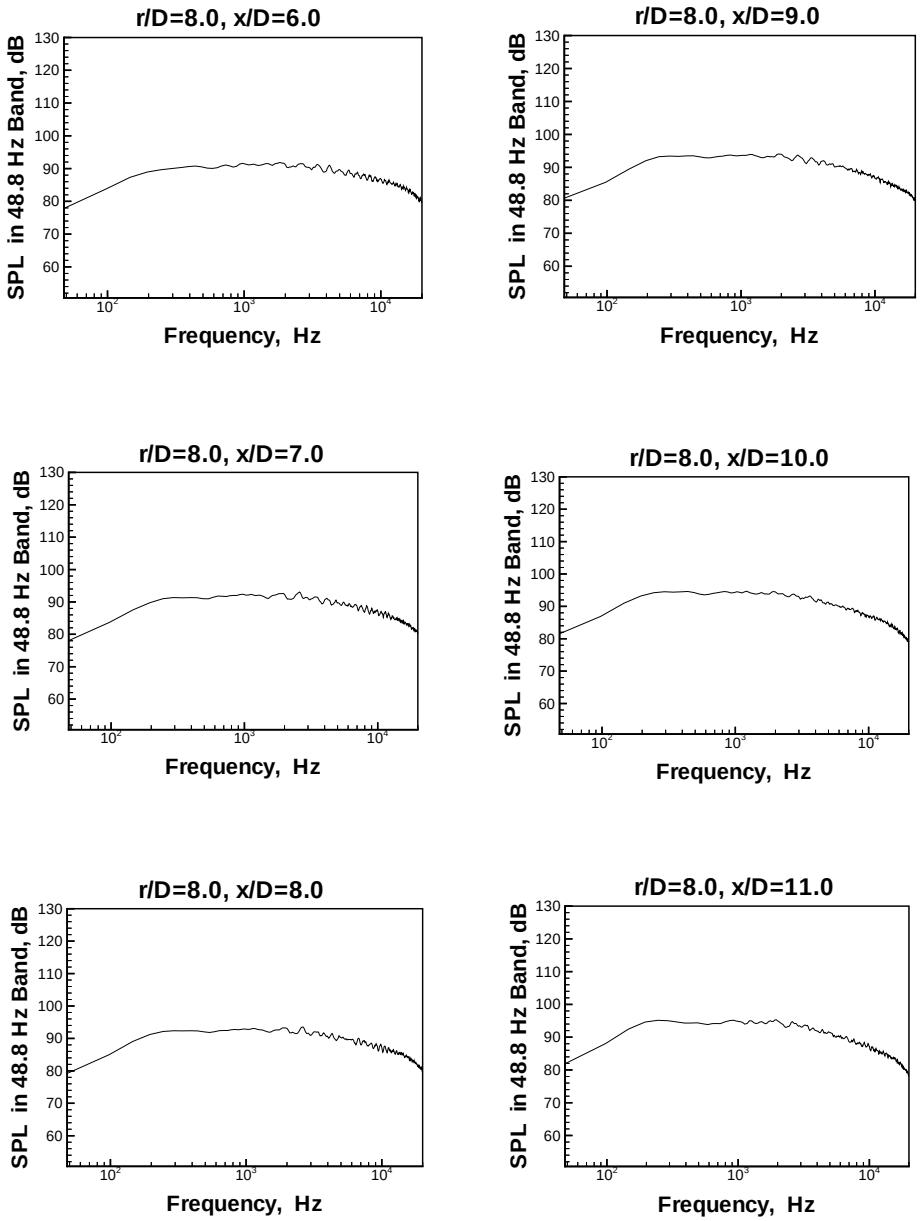

Figure 47: Near Field Pressure Spectra, Ma_e=0.85, r/D=8.0

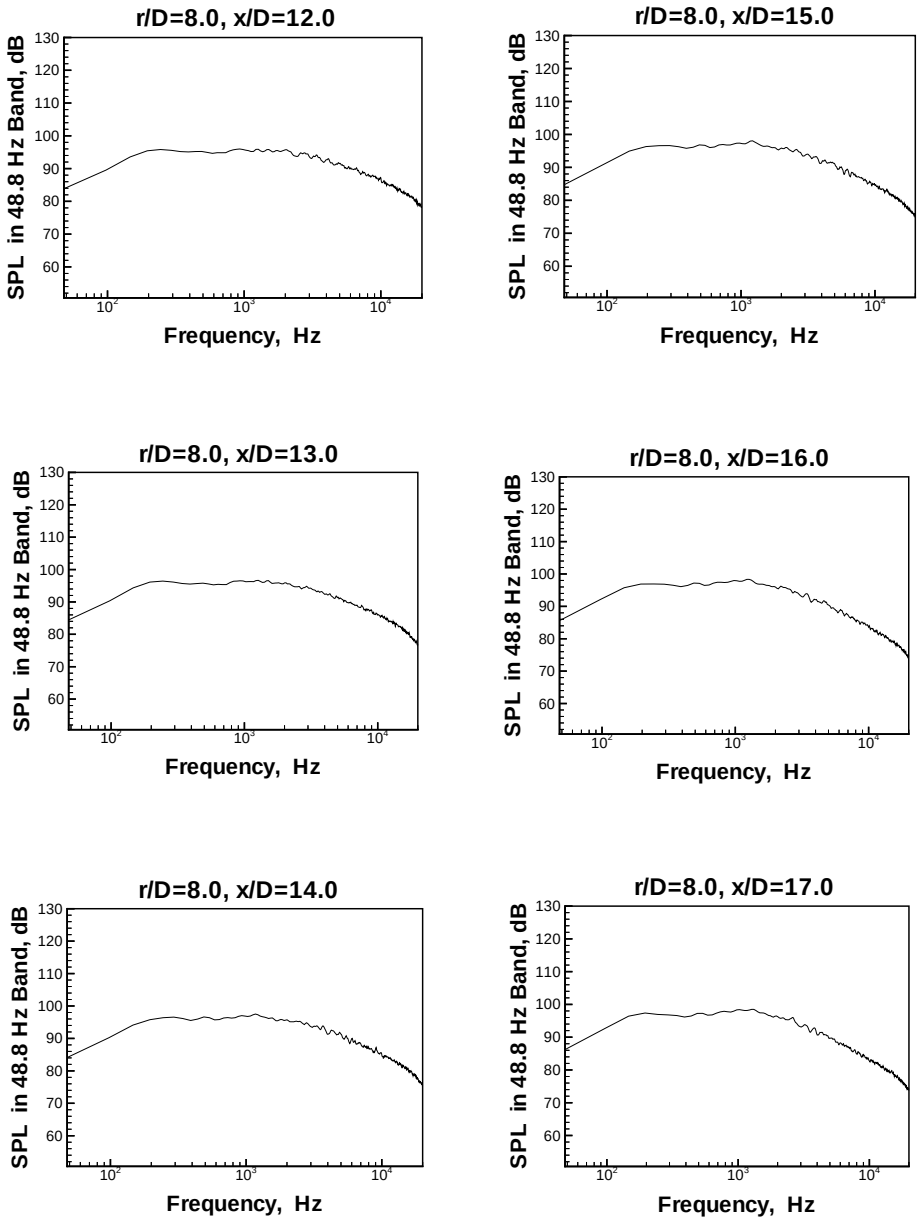

Figure 48: Near Field Pressure Spectra, Ma_e=0.85, r/D=8.0

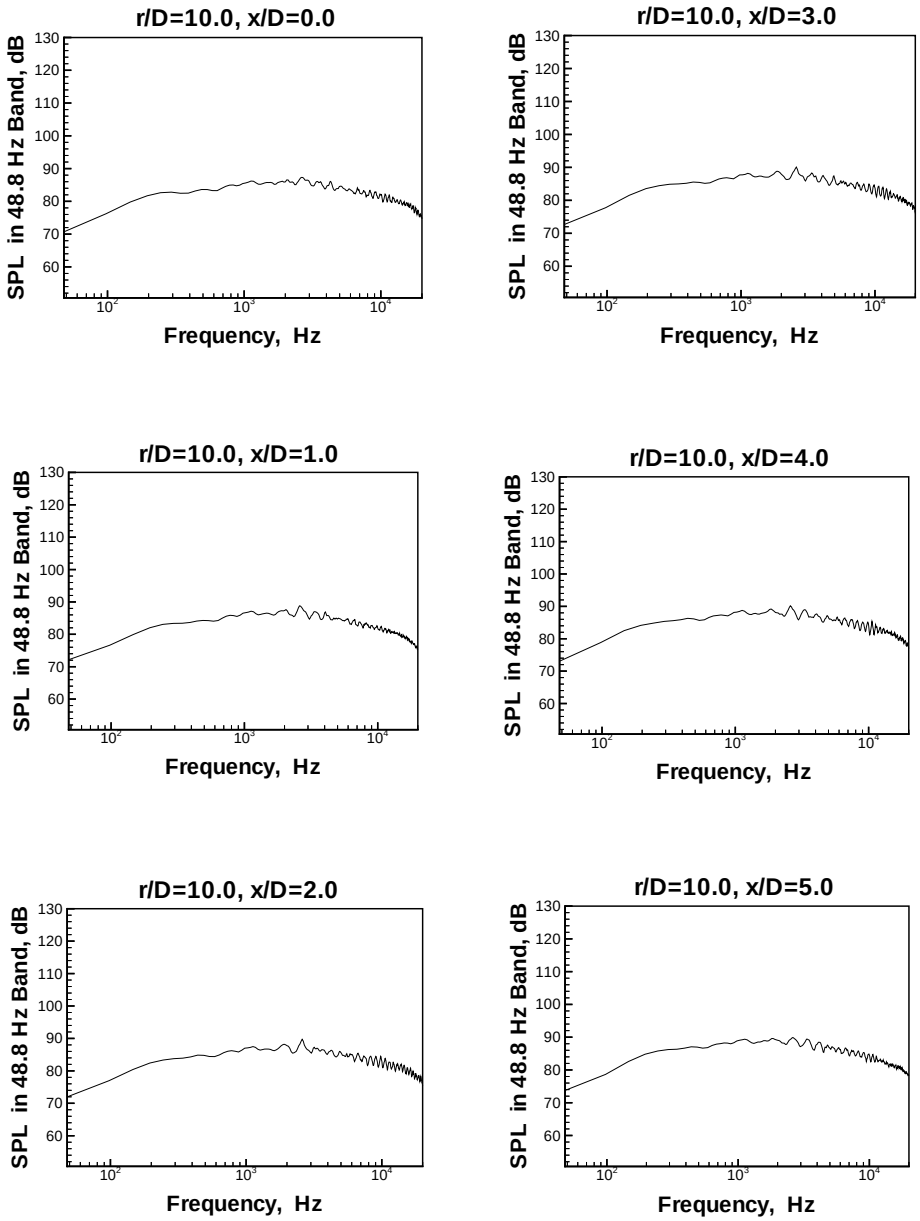

Figure 49: Near Field Pressure Spectra, Ma_e=0.85, r/D=10.0

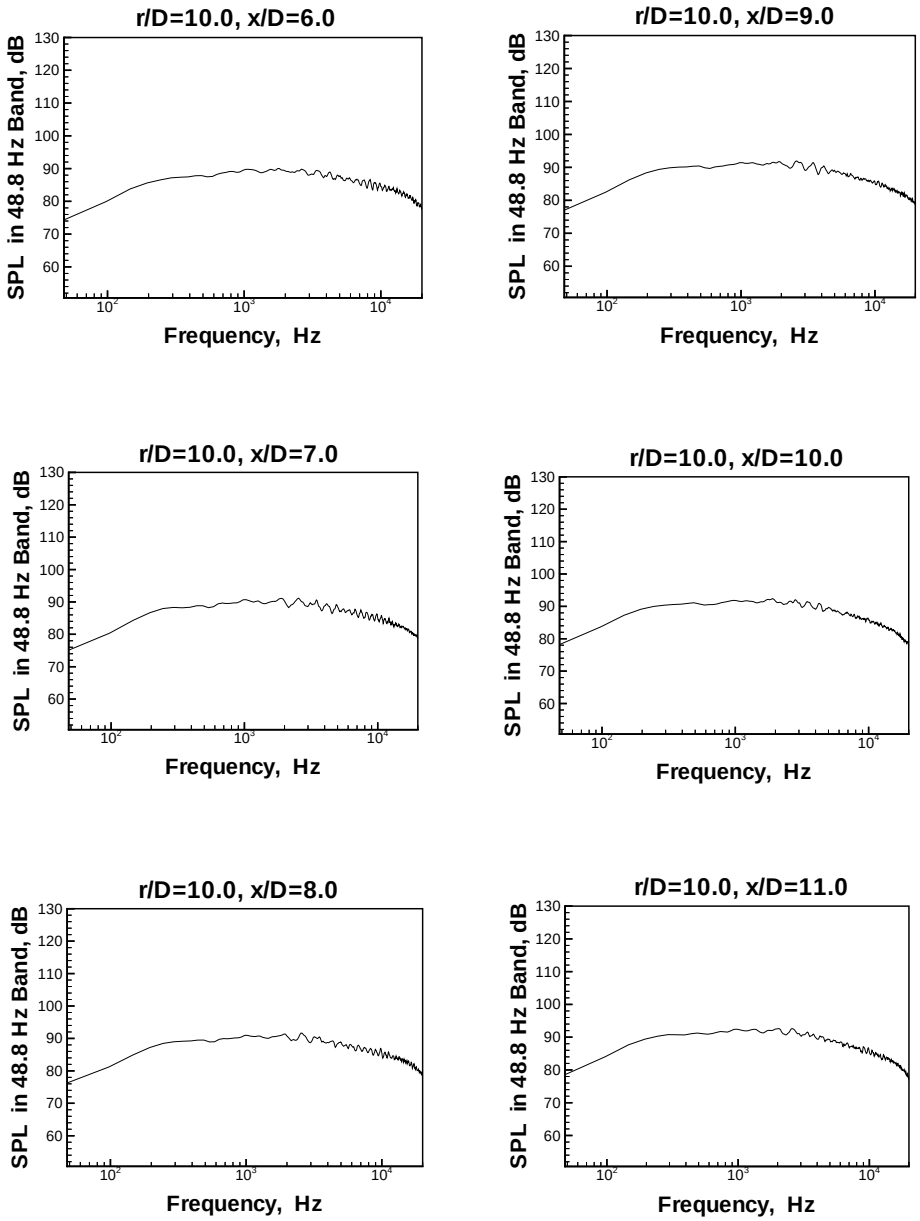

Figure 50: Near Field Pressure Spectra, Ma_e=0.85, r/D=10.0

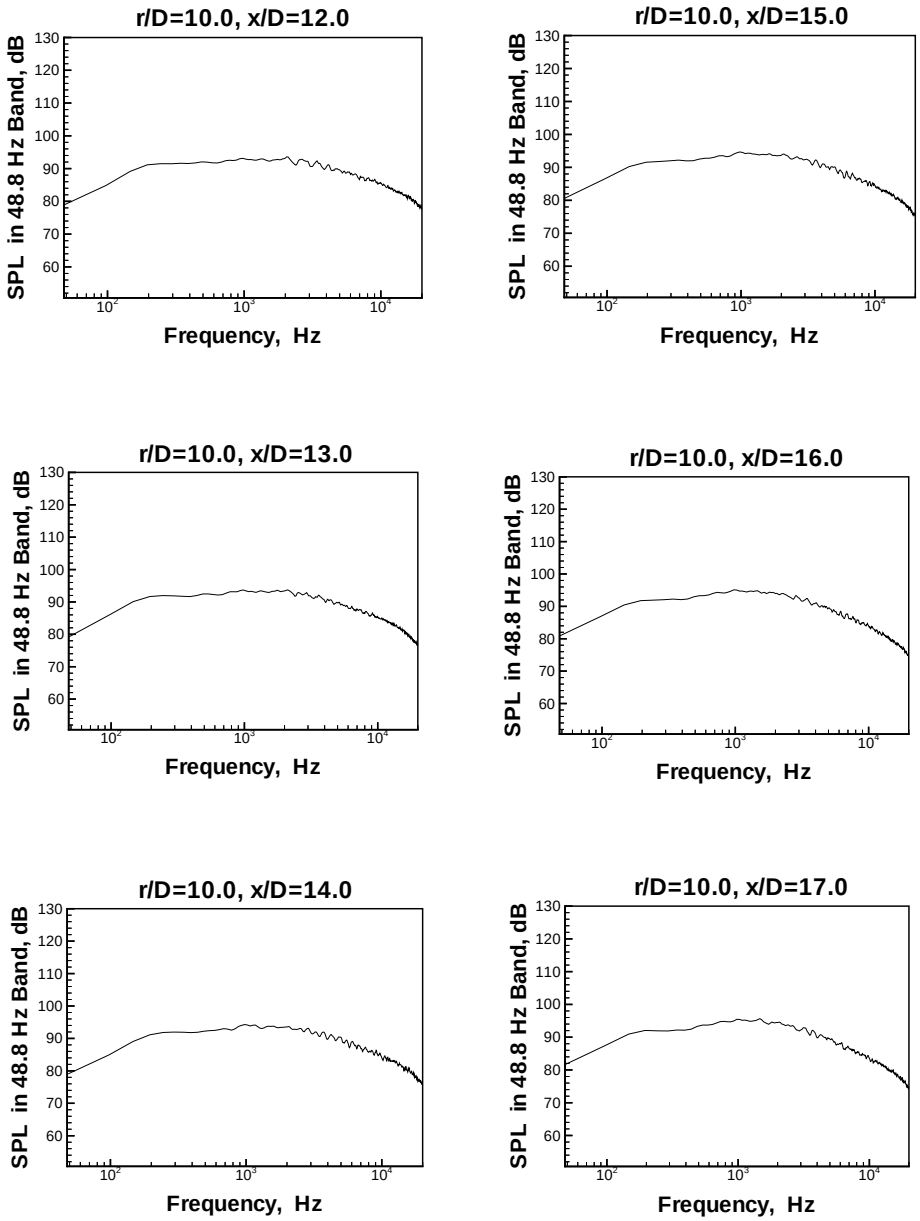

Figure 51: Near Field Pressure Spectra, Ma_e=0.85, r/D=10.0

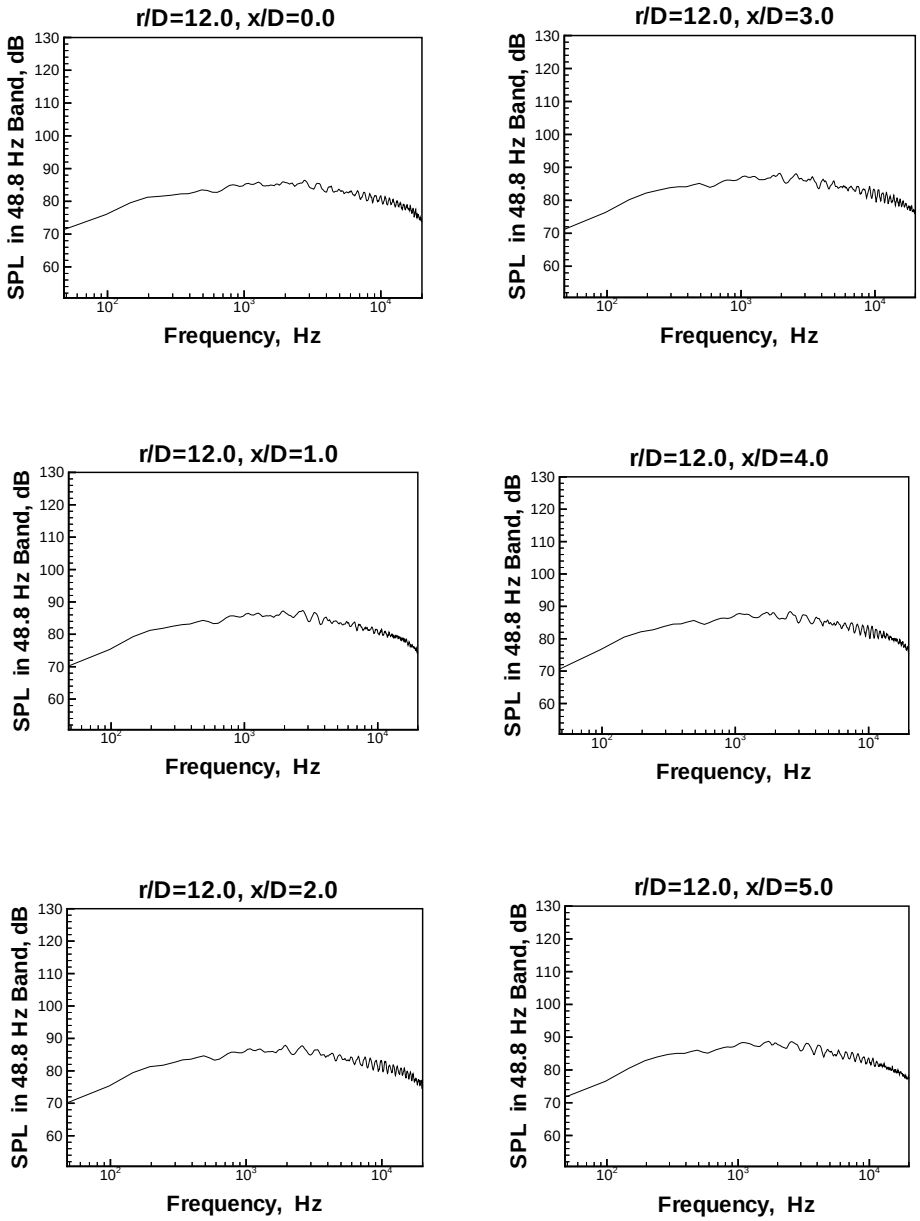

Figure 52: Near Field Pressure Spectra, Ma_e=0.85, r/D=12.0

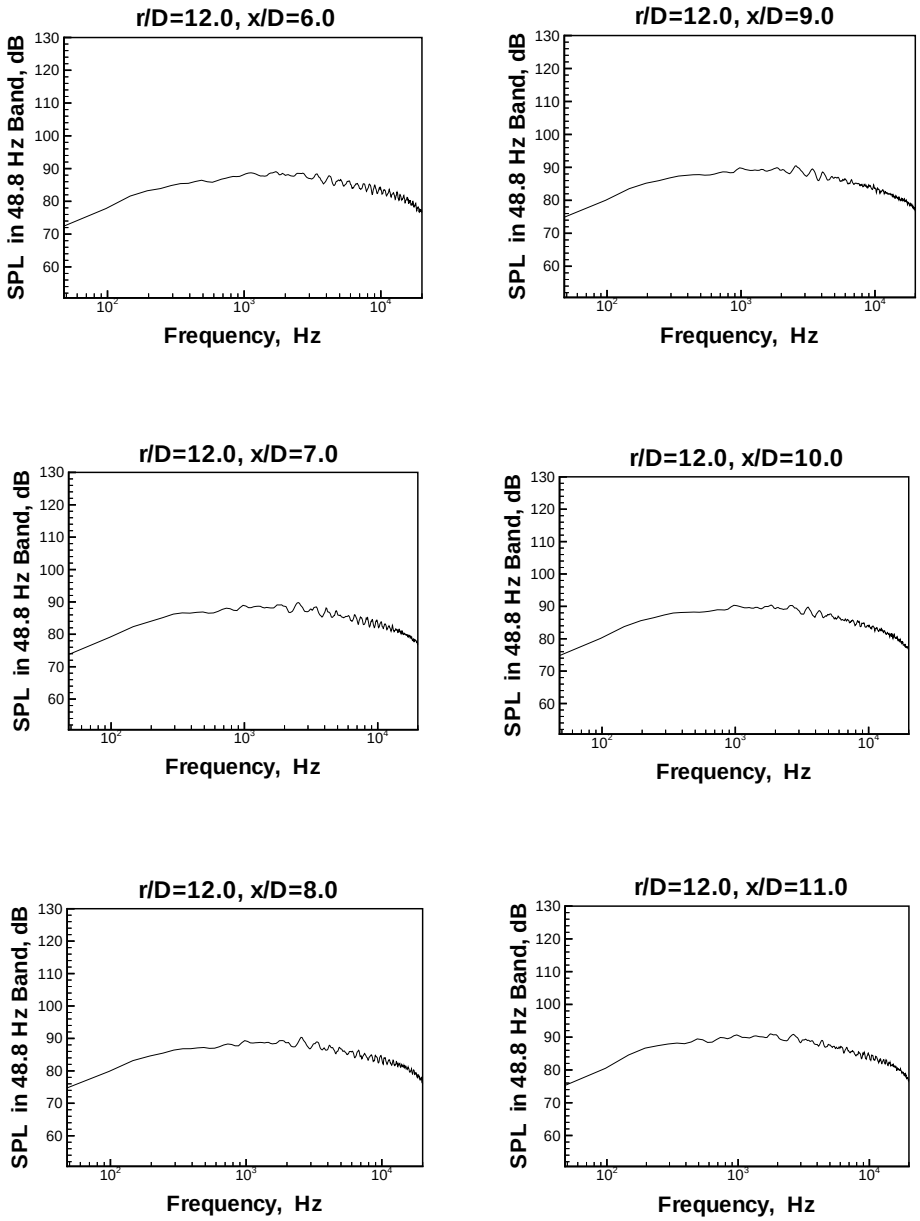

Figure 53: Near Field Pressure Spectra, Ma_e=0.85, r/D=12.0

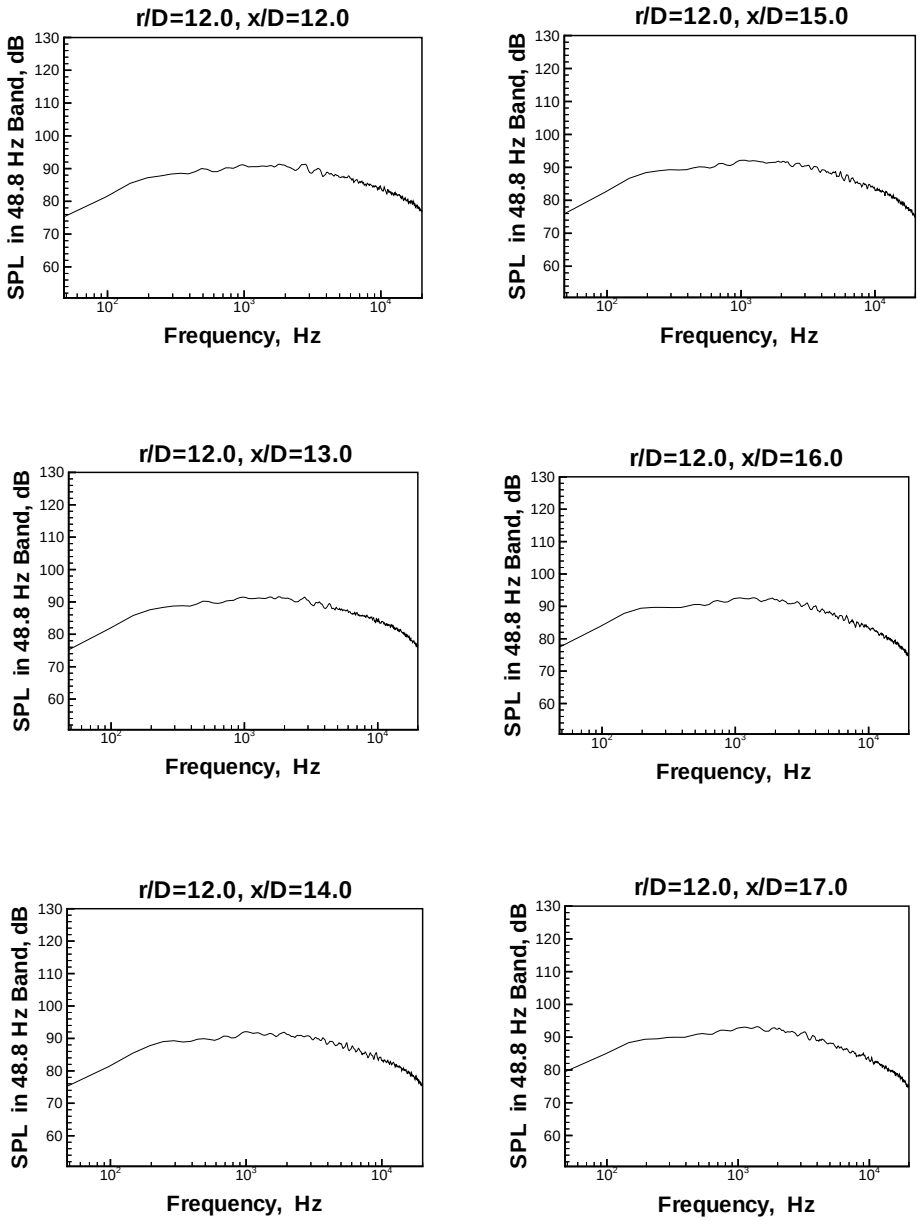

Figure 54: Near Field Pressure Spectra, Ma_e=0.85, r/D=12.0

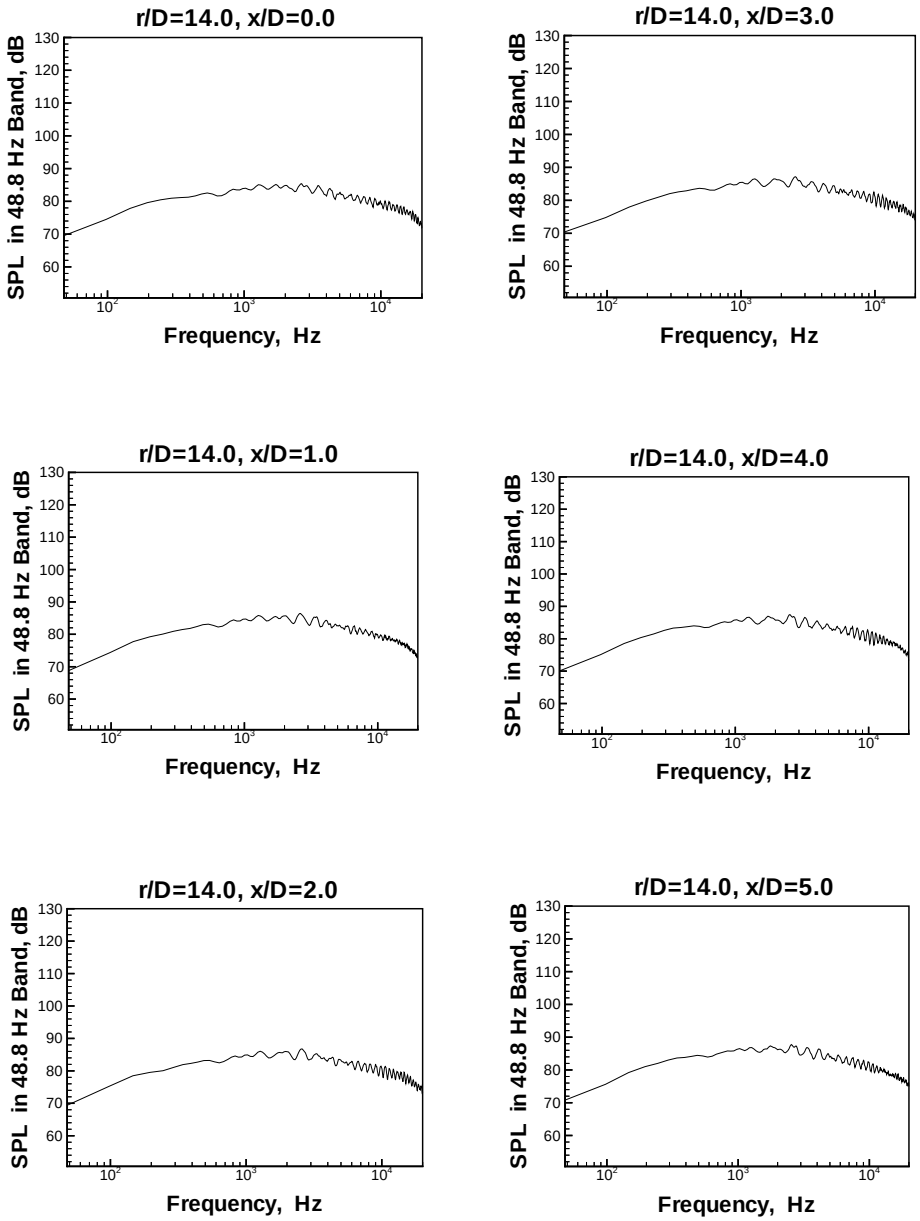

Figure 55: Near Field Pressure Spectra, Ma_e=0.85, r/D=14.0

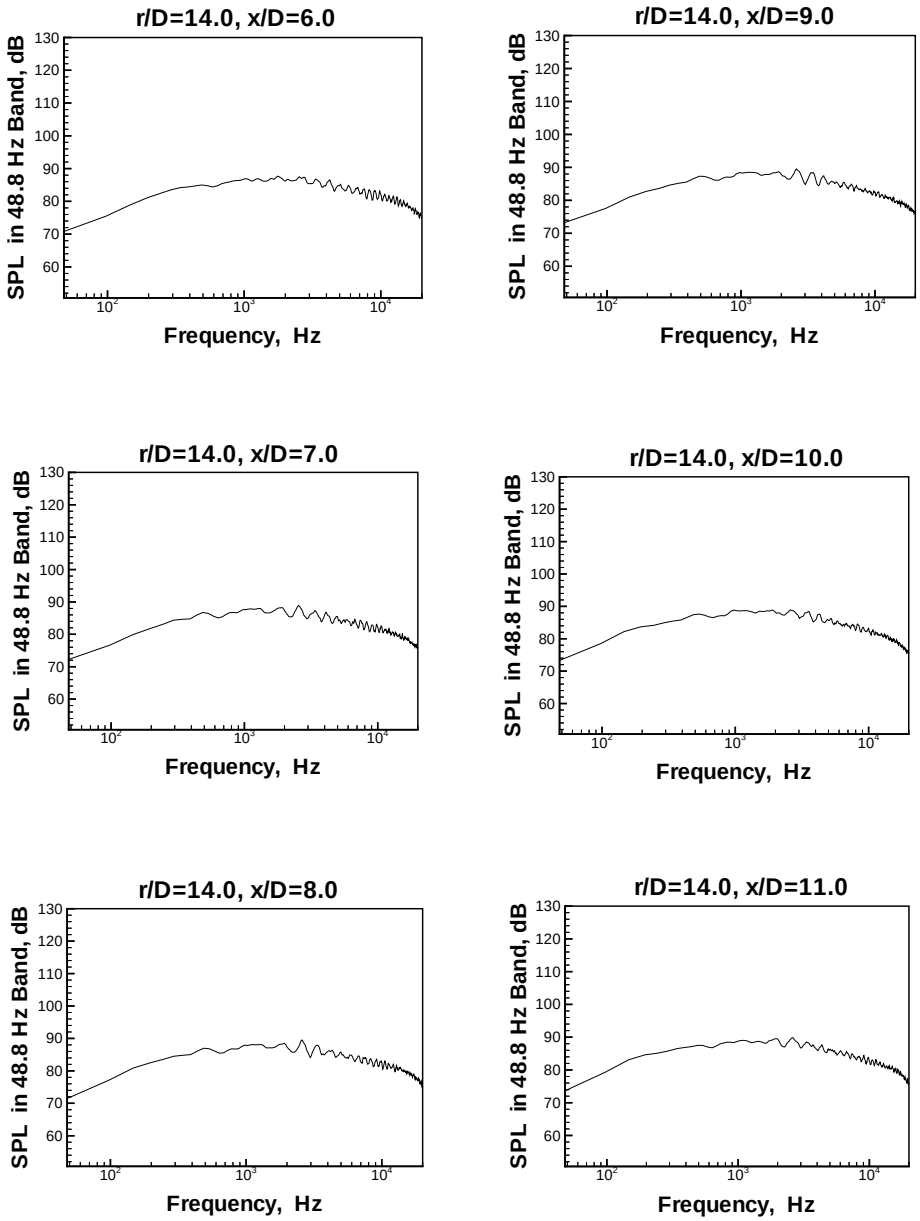

Figure 56: Near Field Pressure Spectra, Ma_e=0.85, r/D=14.0

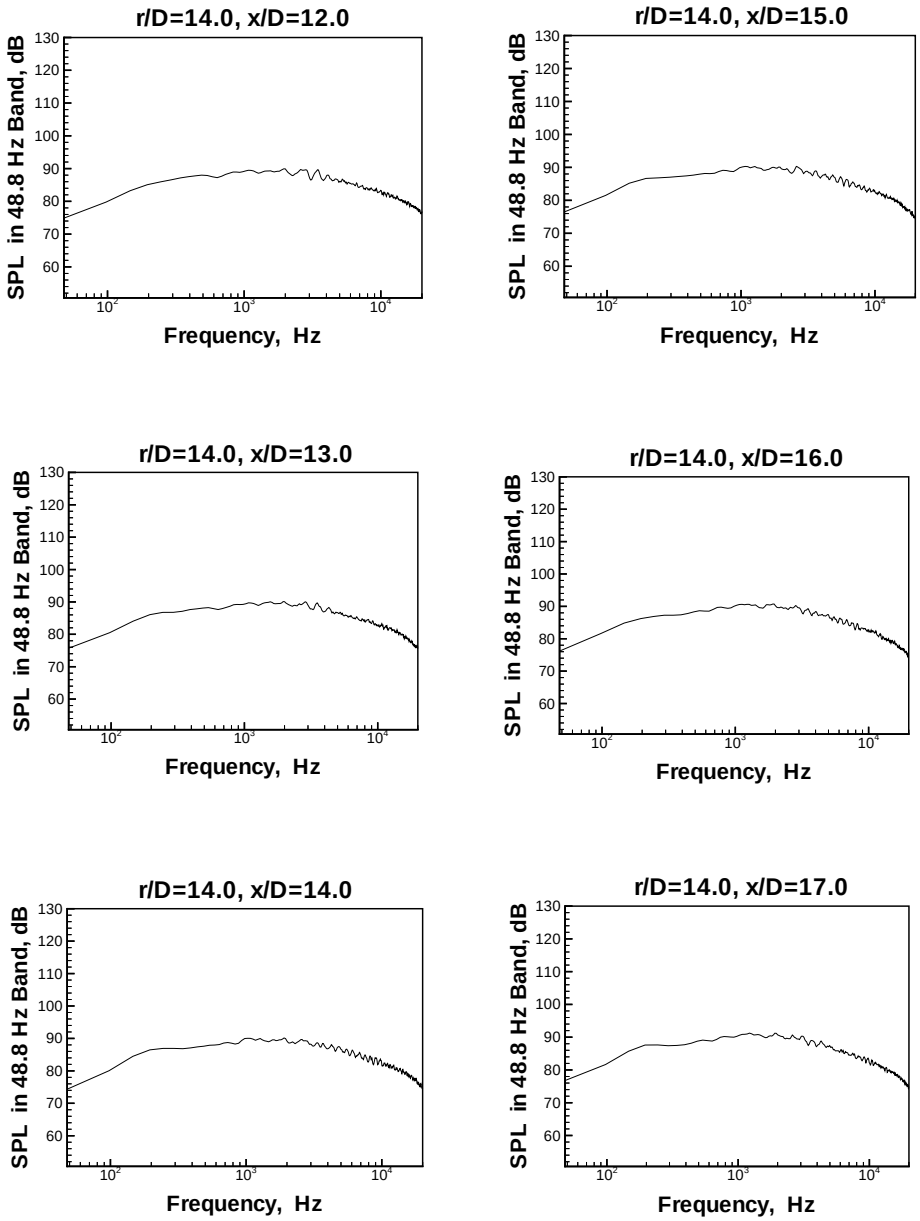

Figure 57: Near Field Pressure Spectra, Ma_e=0.85, r/D=14.0

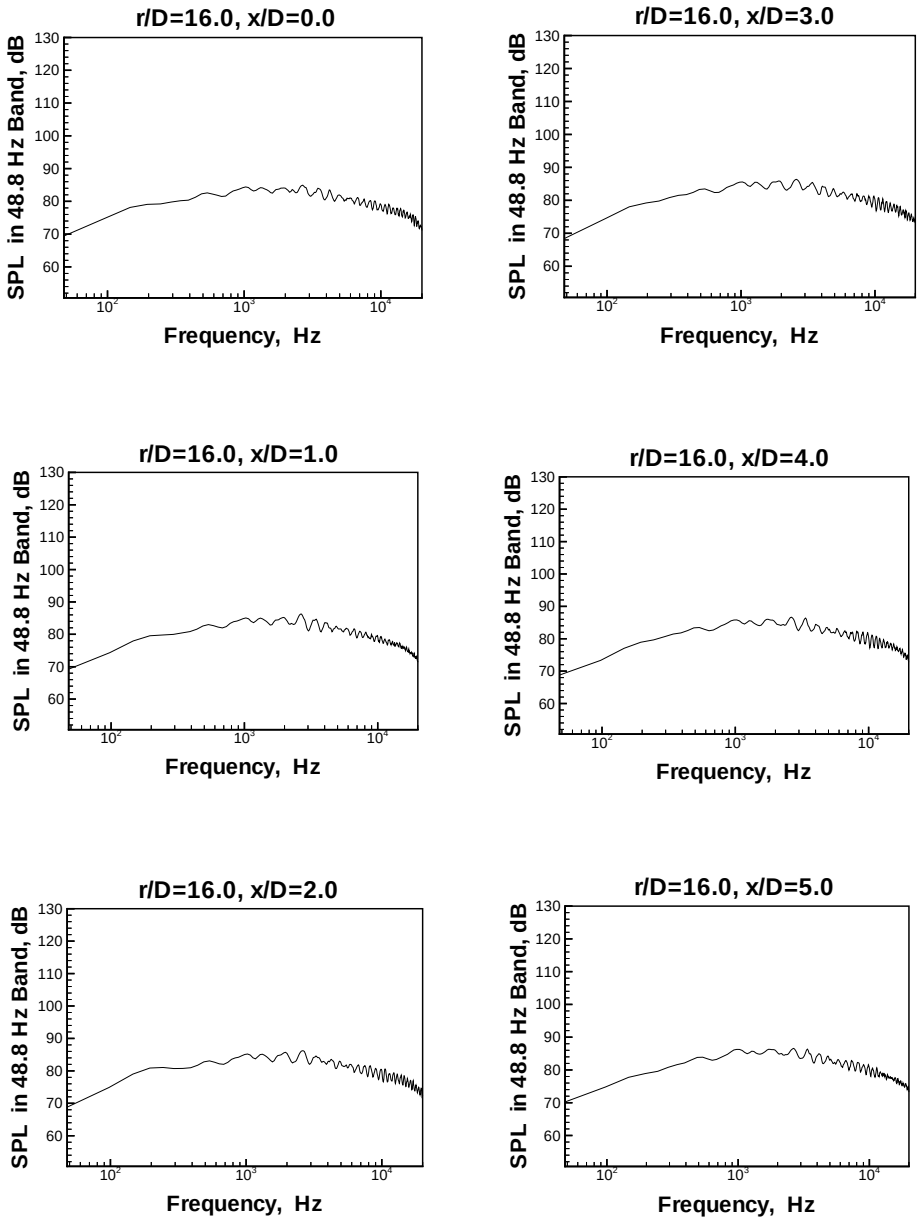

Figure 58: Near Field Pressure Spectra, Ma_e=0.85, r/D=16.0

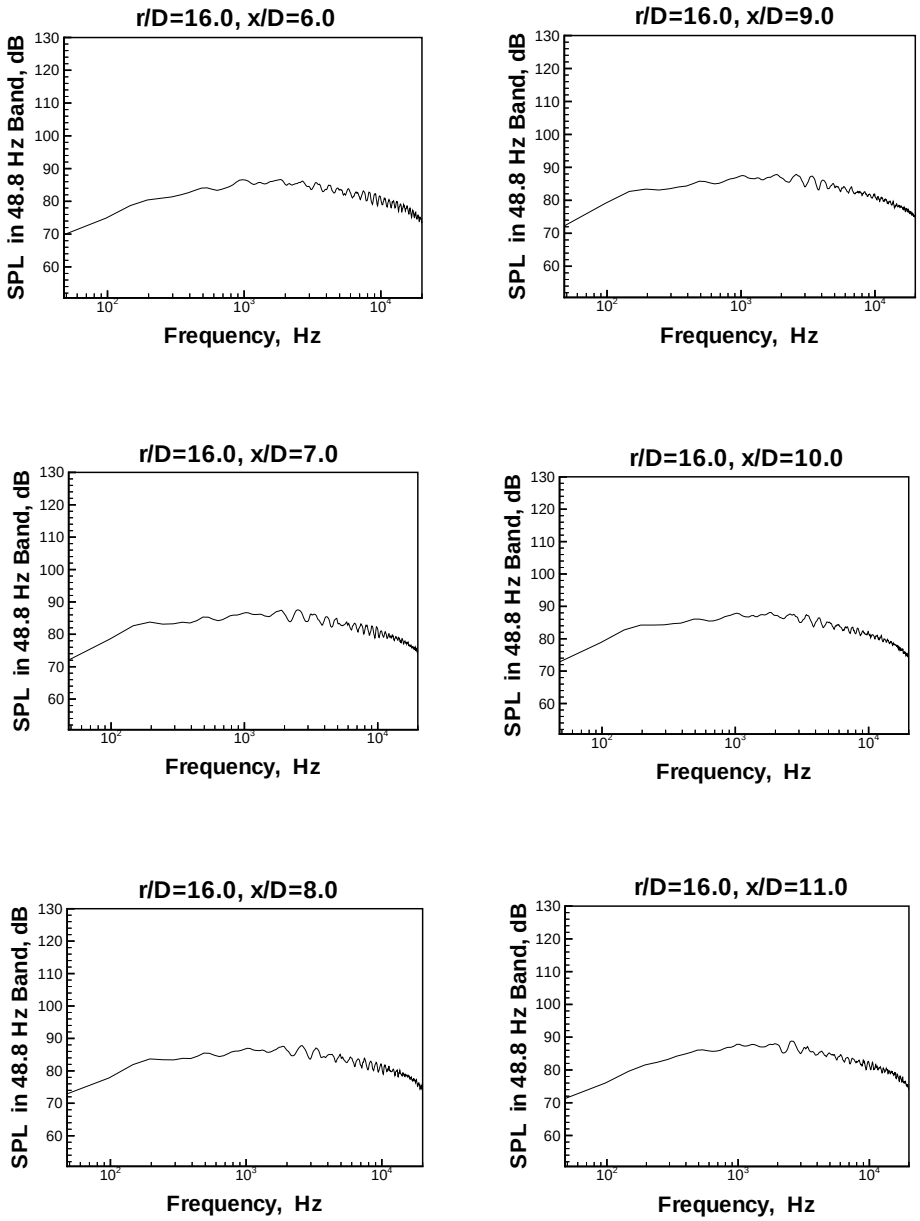

Figure 59: Near Field Pressure Spectra, Ma_e=0.85, r/D=16.0

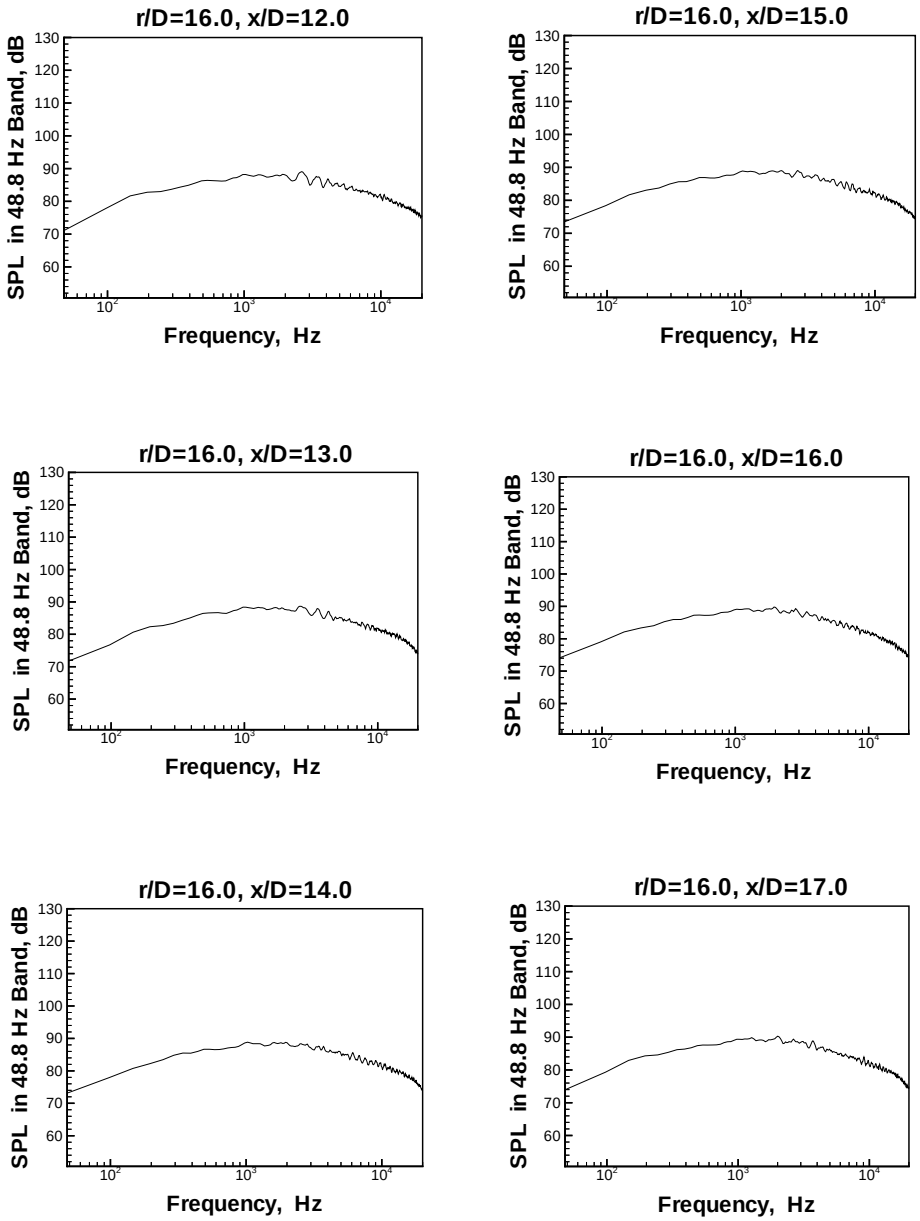

Figure 60: Near Field Pressure Spectra, Ma_e=0.85, r/D=16.0

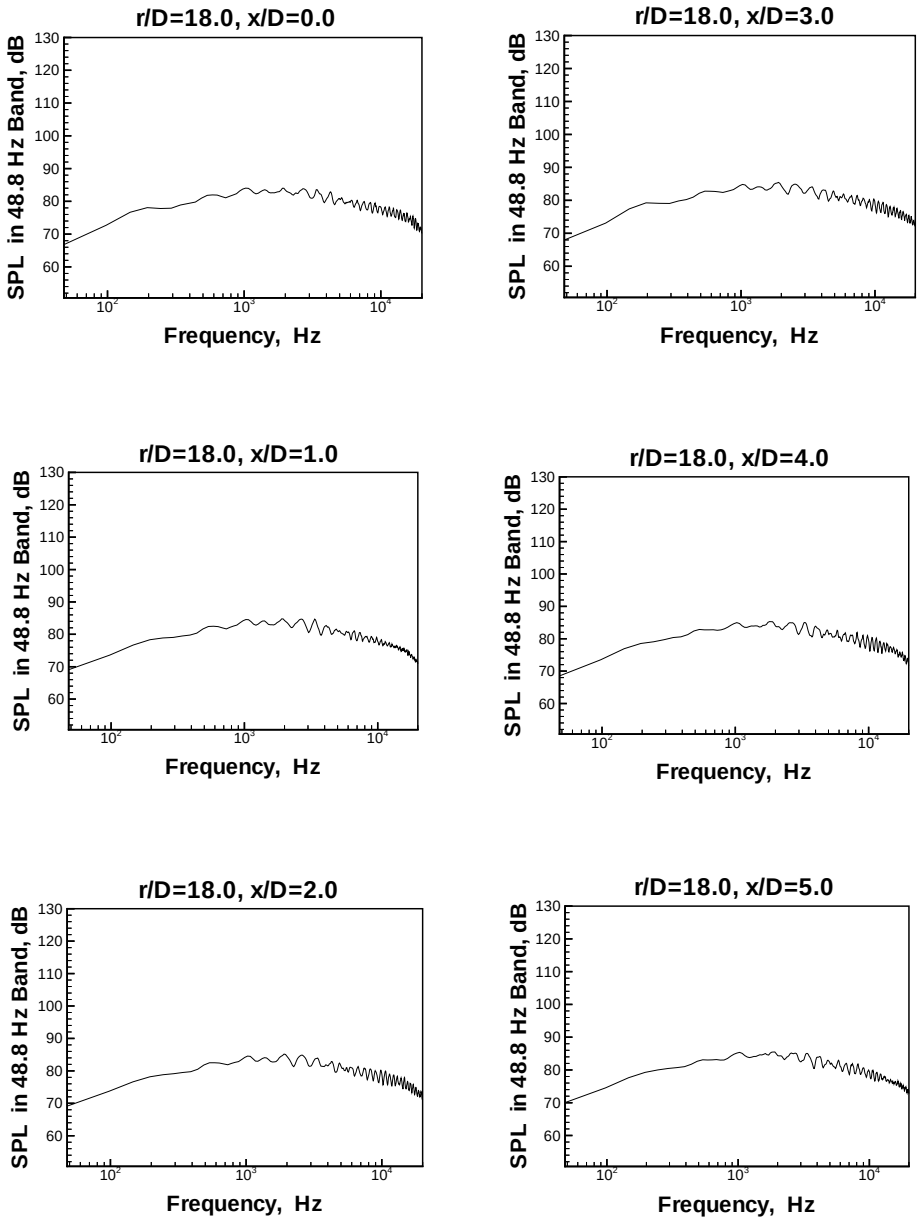

Figure 61: Near Field Pressure Spectra, Ma_e=0.85, r/D=18.0

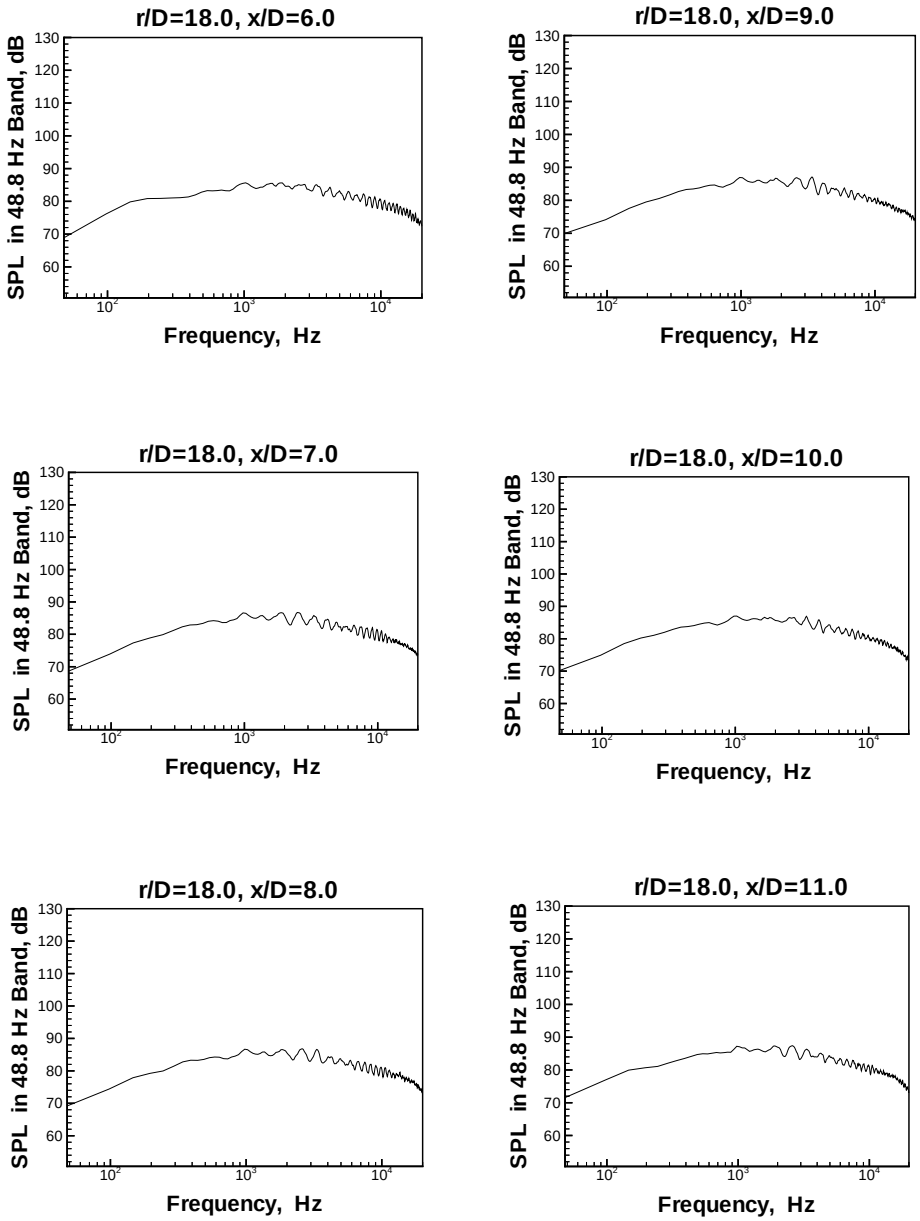

Figure 62: Near Field Pressure Spectra, Ma_e=0.85, r/D=18.0

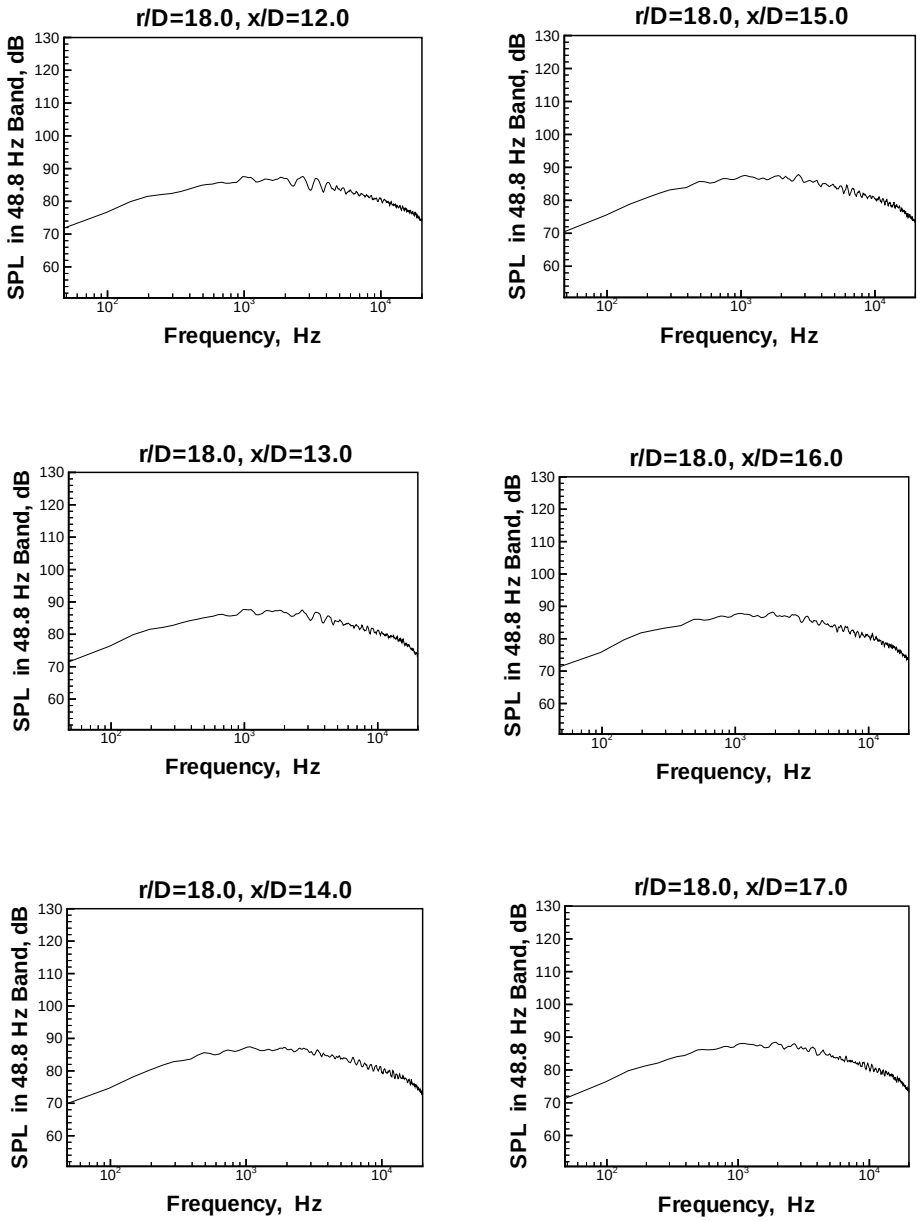

Figure 63: Near Field Pressure Spectra, Ma_e=0.85, r/D=18.0

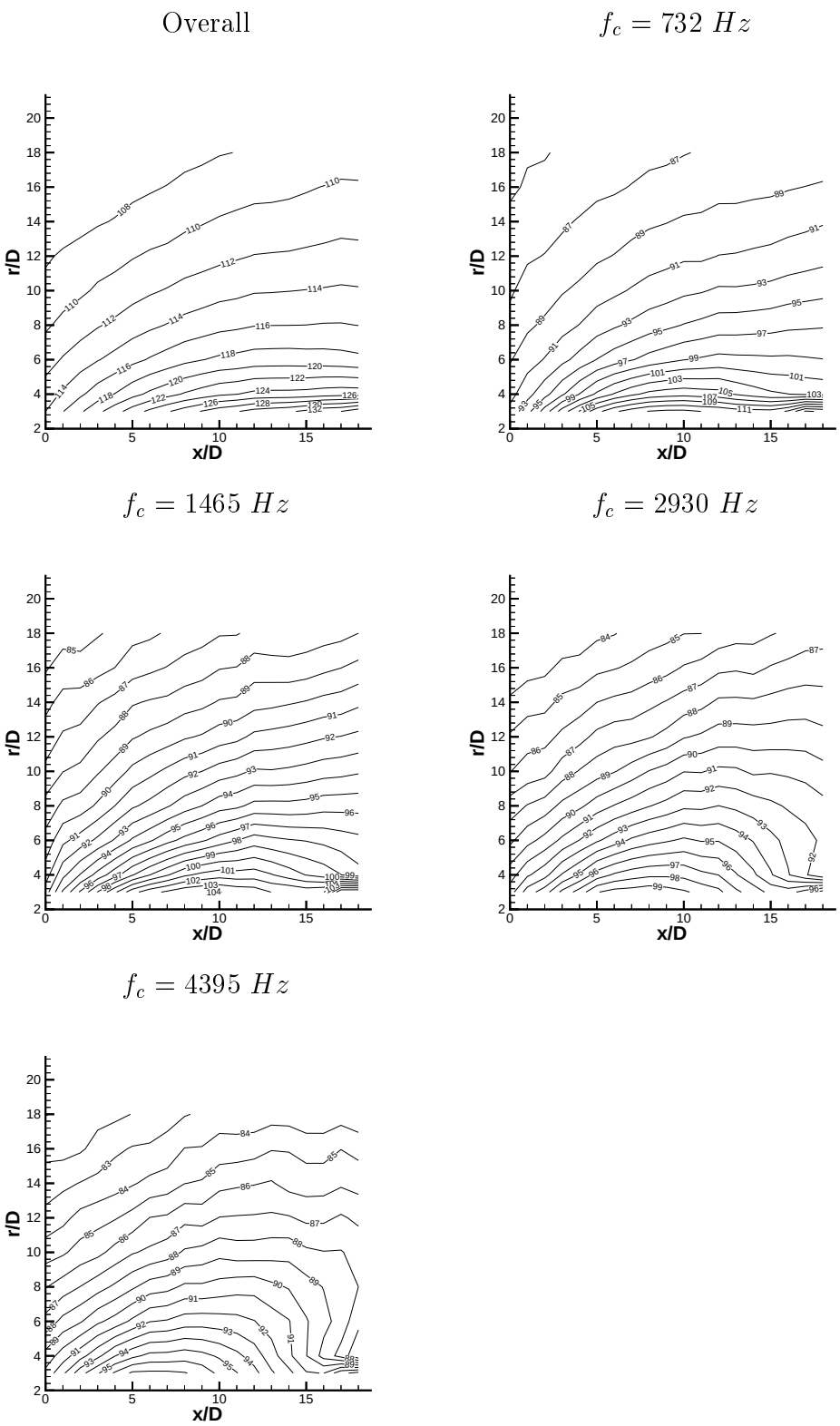

Figure 64: Contours of Acoustic Near Field for Ma_e=0.60, Overall and Bandpassed at Center Frequency Denoted

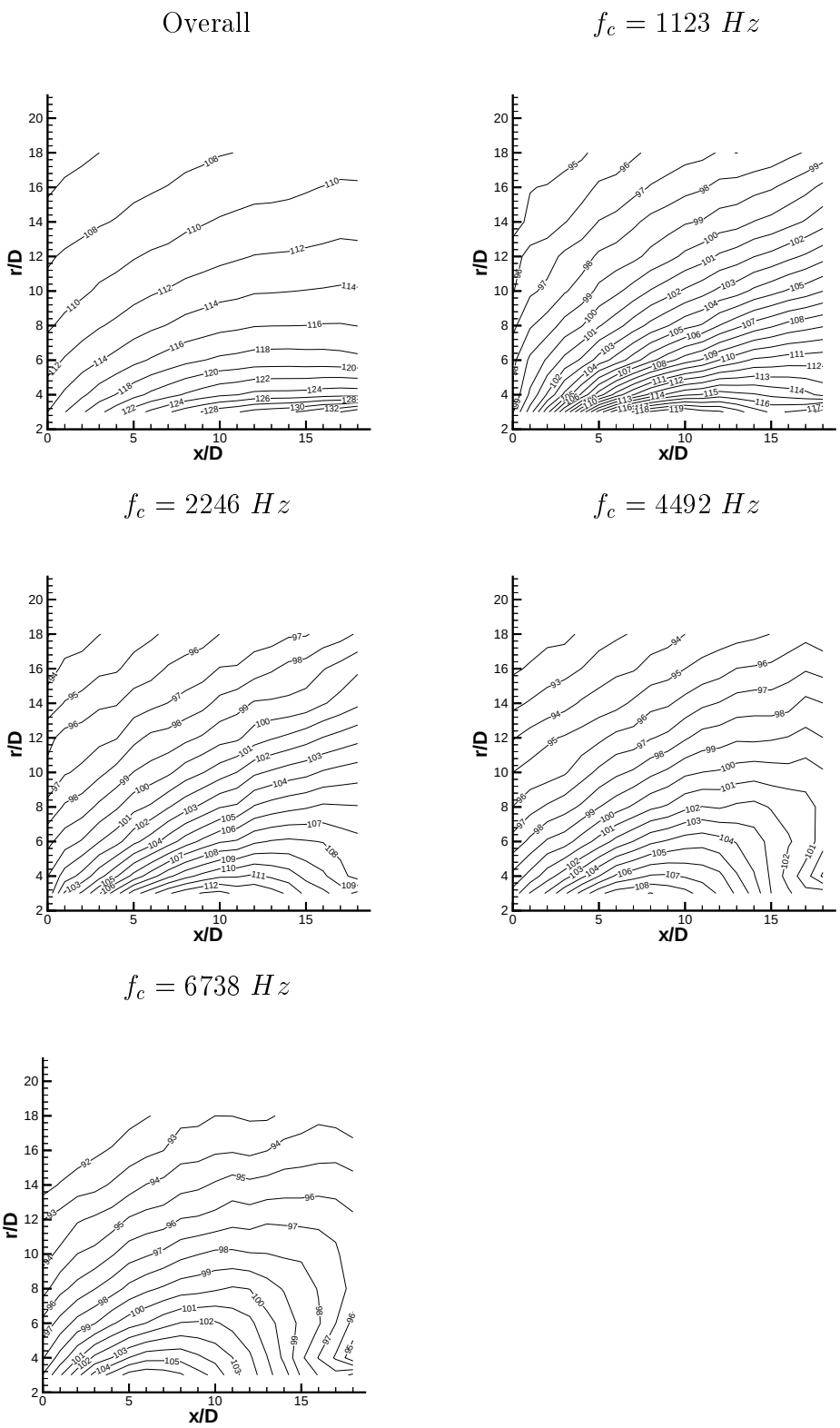

Figure 65: Contours of Acoustic Near Field Ma_e=0.85, Overall and Bandpassed at Peak Frequency Denoted

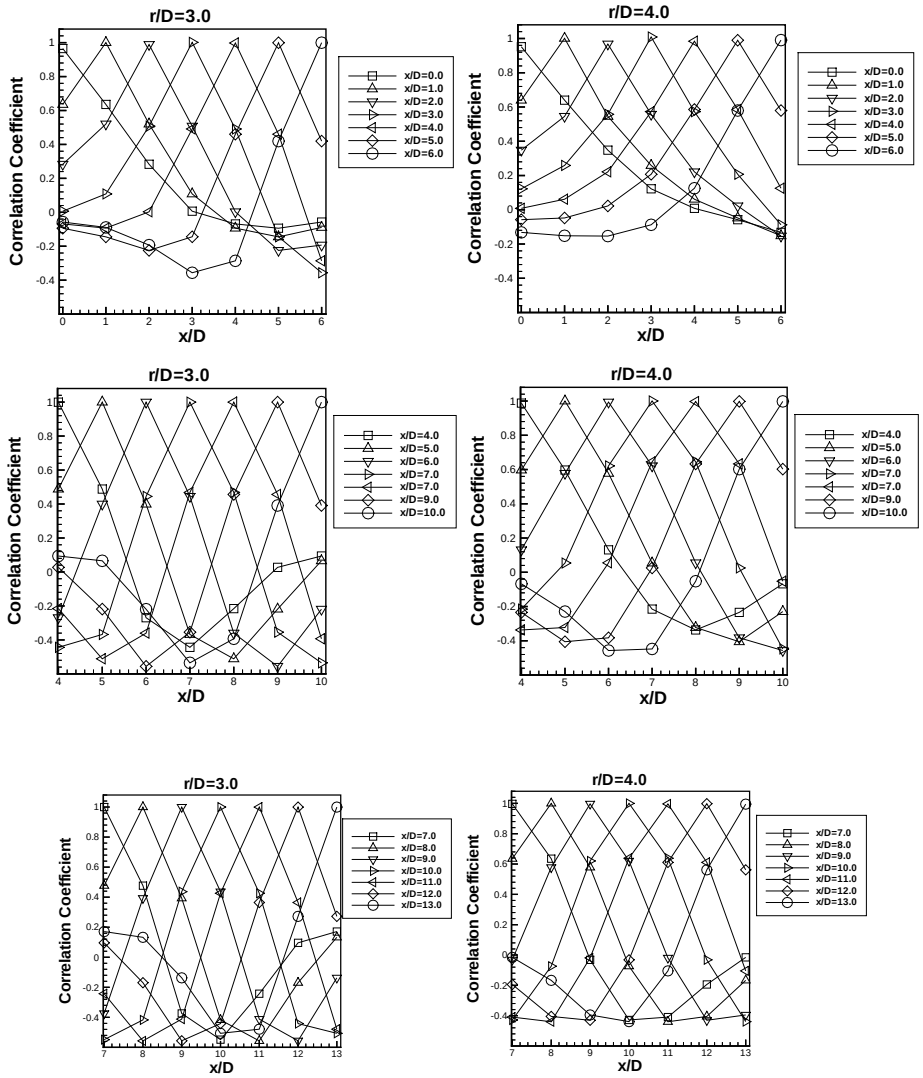

Figure 66: Zero Time Lag Pressure Correlations, Ma_e=0.30

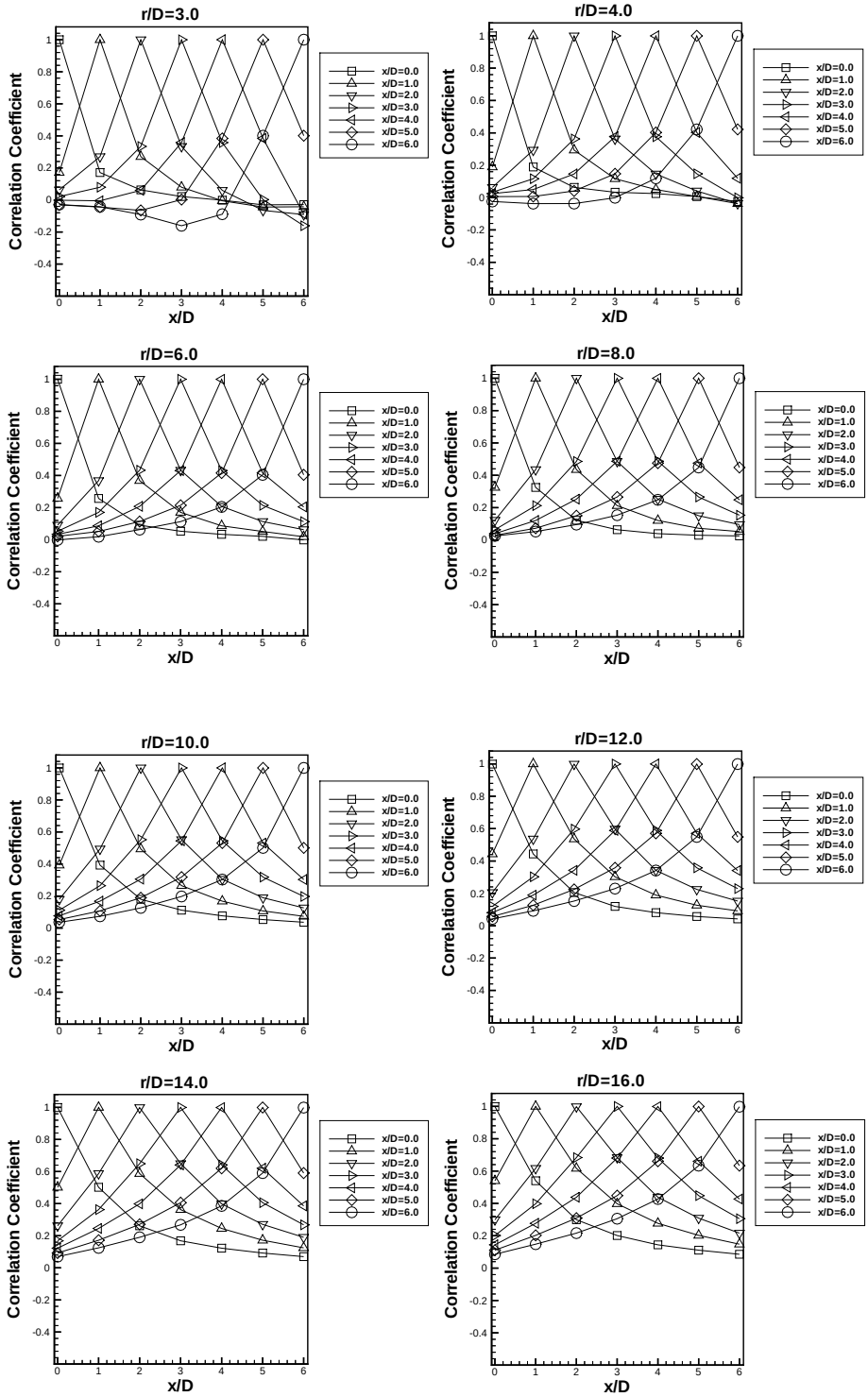

Figure 67: Zero Time Lag Pressure Correlations, Ma_e=0.60

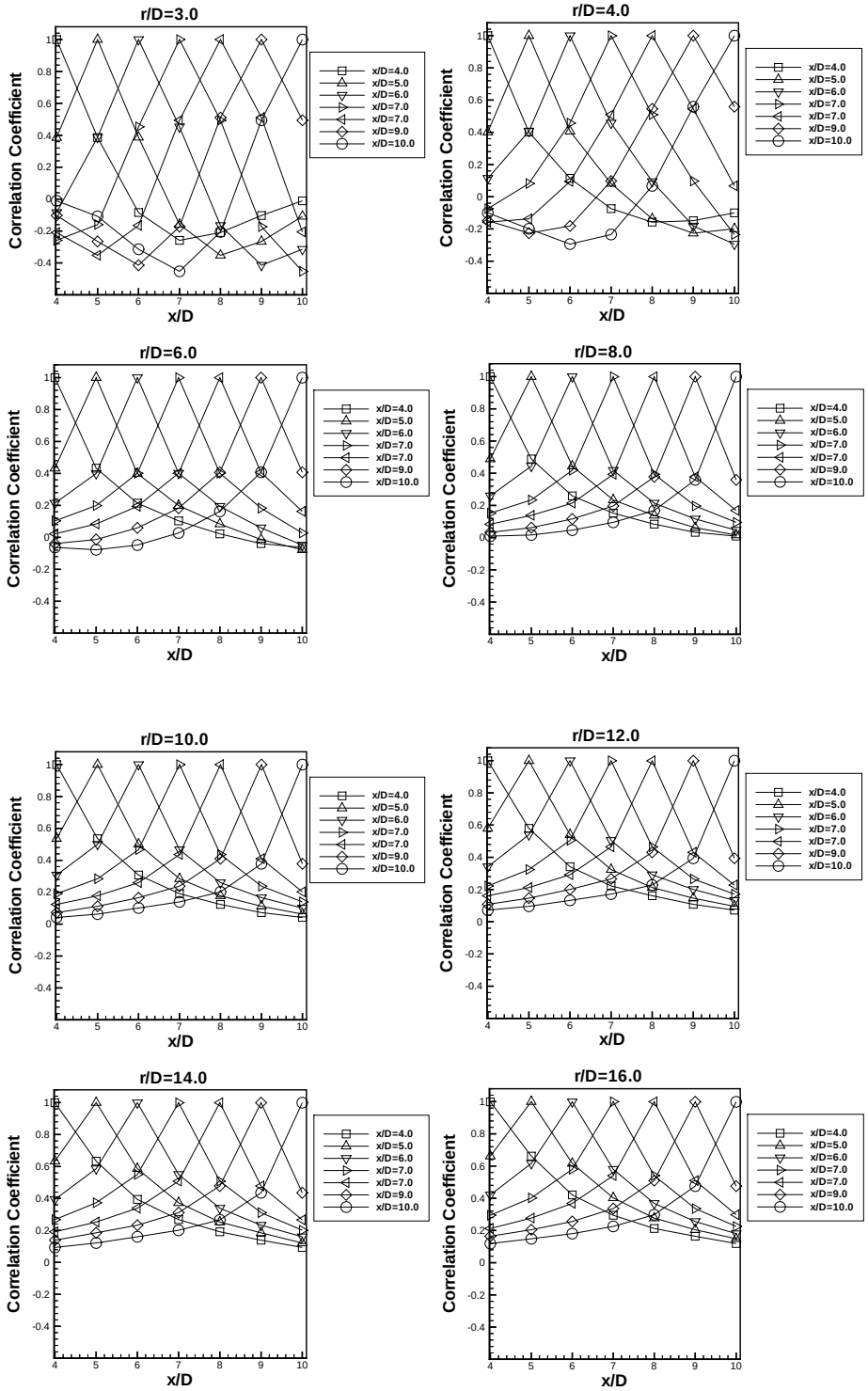

Figure 68: Zero Time Lag Pressure Correlations, Ma_e=0.60

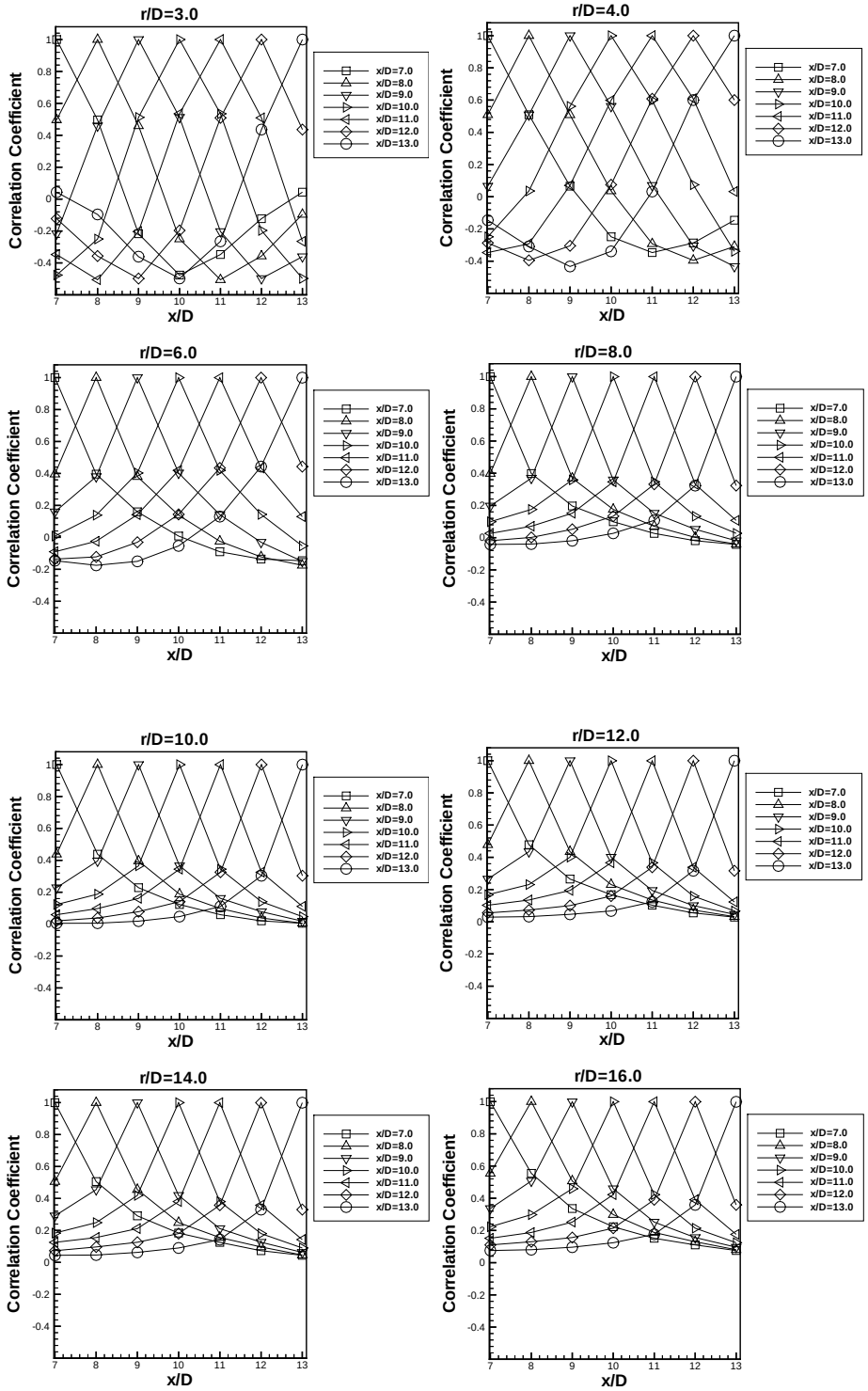

Figure 69: Zero Time Lag Pressure Correlations, Ma_e=0.60

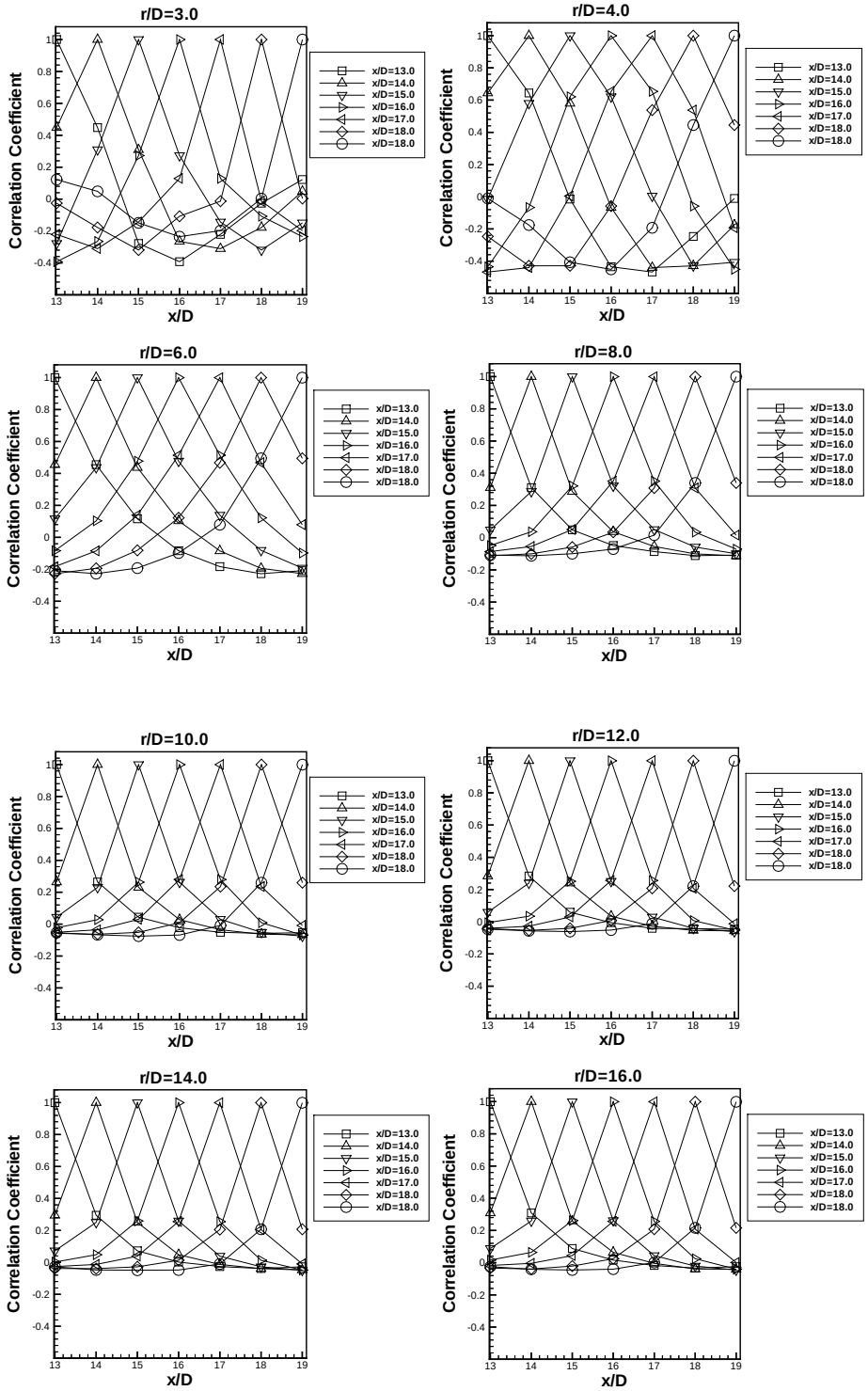

Figure 70: Zero Time Lag Pressure Correlations, Ma_e=0.60

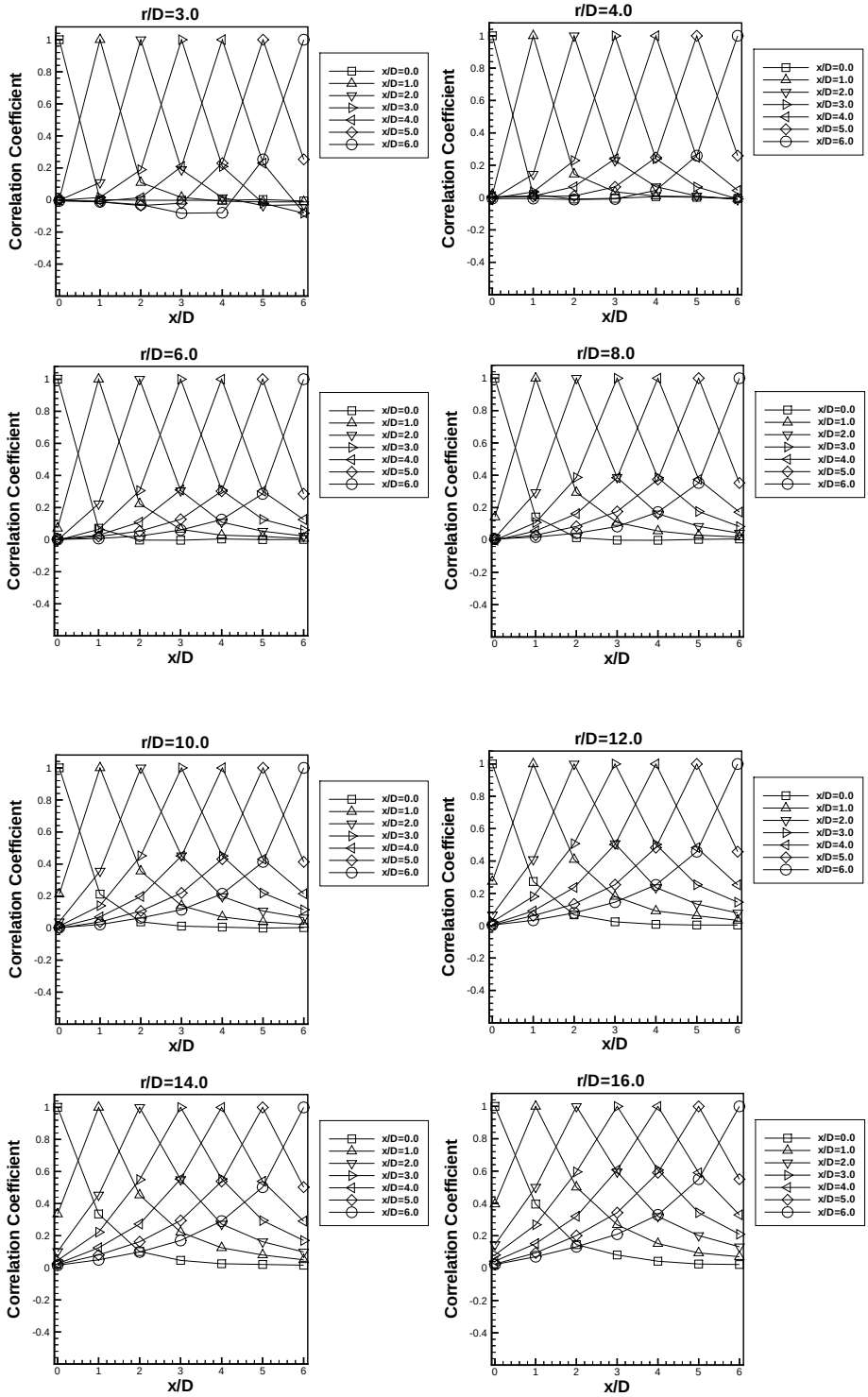

Figure 71: Zero Time Lag Pressure Correlations, Ma_e=0.85

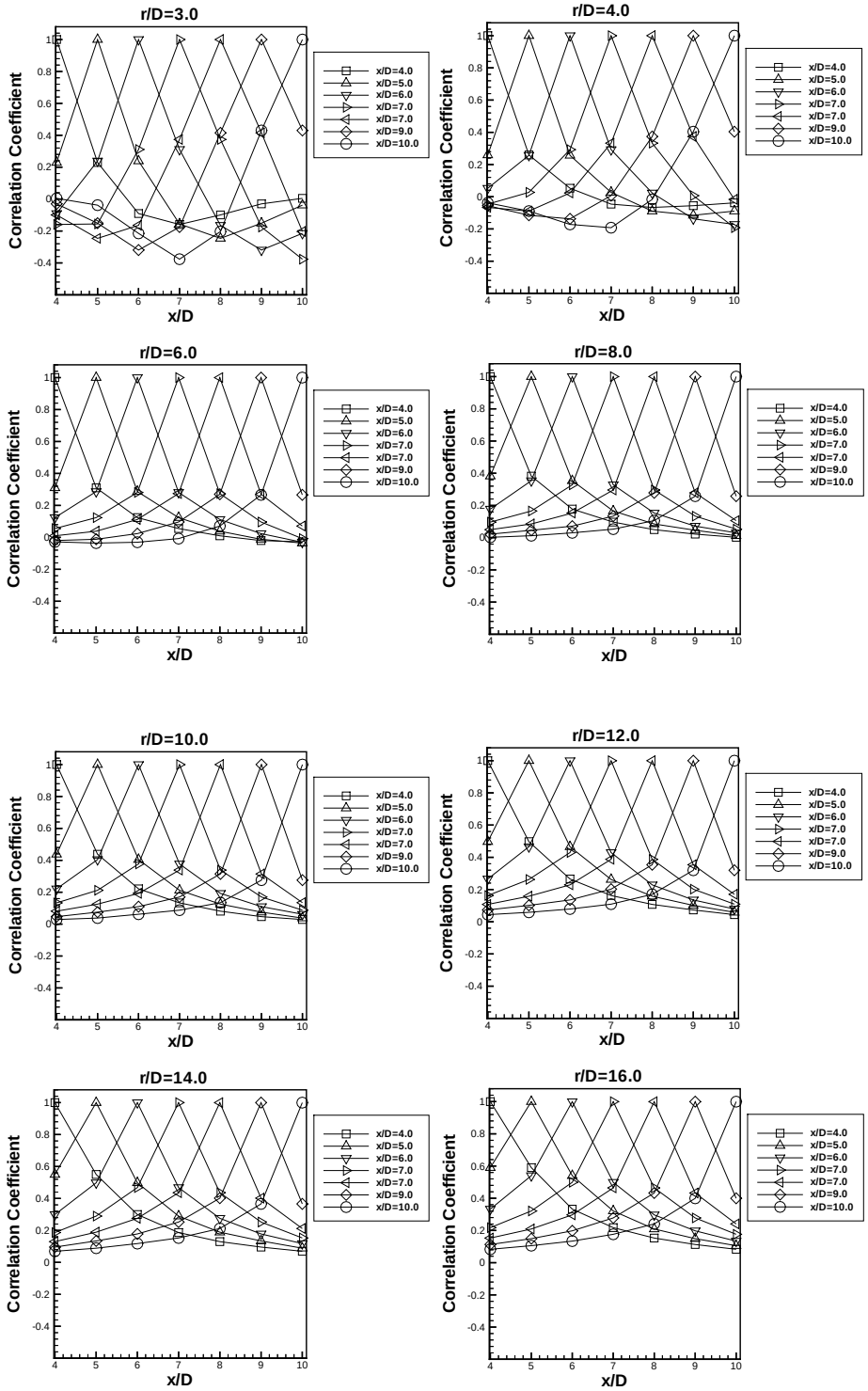

Figure 72: Zero Time Lag Pressure Correlations, Ma_e=0.85

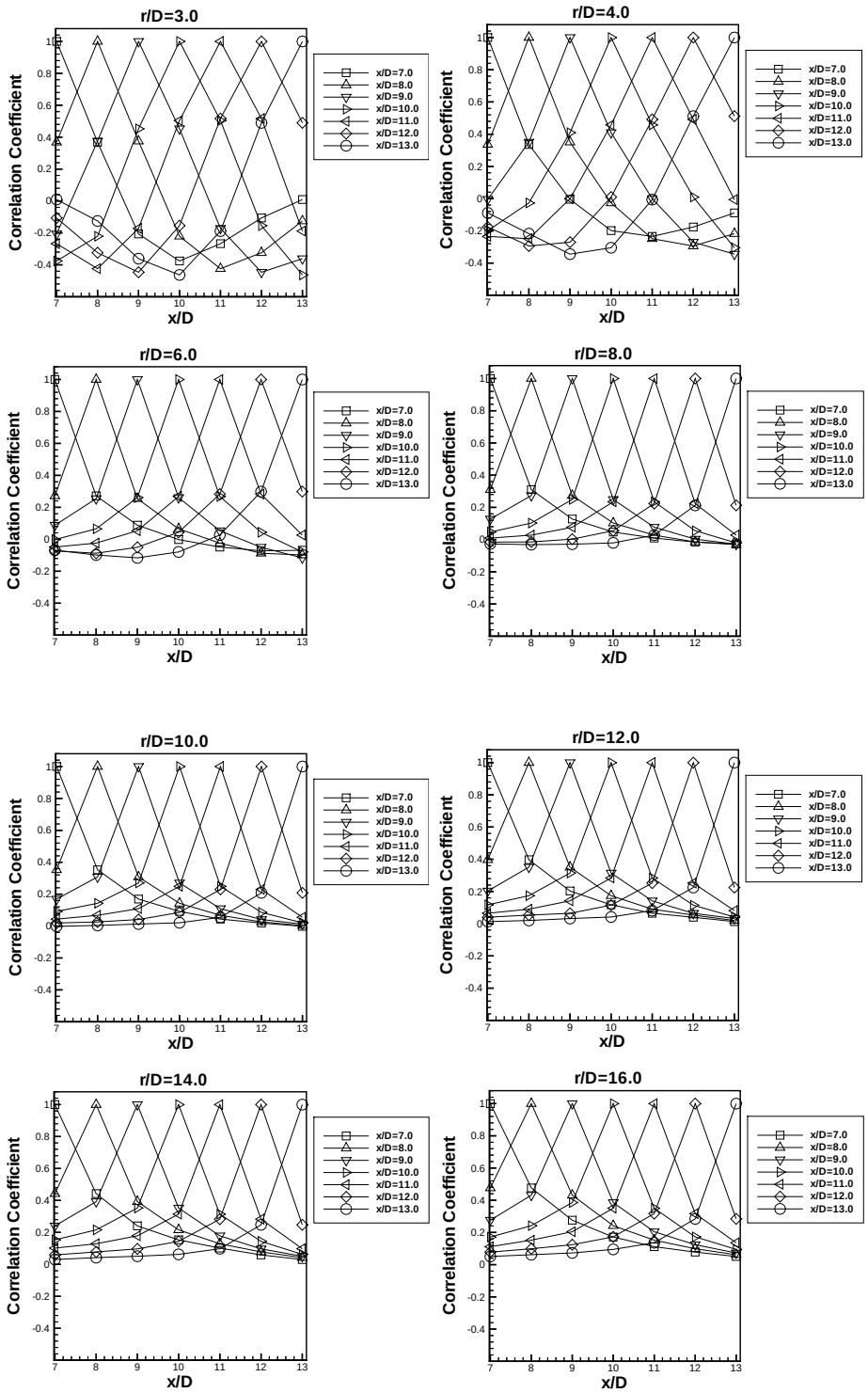

Figure 73: Zero Time Lag Pressure Correlations, Ma_e=0.85

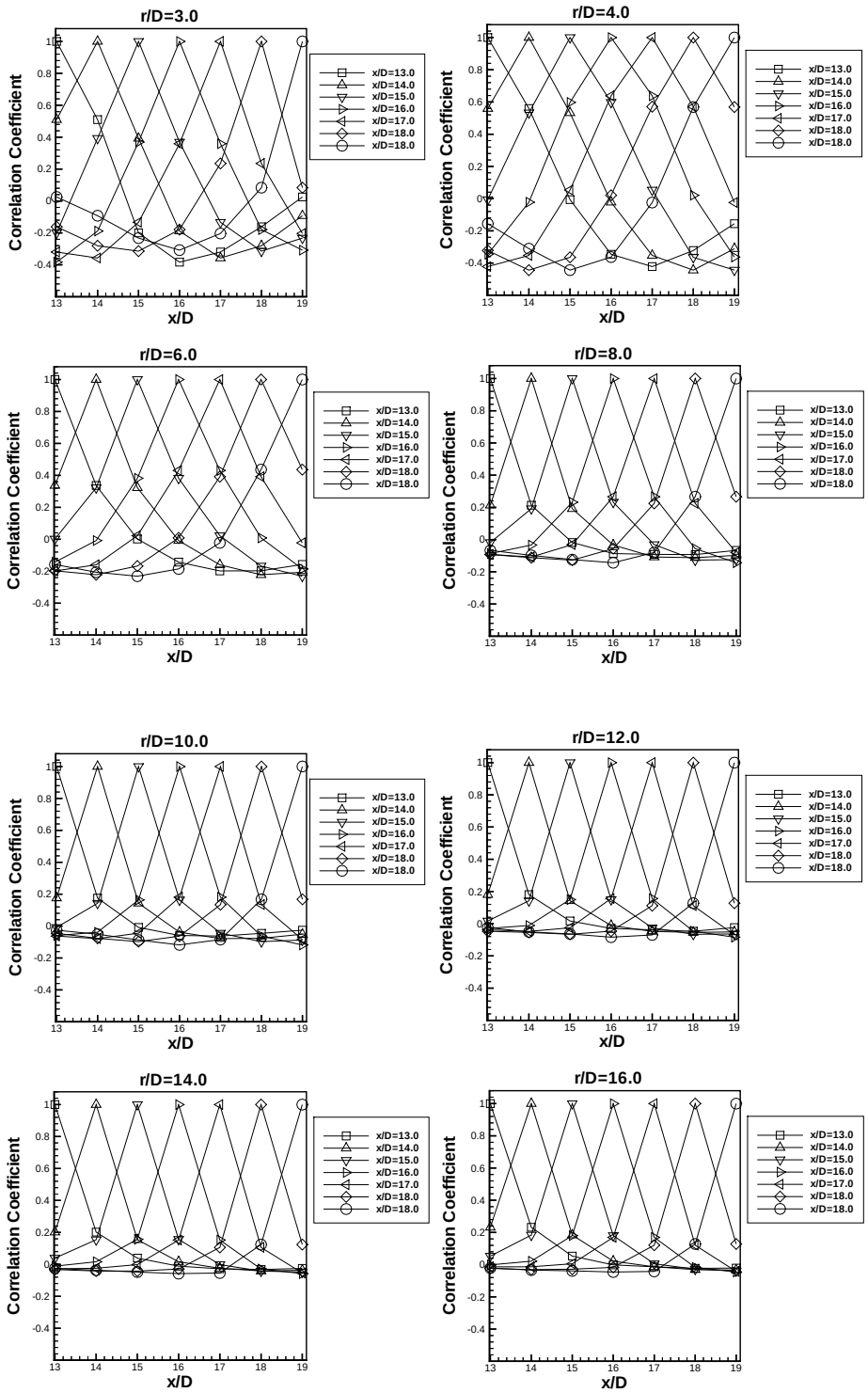

Figure 74: Zero Time Lag Pressure Correlations, Ma_e=0.85

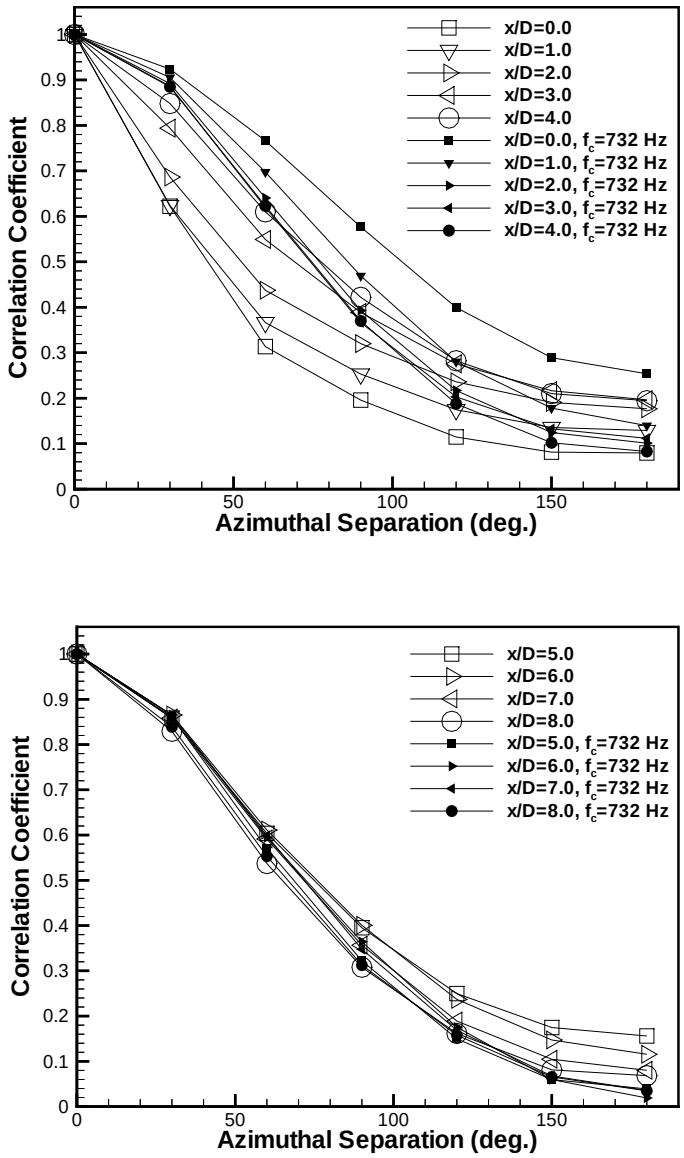

Figure 75: Azimuthal Correlations, Ma_e=0.60

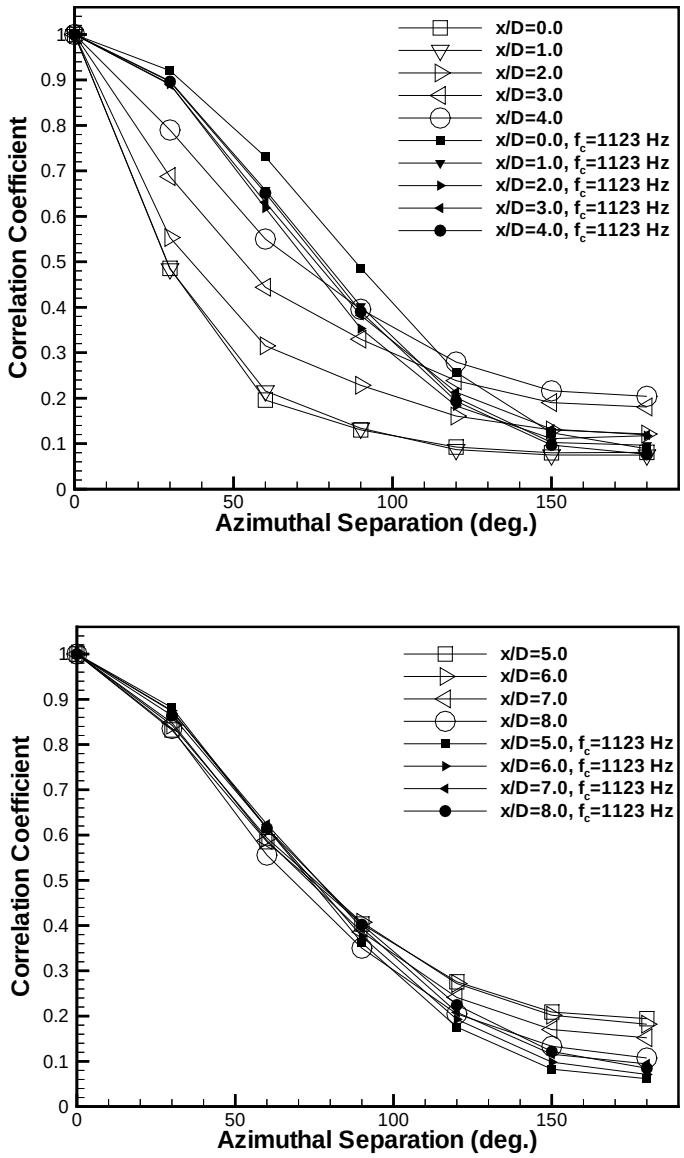

Figure 76: Azimuthal Correlations, Ma_e=0.85

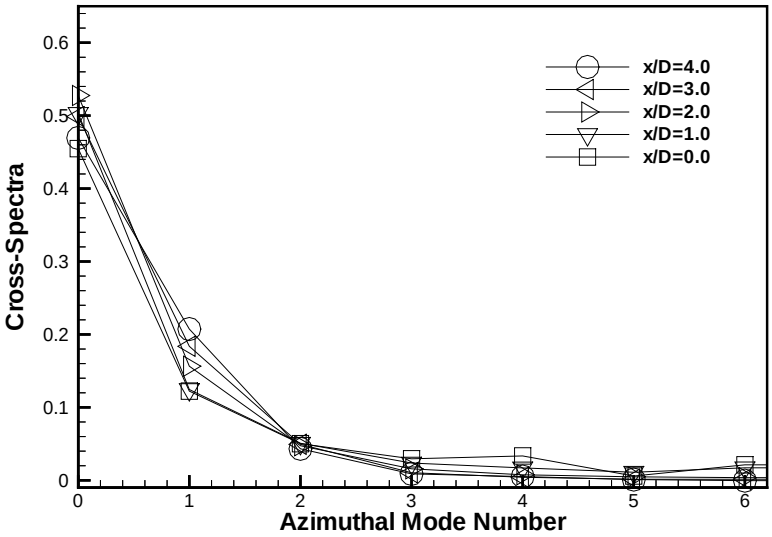

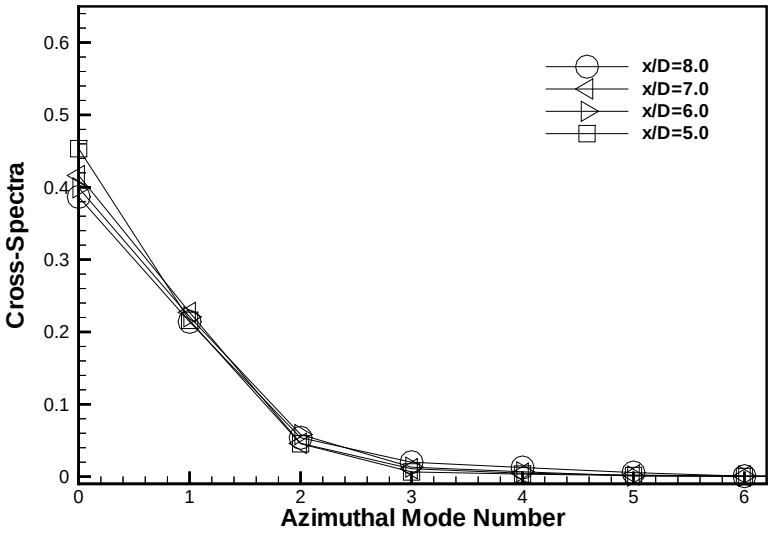

Figure 77: Azimuthal Cross-Spectra, Ma_e=0.30

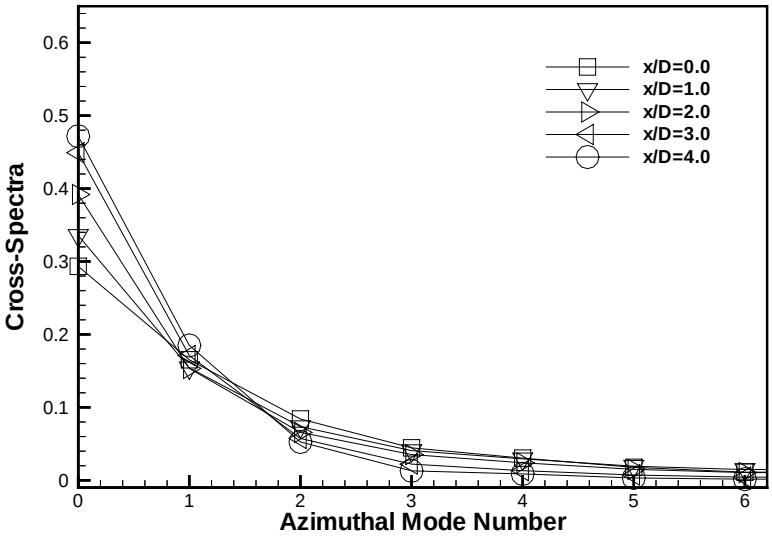

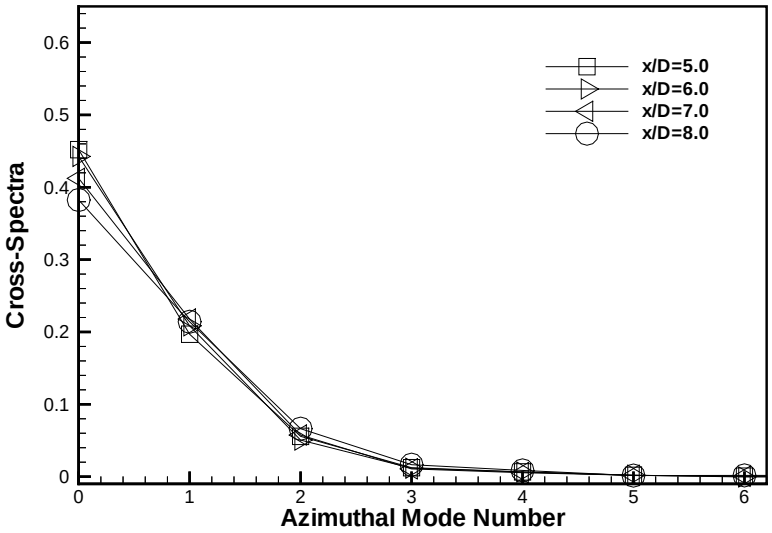

Figure 78: Azimuthal Cross-Spectra, Ma_e=0.60

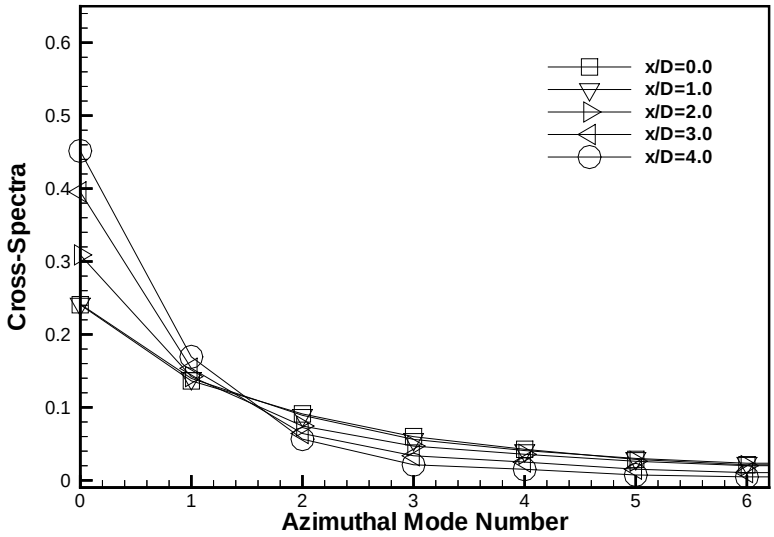

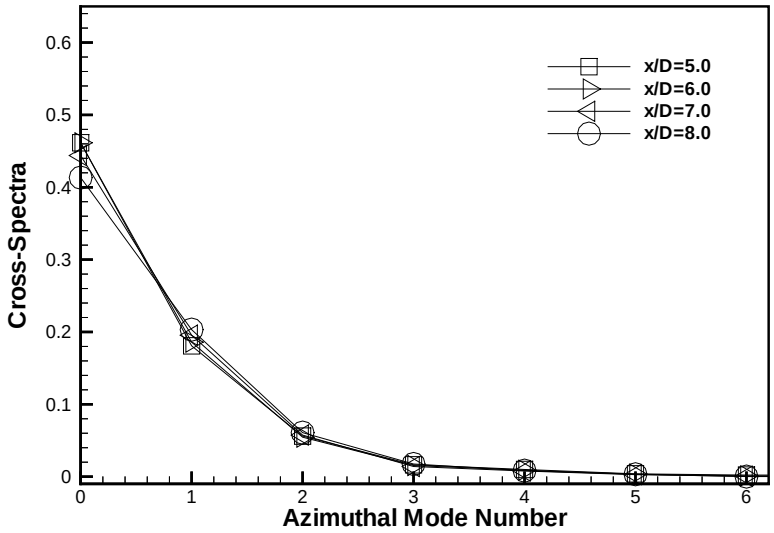

Figure 79: Azimuthal Cross-Spectra, Ma_e=0.85

REPORT DOCUMENTATION PAGE

Form Approved
OMB No. 0704–0188

1. AGENCY USE ONLY *(Leave blank)*

2. REPORT DATE
May 1999

3. REPORT TYPE AND DATES COVERED
Technical Memorandum

4. TITLE AND SUBTITLE
Aeroacoustic Data for a High Reynolds Number Axisymmetric Subsonic Jet

5. FUNDING NUMBERS
522-32-31-02

6. AUTHOR(S)
Michael K. Ponton, Lawrence S. Ukeiley and Sang W. Lee

7. PERFORMING ORGANIZATION NAME(S) AND ADDRESS(ES)
NASA Langley Research Center
Hampton, VA 23681–2199

8. PERFORMING ORGANIZATION REPORT NUMBER
L–17870

9. SPONSORING/MONITORING AGENCY NAME(S) AND ADDRESS(ES)
National Aeronautics and Space Administration
Washington, DC 20546–0001

10. SPONSORING/MONITORING AGENCY REPORT NUMBER
NASA/TM–1999–209336

11. SUPPLEMENTARY NOTES
Ponton: Langley Research Center, Hampton VA; Ukeiley: NRC-Resident Research Associate, Langley Research Center, Hampton VA; Lee: The George Washington University, Joint Institute for Advancement of Flight Sciences, Langley Research Center, Hampton VA.

12a. DISTRIBUTION/AVAILABILITY STATEMENT
Unclassified-Unlimited
Subject Category 71 Distribution: Standard
Availability: NASA CASI (301) 621–0390

12b. DISTRIBUTION CODE

13. ABSTRACT *(Maximum 200 words)*
The near field fluctuating pressure and aerodynamic mean flow characteristics of a cold subsonic jet issuing from a contoured convergent nozzle are presented. The data are presented for nozzle exit Mach numbers of 0.30, 0.60, and 0.85 at a constant jet stagnation temperature of 104°F. The fluctuating pressure measurements were acquired via linear and semi-circular microphone arrays and the presented results include plots of narrowband spectra, contour maps, streamwise/azimuthal spatial correlations for zero time delay, and cross-spectra of the azimuthal correlations. A pitot probe was used to characterize the mean flow velocity by assuming the subsonic flow to be pressure-balanced with the ambient field into which it exhausts. Presented are mean flow profiles and the momentum thickness of the free shear layer as a function of streamwise position.

14. SUBJECT TERMS
Aeroacoustics, Subsonic, Jet, Fluctuating Pressure

15. NUMBER OF PAGES
89

16. PRICE CODE
A05

17. SECURITY CLASSIFICATION OF REPORT
Unclassified

18. SECURITY CLASSIFICATION OF THIS PAGE
Unclassified

19. SECURITY CLASSIFICATION OF ABSTRACT
Unclassified

20. LIMITATION OF ABSTRACT